DESIGN OF Bi_2Te_3 SATURABLE ABSORBER BASED PASSIVE Q-SWITCHED AND MODE-LOCKED ERBIUM DOPED FIBER RING LASER

(Master's Thesis)

Thoalfeqar Ali Razaq ALYASIRI

Kütahya-2023

REPUBLIC OF TÜRKİYE
KÜTAHYA DUMLUPINAR UNIVERSITY
GRADUATE EDUCATION INSTITUTE
ELECTRICAL AND ELECTRONICS ENGINEERING DEPARTMENT

Master's Thesis

DESIGN OF Bi_2Te_3 SATURABLE ABSORBER BASED PASSIVE Q-SWITCHED AND MODE-LOCKED ERBIUM DOPED FIBER RING LASER

Supervisor:
Prof. Dr. Ahmet ALTUNCU

Prepared By:
Thoalfeqar Ali Razaq ALYASIRI

Kütahya-2023

Kabul ve Onay

KÜTAHYA DUMLUPINAR ÜNİVERSİTESİ

LİSANSÜSTÜ EĞİTİM ENSTİTÜSÜ

Elektrik-Elektronik Mühendisliği Anabilim dalında, 202085221012 öğrenci numaralı, Thoalfeqar Ali Razaq ALYASIRI'nın hazırlamış olduğu "DESIGN OF Bi_2Te_3 SATURABLE ABSORBER BASED PASSIVE Q-SWITCHED AND MODE-LOCKED ERBIUM DOPED FIBER RING LASER" başlıklı yüksek lisans tez çalışması ile ilgili tez savunma sınavı jüri tarafından yapılmış ve adayın tezinin OY BİRLİĞİ ile kabul edilmesine karar verilmiştir.

15/02/2023

Tez Jürisi	**İmza**	
	Kabul	Red
Prof. Dr. Ahmet ALTUNCU (Danışman)		
Prof. Dr. İsa NAVRUZ		
Dr. Öğr. Üyesi Fırat Ertaç DURAK		

Onay

Doç. Dr. Arif KOLAY

Enstitü Müdürü

Scientific Ethics Statement

I have carefully complied with scientific ethics and academic rules in the process from the proposal stage to the finalization stage of the study titled "Design Of Bi_2Te_3 Saturable Absorber Based Passive Q-Switched And Mode-Locked Erbium Doped Fiber Ring Laser", which I prepared as a master's thesis, that I have obtained all the information in the thesis within the framework of scientific ethics and tradition, and that I have prepared it in accordance with the rules of writing the thesis. I declare that I have cited every quotation I have made directly or indirectly in this study and that the works I have benefited from are those shown in the bibliography.

15/02/2023

Thoalfeqar Ali Razaq ALYASIRI

Resume

Thoalfeqar Ali Razaq ALYASIRI joined Al-Mustanseriya University Faculty of Engineering in 1999 and graduated in 2004 with an engineering degree in electrical engineering. In the 2020 academic year, he attended Kütahya Dumlupınar University Electrical and Electronics Engineering Department Graduate Education Institute to obtain his master's degree.

1. Passively Mode-Locked Fiber Ring Laser using Lu2O3 Thin Film Based Saturable Absorber

   T. A. Razaq Alyasiri, S. Ali Sadik, F. E. Durak, N. Farhanah Zulkipli, A. Altuncu and S. W. Harun, "Passively Mode-Locked Fiber Ring Laser using Lu2O3 Thin Film Based Saturable Absorber," 2022 30th Signal Processing and Communications Applications Conference (SIU),2022, pp. 1-4, doi: 10.1109/SIU55565.2022.9864845.

2. Nanosecond Mode-Locked Erbium Doped Fiber Laser Based on Few Layer Bismuth Telluride Ultra Thin Film Saturable Absorber

   T. A. Razaq Alyasiri, S. A. Sadik, F. E. Durak, N. F. Zulkipli, A. Altuncu and S. W. Harun, "Nanosecond Mode-Locked Erbium Doped Fiber Laser Based on Few Layer Bismuth Telluride Ultra Thin Film Saturable Absorber," 2022 IEEE 9th International Conference on Photonics (ICP), 2022, pp. 35-36, doi: 10.1109/ICP53600.2022.9912495.

3. Wavelength Tunable Passively Q-Switched Fiber Ring Laser Using Gallium Arsenide Based Microchip Saturable Absorber

   T. A. R. Alyasiri , A. Aşkın , B. Kaya , Ş. A. Sadık , F. E. Durak ve A. Altuncu , "WAVELENGTH TUNABLE PASSIVELY Q-SWITCHED FIBER RING LASER USING GALLIUM ARSENIDE BASED MICROCHIP SATURABLE ABSORBER", Journal of Scientific Reports-A, sayı. 051, ss. 73-80, Ara. 2022

ABSTRACT

DESIGN OF Bi_2Te_3 SATURABLE ABSORBER BASED PASSIVE Q-SWITCHED AND MODE-LOCKED ERBIUM DOPED FIBER RING LASER

ALYASIRI, Thoalfeqar Ali Razaq
Master Thesis, Department of Electrical and Electronics Engineering
Supervisor: Prof. Dr. Ahmet ALTUNCU
February, 2023, 150 pages

The work proposed in this thesis is focused on developing a new method for ultra thin film saturable absorber fabrication, and express different pulsed fiber laser sources based on the new fabricated saturable absorber. Various kinds of passively Q-switched EDFRL were demonstrated. The best result was obtained by using bidirectional pumping method where stable operating within wide repetition rate range of 6.9512 kHz-63.37 kHz, was obtained as the pumping power varied between 57.3 mW-417.6 mW. The highest realized output power, output pulse energy, peak pulse power, the shortest pulse duration, and related pulse train repetition rate were, 3.8mW, 65.459 nJ, 22.3 mW, 2.533 μs, and 63.37 kHz, respectively, at maximum pump power of 417.6mW. Also various kinds of wavelength tunable passively Q-switched EDFRL were demonstrated. The best result was obtained by using unequally pumping powers where a forward pumping 99.9 mW and backward pumping 83.7 mW, respectively. The wavelength tuning range was of 47.1 nm. The shortest pulse width that realized by this experiments with total cavity length about ~ 10.5 m was 3.769 μs with repetition rate of 49.73 kHz, as well as, the related output power spectrum was around 1529.45 nm central wavelength with output average power, pulse energy, peak pulse power, laser extraction efficiency and SNR of 0.7 mW, 12.9 nJ, 3.4 mW, 0.3716% and -67 dB at -105 dB reference level, respectively. Various kind of mode-locked EDFRLs were realized with using different pumping methods and different single mode fiber SMF28 lengths, for instant, 171.5 m from SMF-28 was added to the Q-switched EDFRL cavity to have a total cavity anomalous dispersion of $3.1ps^2.nm^{-1}.km^{-1.}$ By using bidirectional pumping power from 161.3 mW to 365.4 mW, the laser output pulse width, pulse train repetition rate, output average power, output pulse energy, output pulse peak power, and the laser cavity extraction efficiency were varying from (559.5 ns-554 ns), (948.8 kHz–950.6 kHz), (1.2 mW-3.3 mW), (1.244 nJ-3.5178 nJ), (2.2 mW-6.3 mW) and (0.7316%-0.9147), respectively.

Keywords: Bismuth Telluride, Erbium-doped fiber, Q-switched, Saturable Absorber, Ultra thin film $Bi_2Te_{3,}$ Wavelength unable Q-switched, and Mode locked,

ÖZET

DESIGN OF Bi_2Te_3 SATURABLE ABSORBER BASED PASSIVE Q-SWITCHED AND MODE-LOCKED ERBIUM DOPED FIBER RING LASER

ALYASIRI, Thoalfeqar Ali Razaq
Yüksek Lisans Tezi, Elektrik-Elektronik Mühendisliği Anabilim Dalı
Tez Danışmanı: Prof. Dr. Ahmet ALTUNCU
Şubat, 2023, 150 sayfa

Bu tezde önerilen çalışma, ultra ince film doyurulabilir soğurucu üretimi için yeni bir yöntem geliştirmeye ve yeni üretilmiş doyurulabilir soğurucuya dayalı farklı darbeli fiber lazer kaynaklarını ifade etmeye odaklanmıştır. Çeşitli pasif Q-anahtarlı EDFRL türleri gösterildi. En iyi sonuç, pompalama gücü 57,3 mW-417,6 mW arasında değişirken, 6,9512 kHz-63,37 kHz geniş tekrarlama oranı aralığında kararlı çalışmanın elde edildiği çift yönlü pompalama yöntemi kullanılarak elde edilmiştir. Maksimum pompa gücünde gerçekleşen en yüksek çıkış gücü, çıkış darbe enerjisi, tepe darbe gücü, en kısa darbe süresi ve ilgili darbe dizisi tekrar oranı sırasıyla 3,8 mW, 65,459 nJ, 22,3 mW, 2,533 µs ve 63,37 kHz idi. 417,6mW. Ayrıca pasif olarak Q-anahtarlı EDFRL ile ayarlanabilen çeşitli dalga boyu türleri de gösterildi. En iyi sonuç, sırasıyla ileri pompalama 99,9 mW ve geri pompalama 83,7 mW olmak üzere eşit olmayan pompalama güçleri kullanılarak elde edilmiştir. Dalga boyu ayarlama aralığı 47.1 nm idi. Yaklaşık ~ 10,5 m toplam kavite uzunluğuna sahip bu deneyler tarafından gerçekleştirilen en kısa darbe genişliği, 49,73 kHz tekrarlama oranı ile 3,769 µs, ayrıca ilgili çıkış gücü spektrumu, çıkış ortalama gücü, darbe enerjisi ile 1529,45 nm merkezi dalga boyu civarındaydı. pik darbe gücü, lazer ekstraksiyon verimliliği ve -105 dB referans seviyesinde sırasıyla 0,7 mW, 12,9 nJ, 3,4 mW, %0,3716 ve -67 dB SNR. Farklı pompalama yöntemleri ve farklı tek modlu fiber SMF28 uzunlukları kullanılarak çeşitli türde mod kilitli EDFRL'ler gerçekleştirilmiştir, anlık olarak, Q-anahtarlı EDFRL boşluğuna SMF-28'den 171,5 m eklenerek toplam boşluk anormal dağılımı 3,1ps2 elde edilmiştir. .nm-1.km-1. 161,3 mW ila 365,4 mW arasında çift yönlü pompalama gücü kullanılarak, lazer çıkış darbe genişliği, darbe dizisi tekrarlama oranı, çıkış ortalama gücü, çıkış darbe enerjisi, çıkış darbe tepe gücü ve lazer boşluğu çıkarma verimliliği (559,5 ns-554) arasında değişiyordu. ns), (948,8 kHz–950,6 kHz), (1,2 mW-3,3 mW), (1,244 nJ-3,5178 nJ), (2,2 mW-6,3 mW) ve (%0,7316-0,9147).

Anahtar Kelimeler: Bizmut Tellürid, Dalgaboyu Q-anahtarlı olmayan ve Mod kilitli, Doyurulabilir Soğurucu, Erbiyum katkılı fiber, Q-anahtarlı, Ultra ince film Bi2Te3

ACKNOWLEDGEMENTS

First of all, I would like to thank Allah for the blessings He has given me throughout my life and for my academic research work.

I would like to thank all the members of the photonics research group (FOTAM) at Dumlupınar University, specifically, my advisor Prof. Ahmet ALTUNCU, Dr. Şerif Ali SADIK, and Dr. Fırat Ertaç DURAK.

I would like to thank my colleague Dr. Farhanah Zulkipli and Prof.Ir.Dr. Sulaiman Wadi Harun from the University of Malaya, Malaysia for the scientific support they provided me.

Thank you to my family members, my wife, and my three children Deemah, Abdulazeez, and Muhamed.

Finally, I would like to thank Kütahya Dumlupınar University, Graduate Education Institute, and the Republic of TÜRKİYE.

CONTENTS

Page

CHAPTER THREE

BIZMUTH TELLURIDE (Bi_2Te_3) BASED SATURABLE ABSORBER

CHAPTER FOUR

BISMUTH TELLURIDE (Bi_2Te_3) SATURABLE ABSORBER BASED Q-SWITCHED EDFRL

CHAPTER FIVE

MODE-LOCKED EDFRL OPERATING AT 1.5-MICRON REGION BASED ON Bi_2Te_3-PVA SATURABLE ABSORBER

CHAPTER SIX

CONCLUSION AND FUTURE WORK

LIST OF FIGURES

Page

LIST OF TABLES

LIST OF SYMBOLS AND ABBREVIATIONS

Al_2O_3	Aluminium Oxide
Bi_2Te_3	Bismuth Telluride
BP	Black Phosphorus
CNT	Carbon Nanotube
CW	Continuous Waveform
XPM	Cross phase Modulation
CVD	Chemical vapor deposition
C_5H_5OH	Ethanol alcohol
C_3H_8O	Isopropyl alcohol
dB	Decibel
DI	De-ionized
EDFA	Erbium Doped Fiber Amplifier
EDFL	Erbium Doped Fiber Laser
EDFRL	Erbium Doped Fiber Ring Laser
EDS	Energy Dispersive Spectroscopy
Er^{3+}	Erbium ion
eV	Electron volt
FESEM	Field Emission Scanning Electron Microscope
FWHM	Full Width Half Maximum
Fe_2O_3	Iron oxide
GVD	Group Velocity Dispersion
HAZ	Heat Affected Zone
Ho^{3+}	Hollium ion
h	Plancks constant
IMG	Index maching gel
ISO	Isolator
Lu_2O_3	Lutetium Oxide
LD	Laser Diode
LPE	Liquid phase exfoliation
ME	Mechanically exfoliated
MBE	Molecular beam epitaxial
MoS_2	Molybdenum Disulfide

NLDR	Nonlinear Dispersive Regime
NLO	Nonlinear optical
NiO	Nickel Oxide
Nd	Nedimium
nm	Nano meter
ONLM	Optical nonlinear material
OSA	Optical Spectrum Analyzer
OSC	Oscilloscope
PD	Photodetector
PEG	Polyethylene Glycol
PVA	Poly(vinyl Alcohol)
Pr^{3+}	Promum ion
RBW	Resolution Bandwidth
RF	Radio Frequency
SA	Saturable Absorber
SESAM	Semiconductor saturable absorber mirror
SEM	Scanning Electron Microscope
SMF	Single Mode Fiber
SNR	Signal to Noise Ratio
SPM	Self-Phase Modulation
TBP	Time Bandwidth Product
Tm	Thulium
TMDs	Transition Metal Dichalcogenides
TMO	Transition Metal Oxide
TI	Topological Insulators
TiO	Titanium Oxide
VBW	Video Bandwidth
V_2O_5	Vanadium Oxide
WDM	Wavelength Division Multiplexing
WS_2	Tungsten Disulfide
XRD	X-ray Diffraction
Xe	Periodic element symbol
Yb^{3+}	Ytterbium ion

ZnO	Zinc Oxide
Ω	Ohm
0D	Zero-dimensional
1D	One-dimensional
2D	Two-dimensional
3D	Three-dimensional

THESIS TEXT

INTRODUCTION

Of the very importance of pulsed laser technology in various fields of applications, for example, medical diagnostics, material processing, scientific research, and telecommunications, the need for robust pulsed laser sources has grown. Up to date, different kinds of saturable absorbers (SAs) were proposed to realize passively pulsed laser sources. However, great efforts have been dedicated to investigate SA materials that are fabricated simple, fast and cheap methods with high performance. This thesis presents the usability of Bi_2Te_3-PVA based saturable absorbers in pulsed erbium doped fiber ring lasers to be able to use in fiber optical laser sources operating in the 1.5 micron region. To fabricate a saturable absorber thin film, firstly, polyvinyl alcohol (PVA) was doped by Bi_2Te_3 nanoscale powder. Next, thin film SA was placed between two fiber ferrule connectors connected with an adapter to make a fiber coupled SA device. In addition to traditional methods, Bi_2Te_3-PVA based thin film SA was sandwiched between firmly fixed connector tips to convert thin film SA to an ultra-thin film SA. The newly fabricated ultra-thin film SA has presented the properties better than the original thin film SA. Various passively Q-switched, wavelength-tunable Q-switched and passively mode-locked erbium doped fiber ring lasers were successfully demonstrated in 1.5-micron regimes based on the newly developed ultra-thin film SAs.

The new fabricated ultra-thin film Bi_2Te_3 was used to demonstrate various kinds of EDFRLs and the best results obtained were:

First, an ultra-thin film Bi_2Te_3 SA device fabricated with the new method for passively Q-switched EDFRL was demonstrated by using bidirectional-pumping method. It was stably operating at 1565.23 nm-1567.2 nm, with a wide repetition rate range of 6.9512 kHz-63.37 kHz for a pump power range of 57.3 mW-417.6 mW. At the maximum pump power, the highest output power and pulse energy of 3.8 mW and 65.459 nJ were obtained respectively. Additionally, the maximum peak power of 22.3 mW, the shortest pulse width of 2.533 μs and the highest pulse frequency of 63.37 kHz were observed at the pump power of 417.6 mW.

Second, an ultra-thin film Bi_2Te_3 SA device fabricated with the new method for wavelength tunable passively Q-switched EDFRL operation was demonstrated by using unequally pumping powers in both directions, with a forward pump power of 99.9 mW and a backward pump power of 83.7 mW. The proposed EDFRL had a tunable wavelength range of 47.1 nm (from 1523.9 nm to 1571 nm). The shortest observed pulse width for a total EDFRL cavity length of ~10.5 m was 3.769 µs with a repetition rate of 49.73 kHz. The corresponding central lasing wavelength observed in optical output spectrum was 1529.45 nm with an output average power of 0.7 mW, pulse energy of 12.9 nJ, peak pulse power of 3.4 mW, laser extraction efficiency of 0.3716% and SNR of 67 dB, respectively. The widest observed pulse width was 6.106 µs with a repetition rate of 20.661 kHz. The corresponding central lasing wavelength observed in optical output spectrum was 1571 nm with an output average power of 1.0 mW, pulse energy of 44.56 nJ, peak pulse power of 7.3 mW, power conversion efficiency of 0.5334% and SNR of 60 dB, respectively.

Third, an ultra-thin film Bi_2Te_3 SA device fabricated with the newly method for passively mode-locked EDFRL was demonstrated by adding a 171.5 m SMF-28 standard fiber within the Q-switched EDFRL cavity and using a bidirectional pumping power range from 161.3 mW to 365.4 mW. The obtained results in these measurements were a pulse width range from 559.5 ns to 554 ns, a repetition rate range from 948.8 kHz to 950.6 kHz, an output average power range from 1.2 mW to 3.3 mW, a pulse energy range from 1.244 nJ to 3.5178 nJ, a pulse peak power range from 2.2 mW to 6.3 mW. Using the same length of SMF-28 fiber and a forward pumping power range from 168.3 mW to 284.7 mW, the obtained results in these measurements were a pulse width range from831 ns to 996 ns, a repetition rate range from 501 kHz to 502.3 kHz, an output average power range from 1.0 mW to 1.8 mW, a pulse energy range from 1.001 nJ to 1.8674 nJ, a pulse peak power range from 1.8 mW to 3.3 mW and a laser extraction efficiency range from 0.5648% to 0.6232%.

CHAPTER ONE

INTRODUCTION

1.1. BACKGROUNDAND MOTIVATION

In spite of the success of solid-state lasers as ultra-short pulse laser sources, like titanium sapphire lasers, all-solid-state lasers have negative aspects regarding their performances. They have some disadvantages such as high cost, cooling requirements, difficulty in accurate alignment, big size, and continuous maintenance. These drawbacks make use of these kinds of lasers limited in real-world applications (Bourziex et al., 1993, Walsh et al., 1997). Over the past decade, fiber lasers have been proposed as an alternative way to produce short optical pulses with a high pulse energy(Walsh et al., 1997).Fiber lasers are preferred over the solid-state laser sources due to their advantages rare earth doped fibers are used as the gain medium. Therefore, the large surface area of the active fiber cancels the need for external cooling. In addition, there is no need for precise optical alignment in the cavity design due to the fiber optical waveguide structure providing optimum pump and signal overlapping in the gain medium. Furthermore, an excellent laser beam quality can be achieved at the output of a single mode fiber. In practice, setup cost of a fiber laser is less than a solid-state laser counterpart, leading to a widespread adoption of fiber laser technology in many applications.

Recently, the pulsed fiber lasers have become an essential tool in many practical application fields, for example, medical diagnosis (Nagy et al., 2009, Blaman et al., 2010), multiphoton imaging (C.Xu. et al., 2013), precision instruments (Gatas et al., 2008), microscopy and spectroscopy (Freudiger et al., 2014), and optical communications (Salihi et al., 1990). Two approaches are used to generate pulses in fiber lasers, which are quality-switching and phase-locking techniques.

In quality switching, the laser cavity quality factor (Q-factor) is rapidly switched between high quality (Q-high) and low quality (Q-low) regimes. The laser cavity stores energy in the gain medium for the Q-high regime. When Q changes from Q-high to Q-low, the laser emits energy as a light pulse with a relatively high peak power in a time scale from microsecond to nanosecond and even picoseconds (Adachi et al., 2002).

Phase-locking or mode-locking is the second approach for ultra fast, narrow pulse generation. For mode-locking of a fiber laser, like Q-switching, a modulator is used with a special cavity arrangement having a balance between group velocity dispersion (GVD) and self-phase modulation (SPM) within the laser cavity. A passively mode-locked fiber laser uses a passive modulator called as saturable absorber (SA) (Haus, 2000). The SA device functions as a light modulator which absorbs light when the light intensity is low and allows light with high intensity to transmit through with low loss. Depending on the laser cavity length and gain spectrum of the active medium, the number of excited laser modes and the mode spacing will change. The excited laser modes that have a constant phase relation will interfere constructively to generate short pulses inside the laser cavity. Rising and falling edges of each pulse suffer high losses than the central part due to the nonlinear absorption of the SA. After few round trips, the final pulse shape is formed and became as narrow as picoseconds or femtoseconds.

In 1992, first SESAMs were used as SAs (Okhotnikov et al., 2004) and within a few years they became commercial SA devices for optical switching purposes. However, the researchers have focused on finding alternative materials due to their some drawbacks such as high manufacturing costs, narrow absorption bandwidths and bulk structures.

A lot of different materials have recently been investigated as saturable absorbers to generate laser pulses. These materials such as semiconductor saturable absorber mirror (SESAM) (Z.C. Luo. et al., 2010, Gomez, 2004), graphene (Zhang et al., 2009, Sun et al., 2010) carbon nanotube (CNT) (Set et al., 2004, Ahmed et al., 2014), black phosphorous (BP) (Y. Chen et al., 2015), transition metal oxides like zinc oxide (ZnO) (Harith Ahmad et al., 2016) and topological insulator (TI)have been used as SAs in both passively Q-switched and passively mode-locked lasers.

Despite other materials, TIs have high potential and significant advantages due to their properties. As an example of TI, Bismuth Telluride (Bi_2Te_3) was proposed and demonstrated in 1.5 μm region (Wang et al., 2015), in 2 μm region (Ke Yin et al., 2015) (Lu Li et al., 2017), also As_2Te_3 (Jinho Lee and Ju Han Lee, 2020), Bi_2Se_3 (Kexuan Li et al., 2016, Kexuan Li et al., 2015) (K. Li, Y. Song, Z. Yu, and J. Tian,2022), and Sb_2Te_3 (Harith Ahmad et al., 2016, Harith Ahmad et al., 2022) were proposed as highly efficient SAs.

This thesis focus on realizing high performance erbium doped fiber ring lasers (EDFRLs) in Q-switching and mode-locked operations using new kinds of passive optical nonlinear materials (ONL) and Topological Insulators (TI) as thin film SAs.

Specifically, Bi_2Te_3 based thin film and ultra-thin film TI Saturable absorbers have been used in our cavity designs.

1.2. THESIS OBJECTIVES

This thesis aims to evaluate Bi_2Te_3 based thin film and ultra-thin film TI Saturable absorbers in pulsed EDFRLs operating in both Q-switching and mode-locking regimes. This study specifically focuses on converting a thin film SA to ultra-thin film SA for a better Q-switching and mode-locking performance. Several objectives have been outlined:

a) Investigate low cost, simple and fast fabrication method of thin filmBi_2Te_3-PVA SAs and converting a thin film SA to an ultra-thin film SA.

b) Demonstrate Q-switched EDFRL based on Bi_2Te_3-PVA thin film and ultra-thin film SA in 1.5-µm region.

c) Demonstrate wavelength tunable Q-switched EDFRL based on Bi_2Te_3–PVAthin film and ultra-thin film SA in 1.5-µm region.

d) Demonstrate mode-locked EDFRL based on Bi_2Te_3–PVAultra-thin film in 1.5-µm region.

1.3. THESIS OVERVIEW

This thesis contains a comprehensive study to generate two types of pulsed fiber lasers: Q-switched EDFRLs and mode-locked EDFRLs. The thesis is divided into six chapters as follow:

Chapter 1 outlines on the background, motivation and the objectives of the study.

Chapter 2 presents literature review and discussion of the fundamental background on passively Q-switched and mode-locked pulsed fiber lasers based on passive SAs. Specifically, a comprehensive theoretical background has been presented.

Chapter 3 proposes and demonstrates a new method to convert thin film SAs to ultra-thin film SA devices which based on sandwiching a Bi_2Te_3-PVA thin film between two connector ferrules and fastened them very well after adding an index matching gel (IMG) with a few drops from Ethanol Alcohol. Ultra-thin film SA has shown a better switching performance as a passive nonlinear optical modulator within an EDFRL cavity. By inserting a thin film and ultra-thin film Bi_2Te_3-SA device to the EDFRL cavity, passively Q-switched and mode-locked laser operations were achieved.

Chapter 4 demonstrates Q-switched EDFRL at a constant wavelength and wavelength-tunable operation in both C band and L band based on the thin film and ultra-thin film Bi_2Te_3-PVA SA. Q-switching performance of EDFRLs for both SA types are obtained regarding pulse width, pulse repetition rate, pulse amplitude, optical output power and pulse shape for varying pumping powers provided in the EDFA.

Chapter 5 demonstrates mode-locked EDFRL operation based on the ultra-thin film Bi_2Te_3-PVA SA. By adding different lengths of standard single mode fibers (SMF-28) within the Q-switched EDFRL cavity, mode-locked operation was achieved. The mode-locked performance of EDFRLs for both SA types are measured regarding pulse width, pulse repetition rate, pulse amplitude, optical output power and pulse shape for varying pumping powers provided in the EDFA.

Chapter 6 summarizes significant research findings in the thesis and presents future works.

CHAPTER TWO

LITERATURE REVIEW

2.1. INTRODUCTION

Optical fiber lasers have witnessed a great development due to their use in various scientific fields of research and various industrial applications. High power continuous wave laser is used for many applications such as cutting, welding and additive manufacturing; While Q-switched lasers are used in embossing and engraving processes as well as in telecommunication and optical sensor systems. As for lasers with short pulses of nanoseconds, picoseconds and femtoseconds with high frequencies of the MHz class, they are used in more precise applications such as engraving and decoration on the surfaces of reflective materials, as well as in nonlinear wavelength conversion applications, as pulsed laser pumps.

Passive-based fiber lasers dominate the scientific and industrial fields where the low-power output pulses are amplified to the required power levels by passing them through several stages of optical amplifiers.

A literature review is presented in this chapter on varied topics of fiber lasers such as pulsed fiber lasers types, operation principle and generation of passive pulsed fiber lasers was discussed. In terms of the saturable absorber (SA) importance in the passively pulsed fiber lasers, the principle of SA operation and its function as a nonlinear modulator of the laser cavity losses to produced pulsed laser was explained. The propagation of light within the laser cavity induces self-amplitude modulation. A four-level electronic model system is used to describe the working principle of a saturable absorber. The optical pulse transmits within the optical fibers affected by two events, namely, group velocity dispersion (GVD) and self-phase modulation (SPM) which contributes to form a solid and robust laser pulse shape. The generic parameters of the pulsed fiber laser are also explained.

The material of SA used in this thesis is based on the topological insulator (TI), Bismuth Telluride (Bi_2Te_3), which was used in different methods. This material is also briefly explained in chapter3 of this thesis.

2.2. APPLICATIONS OF PULSED FIBER LASERS

Through the second half of the last century, fiber laser Technologies have advanced and witnessed a great development due to their importance in many fields such as industrial, optical communications, sensing and research applications. Fiber lasers are classified into two types: continuous (CW) wave and pulsed fiber lasers. In CW, laser light is generated with a constant power output during the entire operation process, the phase and intensity of the light varying continuously. In pulsed laser, it is generated in a form of light pulses. These pulses are characterized regarding peak power, pulse energy, pulse width, and the pulse train repetition rate (or frequency) during the laser operation (Spuhler et al., 2001).

Pulsed fiber lasers are preferred over CW fiber laser in considerable fields such industrial, telecommunications, materials processing, engineering, and remote sensing (Luo et al., 2013).

Figure 2.1: Interaction and Performance Efficiency of Three Types of Lasers with Materials

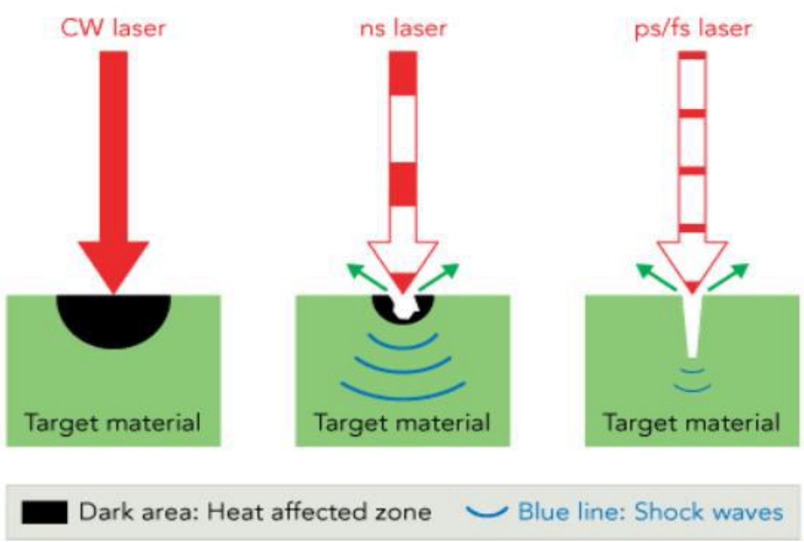

Reference: Lucas and Zhang, 2012.

CW lasers and long-pulse lasers were previously used in traditional processing methods, where the materials' ablation occurs through the ejection of molten vapor pressure and the return pressure of metal vapor. It is unstable process with compared to ultrafast pulsed lasers (ultra-short pulse and high frequency), as shown in Figure 2.1. The interaction of CW laser light with a materials shown in Figure 2.1a where the black region shows the size of the heat-affected zone (HAZ). While in a long-pulse laser light (nanosecond pulsed laser), in Figure 2.1b, the curved lines refer to the shock waves resulting from the metal's vapor, the fusion is mainly happens by expulsion of the melt by the vapor and the pressure of the rebound, and due to this the formation of the HAZ area is smaller than with use of CW laser lights. As with the ultra short pulsed laser

(Pico/femtoseconds pulsed laser) one can notice that there is no presence to the (HAZ) as shown in Figure 2.1c. Because the material evaporates away from the surface, so the outlines of punctures and cuts are precisely clean (Lucas & Zhank, 2012).

2.3. MATERIALS FOR FIBER LASERS

The materials around us are either free elements, the number of which is 118, as shown in the periodic table in Figure.2.2, or they are based on the union of two or more elements together to form new materials. The elements in a single substance are linked to each other by chemical and physical bonds. Substances differ based on their chemical composition, electronic structure, and surrounding environmental conditions to be solid, liquid, gaseous, or in the plasma state, which is the ionic state.

Based on their electronic structure, some of these materials are good conductors of electrical currents, insulators, or semiconductors, as the electrons in their outer atomic shells (conduction and covalent bands) are strongly bonded with the atom (atomic nucleus). For conductors, their conduction band electrons have the ability to interact with the electric and electromagnetic fields.

Light as an electromagnetic field, by nature, interacts with materials and makes their electrons vibrate based on the intensity of light, so materials absorb part of the light and allow the rest to pass through it. Based on the interaction of materials with light, we can classify them into opaque, transparent or semi-transparent materials.

Figure 2.2: The Periodic Table Elements, Lanthanide Elements (Marked in Black-Bordered Bracket)

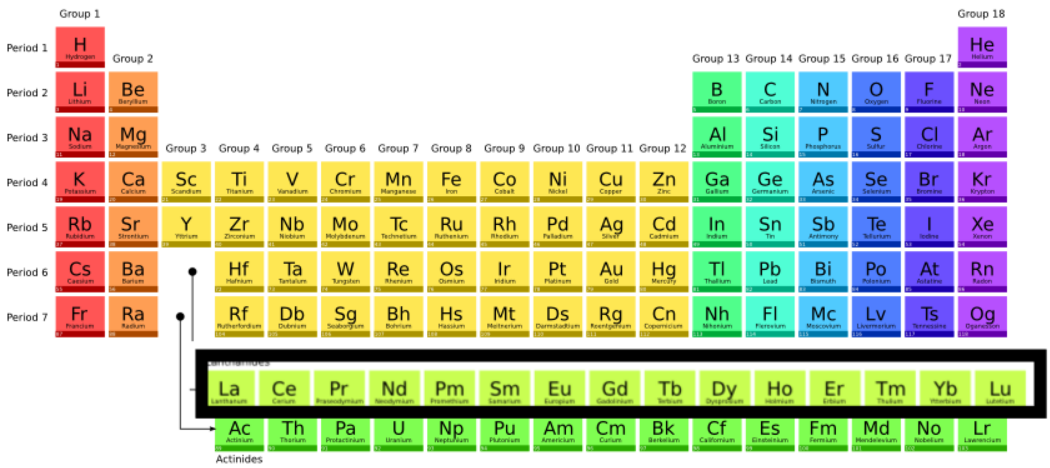

Reference: D. F. Shriver & P. W, 2010.

Materials also differ in the degree of their absorption of light based on their thickness, which means the number of atomic layers forming it. Thus, bulk materials consist of thousands or perhaps millions of atomic layers, while films consist of several atomic layers, a few layers or a monolayer. The absorption of light means energy absorption measured in the electron volt unit (eV). When materials absorbing a photon coincides with any two energy level differences an electron can liberate from the covalent band to the conduction band, and this electron remains in the conduction band for a limited period that varies from one material to another. This length of time is called the lifetime of the electron in the energy state or level. In the event that the optical field is removed away from the material, the excited electron remains in the upper energy state for a period of time, and then returns back to the lower energy state in a phenomenon called spontaneous emission, which is usually a long period of time that may reach a few seconds for some materials and less for others, thus, there are slow absorbers and fast absorbers. In the event that the optical field continues to affect the matter, the electron in the upper level will be induced by another photon corresponding to the energy difference between the energy states/levels in which the first electron settled and the lower energy level, to return to lower energy level and emit a photon identical to the excited photon in a phenomenon called stimulated emission, and coherent light is emitted, thus, lasing happens. It is possible for the electron to move between energy levels that are close to each other with irradiative emissions, whose length of time is very, very short.

The most materials absorb the optical field in a linear manner, but some of them have the ability to reduce their absorption of light with the increase of the optical field; these are called as saturable absorber (SA) materials.

In Figure 2.2, the series of elements in block F, which is called lanthanide, mainly its ions used widely as an optical gain/amplification provide medium in the construction of laser systems; this series consists of 14 elements, which starts with La and ends with Lu, have the electronic structure of $[\boldsymbol{Xe}]\ \boldsymbol{4f}^{\,\boldsymbol{0-14}}\boldsymbol{5d^{0-1}6s^{2}}$; their atomic numbers are from 57 to 71. Because its outer atomic shell contains f orbital’s, their ionization energies are very low, therefore they can lose electrons and become positive ions. It is possible to improve the properties of the gain media by adding other elements, compounds or ions to these materials as well. With regard to the subject of this thesis, the element erbium was used as doped ions in the optical fiber to use as a laser gain medium in a form of erbium-doped fiber (EDF).

For materials that have the ability to change their light absorption degree based on the incident optical field intensity, which is inversely proportional to it, they are used as smart optical intensity modulators, and are also called passive modulators, nonlinear optical materials, or saturable absorber (SA) materials.

One can predict which of the elements or compounds could be a candidate to function as a saturable absorber, through the availability of three characteristics in them:

First, the energy of the electronic band gap has to be a positive amount not exceeding 3.7 eV. Secondly, electro negativity should not exceed 4 eV. Thirdly, electrical conductivity has to be much less than $(1\mu\Omega)^{-1}$.

The first class of the materials that have all the characteristics above, are for example, carbon as graphene (Luo, Z.,Zhou, et al., 2010), black phosphorus (Li, J., Luo, et al., 2016), and rose gold (Rosol, A.H.A., et al., 2020).

The second class of the materials are the elements whose energy gap is negative and possess the other two characteristics; their oxides can be used as a saturable absorber, for example, Al_2O_3 (Al-Hayali SKM, et al., 2017), Fe_2O_3 (Peng Wang, et al., 2021). This class also includes materials which are indeterminate, such as ZnO (H. Ahmad, et al, 2016), V_2O_5 (Rizman, Z.I., et al, 2022), and lutetium oxide Lu_2O_3 (T. A. Razaq Alyasiri, et al, 2022). This is because oxygen possesses the first and second properties (energy band gap of 1.47 eV and electro negativity of 3.5 eV), but it lacks the third property (electrical conductivity).

The third class of materials that have two of these characteristics, could also be used as SAs by interaction or doping them with another element that has one or more of the three characteristics mentioned above, for example bismuth telluride Bi_2Te_3 (T. A. Razaq Alyasiri, et. al, 2022), carbon bismuth telluride composite (S. N. M. Halim, et. al, 2022), tungsten sulfide WS (Gang Zhang, et. al, 2019) and sodium carbonate Na_2CO_3 (Najm, Mustafa Mohammed et. al, 2021).

2.4. LASER CAVITY

Generally, laser cavity consists of a resonator, gain medium and pumping source as shown in Figure 2.3a which is used for CW laser. Surely there is a need of coupling elements for coupling the pump light to the gain medium and for the extraction the laser output. A Fabry Perot laser cavity resonator is based on the standing wave principle thereby the laser light bounces back and forth through the gain medium, and a small part of the laser light is allowed to escape from one of the cavity resonator mirrors. An additional element, which is called modulator, can be added to Fabry Perot cavity to modulate the intensity of light to produce pulsed laser instead of a CW one, as shown in Figure 2.3b the modulators can be active or passive elements. Active modulators are, for example, electro-optic modulators (EOM) (El-Sherif, A.F. and King, T.A., 2003), acousto-optic modulators (AOM) (Li, W., et. al, 2016). Passive modulators are optical nonlinear materials that can be used for optical intensity modulation, for example, semiconductor saturable absorber mirrors (SESAMs) (Wang, M., 2014) or bulky laser crystals, as in Figure 2.3c and Figure 2.3d, respectively.

The above discussion belongs to all solid state lasers and dye lasers cavities and these kinds of cavities need precise alignment which is one of their disadvantages.

In 1970 fiber lasers started to appear in the practical use, and from that time extensive efforts were dedicated to develop the rendering of this class of lasers. There are two famous types of fiber laser cavity structures; the first one is the linear cavity as shown in Figure 2.4a and the other is the ring cavity as shown in Figure 2.4b. Both of these structures consist of a pumping source, gain medium, wavelength division multiplexing coupler, an output splitter and a feedback loop in case of the ring cavities for the CW lasers. In pulsed fiber lasers a modulator is also exists as in both solid state and dye lasers.

Figure 2.3: a) The Simple CW Laser Cavity, b) A Simple Pulsed Laser Cavity Structure, c) A Pulsed Laser Cavity Structure Designed with Using Semiconductor Saturable Absorber Mirrors (Sesams) and d) A Simple Mod-Locked Pulsed Laser Cavity Structure

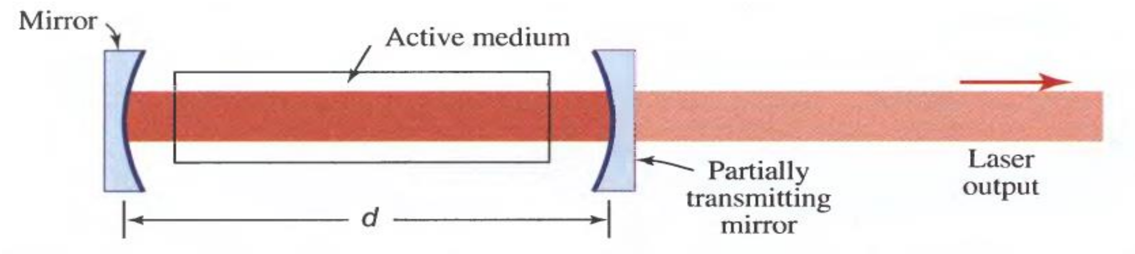

(a)

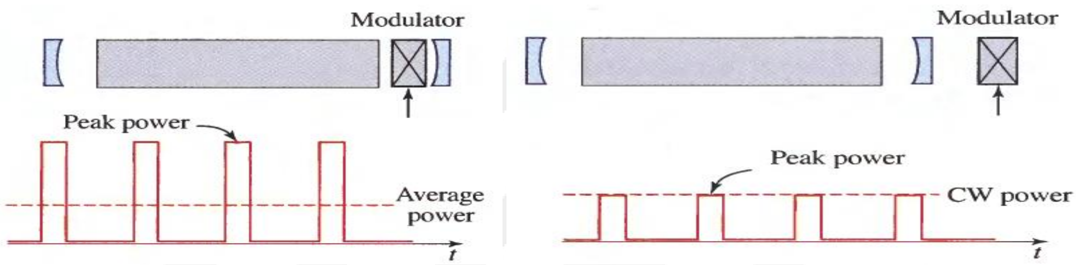

(b)

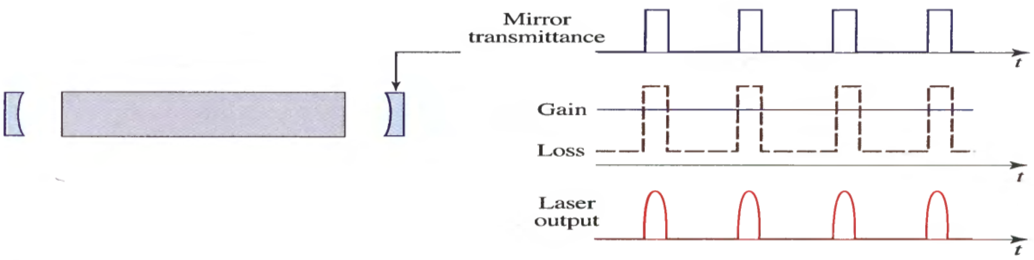

(c)

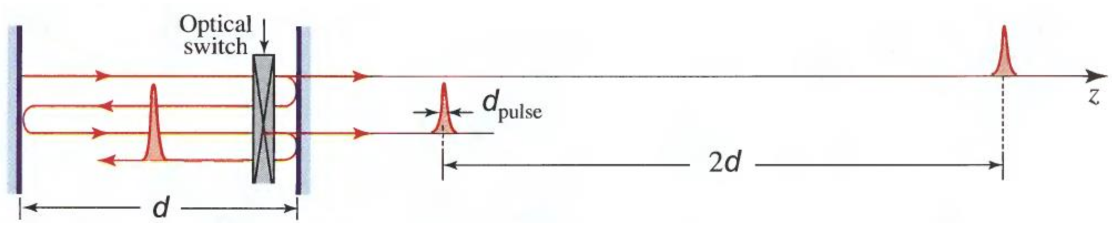

(d)

Reference: Bahaa, E., A., Saleh., Malvin, C., Teich., Richard, E., Slusher., 1991.

Figure 2.4: a) Simple Optical Fiber Linear Cavity Structure and b) Simple Optical Fiber Ring Cavity Structure

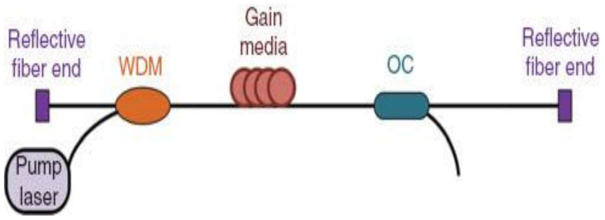

(a)

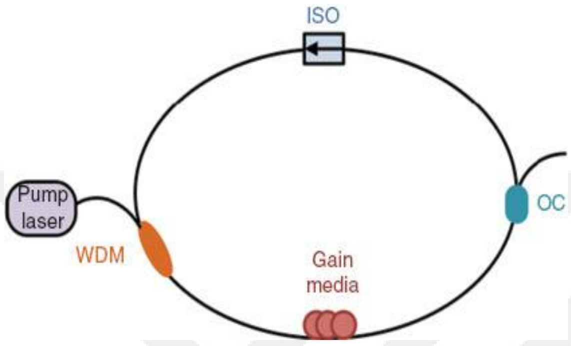

(b)

Reference: Ana M.R. Pinto & Manuel Lopez-Amo, 2013.

The active modulator in fiber laser cavity is the same as the solid state and dye lasers. On the other hand, in addition to what the solid-state and dye passive laser cavities may contain, 3D, 2D, 1D or even 0D materials can be used as a passive modulator.

The pulsed laser cavities are classified into two main types: quality-switching and phase-locking (mode-locking) lasers depending on the laser cavity dynamics.

Table 2.1: Common Rare Earth Doped Glass Fibers Ions Used in Laser Gain Medium and Characteristic Emission Wavelengths

Ion	Common host glasses	Emission wavelength
Erbium (Er3+)	silicate and phosphate glasses	1.5 – 1.6 µm, 0.55 µm
Praseodymium (Pr3+)	Silicate and phosphate glasses	1.3 µm, 0.635 µm, 0.6 µm, 0.52 µm, 0.49 µm
Thullium (Tm3+)	silicate and germinate glasses, fluoride glasses	1.7 – 2.1 µm, 1.45 – 1.53 µm, 0.48 µm, 0.8 µm
Neodymium (Nd3+)	silicate and phosphate glasses	1.03 – 1.1 µm, 0.9 – 0.95 µm, 1.32 – 1.35 µm
Ytterbium (Yb3+)	silicate glasses	1.0 – 1.1 µm
Holmium (Ho3+)	silicate glasses, fluoro-zirconate glasses	2.1 µm, 2.9 µm

Reference: Rudiger Paschotta, 2004b.

Different materials have been dedicated to use as light gain medium in the cavity as well as for amplification purposes to increase the optical signal level as it suffers losses during the transmission over long distances.

For fiber lasers, erbium, ytterbium, thallium, and holmium ions, for example, are usually used as dopants in doped fibers, due to the low ionization energy and having many laser levels, wide operational wavelengths as shown in Table 2.1. Actually, for fiber lasers the gain medium is nothing but a wavelength transformer and pulse shaper, which is because gain medium plays a big role in pulse shaping.

For this thesis 6 meter of erbium doped (EDF) fiber, which has absorption of 30 dB at 1530 nm operation wavelength and 23 dB at pump wavelength of 980 nm was used.

Many schematics are used to explain the energy levels and manifolds of gain media in laser pumping, two levels, three levels, quasi three levels and four levels. Solid-state lasers like spheres are three level lasers so it needs higher pump powers than in EDF where quasi three levels is used, as in Figure 2.5.

Figure 2.5: Gain Media Modeling for, a) Three Level Laser System and b) Four-Level Laser System. In Quasi Three Level Laser Gain Media Modeling System G and L Are Close to Each Other and The Transition Between Them Is Irradiative

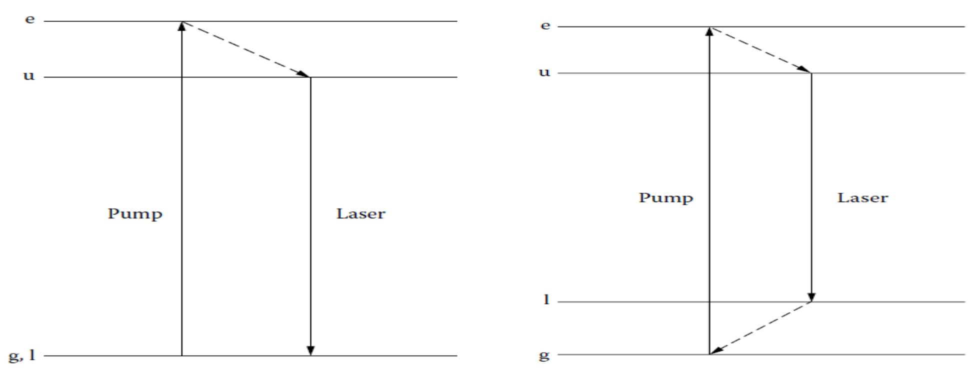

(a) (b)

Reference: Sennaroglu et al., 2007.

2.5. SATURABLE ABSORBER

As explained above, the term saturable absorber (SA) is used to describe the optical nonlinear materials (NLMs), whose absorption is inversely proportional with the intensity of light and this property is described by the term of modulation depth. Figure.2.7 contains the SA material optical properties. (Luo, Z., et. al, 2010), carbon nanotubes (CNTs) (Kasim, N., Al-Masoodi,et. al, 2014), black phosphorus (Li, J., Luo, et. al, 2016), transition materials dichalgogenides (Chen, B., et. al, 2015), and topological insulators (TIs) (Yu, Z., Song, et. al, 2014) have been used as SA materials in fiber laser cavities. Figure 2.6 shows the schematic representation of four-band saturable absorber energy levels' modeling system.

Figure 2.6: Four-Band Saturable Absorber Representation

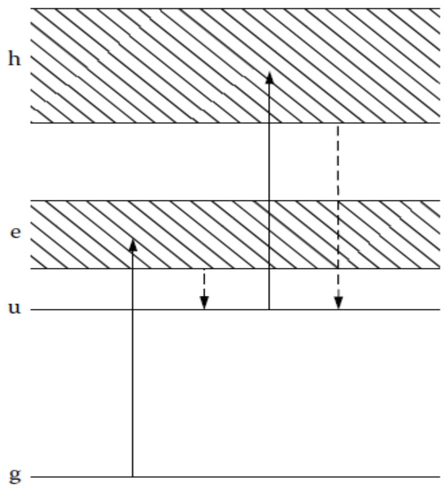

Reference: Sennaroglu et. al, 2007.

In Figure 2.7 shows the linear transmission spectrum and nonlinear transmission variation of Bi_2Te_3-PVA SA thin film that used in EDFRL experiments. The SA material used in this thesis is discussed briefly in Chapter 3.

The SA saturation intensity at the pumping wavelength center can be defined as,

$$I_{p,SA,sat} = \frac{hv_p}{\tau_{SA}\sigma_{SA,g,p}} \tag{2.1}$$

where h = 6.626 * $10^{-34}$$m^2$.kg/s , v_p is the central optical frequency belongs to the pump light, $\sigma_{SA,g,p}$ is the cross section of the ground-state of theSAat the pump wavelength center, and τ_{SA} is the SA response time.

Figure 2.7: The Characteristics of Bi_2Te_3 SA Film as, a) the Linear Transmission and b) Nonlinear Transmission

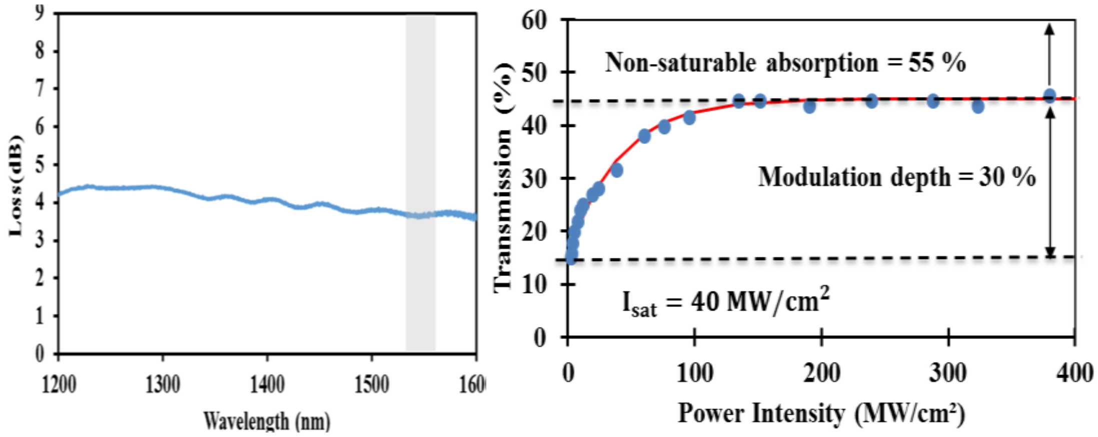

(a) (b)

2.6. ERBIUM DOPED FIBER CONTINUOUS WAVE (CW) AND PULSED RING LASERS

Ring cavity fiber lasers are always used to achieve unidirectional laser beam operation, that for their intrinsic advantages that are represented by having outstanding lasing adequacy and able to suppress the back scattering. Figure2.4bshows the simplest conventional structure for ring laser consists a pair of ports (optical coupler) joined simultaneously to shape the ring cavity and an optical isolator (ISO) to provide unidirectional light operation.

In this thesis, description of the ring fiber lasers using EDF as gain media and SA to produce two types of pulsed laser is discussed.

2.7. Q-SWITCHING AND ITS IMPORTANT PARAMETERS

Q-switching means switching the laser resonator quality between high quality and low quality. High quality is obtained when cavity losses are low and low quality is obtained when losses are high. When the laser output is off, the energy of the cavity is being saved at the cavity gain medium and this energy will be used to create short pulse duration with high energy between the times that the cavity quality factor changes from high to low.

As a result of the continuous pumping provided by the laser pump to the laser gain medium, there is a process of transferring electrons from the ground level to the upper levels. With the continuation of the pumping process and the arrival of the ions in the upper energy level to their lifetime, they return back by the spontaneous emission process, and this successive process provides an abundance of energy accumulated in the laser cavity, specifically in the gain medium. The gain builds up process supported with the stimulated emission due to the continuous pumping process. And whether the used modulator is active or passive (saturable absorber), when the accumulated energy in the gain reaches the limit that is above the losses of the laser cavity, the first laser pulse starts to form. At the same time photons number in the gain decreases as an outcome of extraction photons through the laser through the output coupler as an optical pulse. The process of extraction the energy from the cavity continues to a short time after the gain becomes under the laser cavity low level losses. Again the process of building the gain starts to provide the next laser pulse (Bahaa, E., A., Saleh., Malvin, C., Teich., Richard, E., Slusher., 1991).

Figure 2.8: Q-Switched Fiber Laser Pulse Formation

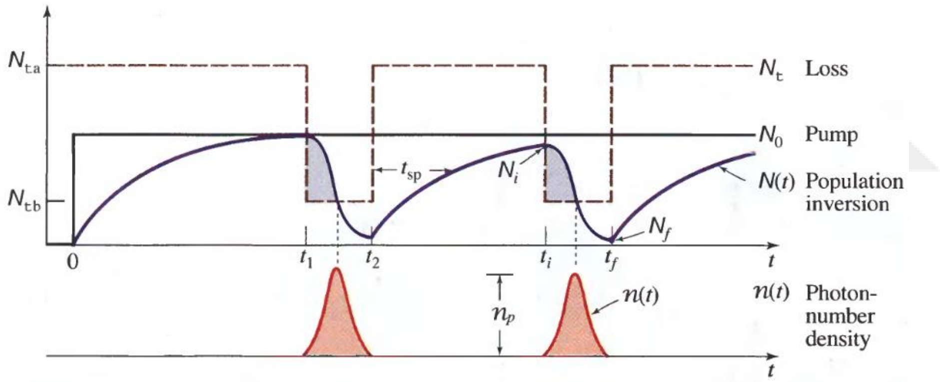

Reference: Bahaa, E., A., Saleh., Malvin, C., Teich., Richard, E., Slusher., 1991.

To determine the pulse width and frequency, energy the following set of equations is used:

$$\mathrm{N}_0 = W_\mathrm{p}\mathrm{N}_\mathrm{g} \tag{2.2}$$

Where W_p is the pump photon number and N_g is the ground state photon number. The stored energy in the gain medium of Q-switching laser is;

$$E_{stored} = \sigma_{ra,g} \,.\, L_g \,.\, N_0 \,.\, h.\, v_p \tag{2.3}$$

Where $N_u$the photon numbers at the upper level is, $hv_p$is the photon energy at the pumping wavelength, $\sigma_{ra,g}$ radiative cross-section area and L_g gain medium optical length at the pumping wavelength.

Pulse width of a Q-switched laser is inversely proportional to the pumping power while repetition rate is directly proportional.

The minimum attainable pulse width is;

$$t_w = \frac{S_p t_{rt}}{\gamma_s} \left[\frac{R(1+R)\eta_{eff}}{R-\ln(1+R)}\right] \tag{2.4}$$

where $S_p$is the pulse shape factor and approximately equal to 0.88, $t_{rt}$is the laser cavity round trip time, $\eta_{eff}$is the laser energy extraction efficiency, γ_s is the saturable loss of the saturable absorber and $R = \gamma_s/(\gamma_{rt,p} + \gamma_0)$ is the saturable to unsaturable laser cavity losses rate. For ultra thin SA films, for instance, the one made with my new fabrication method, discussed in chapter 3 from this thesis, $\gamma_s \ll (\gamma_{rt,p} + \gamma_0)$, equation 2.4 then will be reduced to;

$$t_{w,min} = 4\,\frac{S_p t_{rt}}{\gamma_s} \tag{2.5}$$

Here $\gamma_0 = -\ln(1 - T_0)$ and T_0 is the output coupler extraction ratio. $\gamma_{rt,p}$ are the parasitic loses.

The pulse width of a Q-switched laser is proportional to the laser cavity length, which is mean the time taken in one round-trip, and inversely proportional to the laser cavity saturable losses. The passively Q-switched pulse train repetition ratio is proportional with cavity spontaneous time and can be represented approximately by,

$$R_r = \tau_{spont} \ln\left[\frac{P_a - P_i - (P_{th} - P_i)\frac{N_f}{N_i}}{P_a - P_{th}}\right] \tag{2.6}$$

where τ_{spont} is the cavity spontaneous time, P_a is the total power of the pumping light consumed within the lasing mode size, P_i is the consumed power of pumping light that is required to arrive effective inversion (Neff = 0), P_{th} is the power of the pump light consumed to obtain $N_{eff} = N_i$, N_f the photon final number after the peak of the pulse is being formed, the cavity photon inversion at the time the pulse is being formed is $N_{p,0} = (\gamma_s + \gamma_{rt,p} + \gamma_0)A_g/\sigma_g$ and A_g is the laser mode area in the gain.

The output energy of the pulse can be theoretically calculated;

$$E_{pulse} = S_p \sigma_{ra,g} . L_g . N_{p,0} . h. v_p (1 - \gamma_{rt,t}) T_0 \quad (2.7)$$

Experimentally, the average output Q-switched laser power is measured directly by using an optical power meter and the pulse energy, therefore will be,

$$E_{pulse} = P_{\mathrm{out}} / R_{\mathrm{r}} \quad (2.8)$$

The pulse peak power will be,

$$P_{pp} = S_p E_{pulse} / t_w \quad (2.9)$$

2.8. PULSE PROPAGATION IN OPTICAL FIBERS

Optical fibers can be defending as a cylindrical, thin optical waveguide which can be bent to some degree typically contain two main parts: a core at the center and cladding around the core. It is characterized by the ability to transmit a light due to its structure, where the inner part, core, refractive index is larger than that of the outer part, cladding. Light can transmits in the fiber when inside in appropriate angle that enables the process of complete internal reflection, which can be explain through the modal theory (Y. Jiang et al., 2010). Light, as an optical pulse, propagation in an optical fiber governed by Maxwell equations, given that light is an electromagnetic wave (Agrawal, 2013). Pulse propagation in a linear regime of optical fiber, makes the pulse suffering from time dispersion effect that give rise to broadening of the pulse and therefore may overlap with other neighboring pulses. Such overlap lead to degrade the transmission link capacity (i.e bandwidth).

Propagation of a pulse in a nonlinear regime, Nonlinear Dispersive Regime (NLDR), of optical fiber is influenced by the optical Kerr effect accompanied by SPM and GVD (Agrawal, 2013).

In an anomalous dispersion regime, the contrary effects of the SPM and GVD may allow a very interesting phenomenon, called soliton pulse propagation, causing the propagation of pulses without any changes in the pulse shape over propagation in the fiber.

In the next subsections, dispersion, the Kerr effect, SPM, and soliton generation are discussed.

2.8.1. Chromatic Dispersion (CD)

The phenomenon of splitting visible light into its component colors, for the visible range, is called dispersion. The same thing happens with the other light ranges like infrared. Dispersion of light is caused by the change of speed of the light component's wavelength by a different amount for each. The phenomenon of light propagation at phase velocity and envelope velocity through a transparent that counts on the frequency of the light transmitted in it is called chromatic dispersion of matter/material.

The attribute "chromatic," Figure.2.9, is used to distinguish it from the other classes that are pertinent especially for optical fibers:

The speed of light inside materials is different than in vacuum and can be described by the material refractive index$n$:

$$v_m = \frac{c}{n} \tag{2.10}$$

Material chromatic dispersion is,

$$D_m(\lambda) = \frac{\lambda}{n}\frac{d^2 n}{d\lambda^2} \tag{2.11}$$

The dispersion due to the waveguide, which is an optical fiber characterized by the waveguide dispersion depending on the fiber structure:

$$D_w(\lambda) = -\frac{n_1(\lambda)\Delta}{c\lambda} V \frac{d^2(Vb)}{dV^2} \tag{2.12}$$

where, $n_1(\lambda)$ is the fiber corerefractive index, Δ is the difference between ther efractive indices, b is the normalized propagation constant and V is the normalized frequency.

The optical fiber dispersion is the union of the two dispersion kinds, and is equal to,

$$\mathrm{D}(\lambda) = D_m(\lambda) + D_w(\lambda) \tag{2.13}$$

By using Taylor series to expand the wave number k, which is a function of the angular frequency ω_0, around some center frequency ω_0, (R. Paschotta, 2008), to get the following terms,

$$k(\omega) = \sum_{n=0}^{\infty} \frac{k^{(n)}(\omega_0)}{n!} (\omega - \omega_0)^n \tag{2.14}$$

where $n!$ is the factorial of n, $k^{(n)}$ is the $n'th$ derivative of k evaluated at point ω_0

At n= 0, the equation equal to k_0, which is a common phase shift.

At n= 1, the term $\partial k/\partial\omega$, gives the group delay,

$$k' \equiv \frac{\partial k}{\partial\omega} = \frac{1}{v_g} \tag{2.15}$$

At n= 2, get the GDD (or GVD),

Figure 2.9: a) Fundamentals of Chromatic Dispersion, b) Two Contributors to Chromatic Dispersion: Material and Waveguide

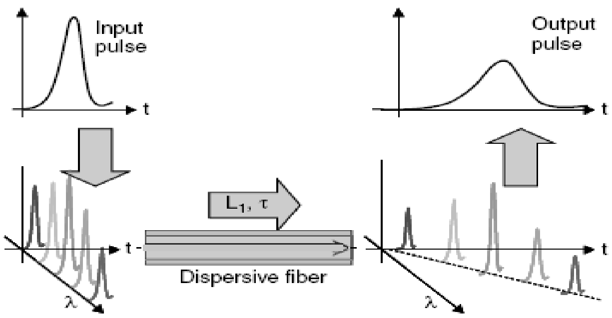

(a)

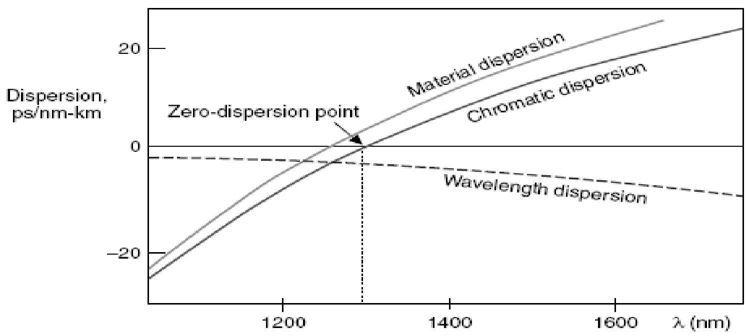

(b)

Reference: Stamatios V. Kartalopoulos, 2004.

$$k'' \equiv \frac{\partial^2 k}{\partial\omega^2} = \frac{\partial}{\partial\omega}\left(\frac{1}{v_g}\right) \tag{2.16}$$

At n= 3, gets the third order dispersion (TOD),

$$k''' \equiv \frac{\partial^3 k}{\partial\omega^3} \tag{2.17}$$

The second-order dispersion measured in units of second^2/meter, for instant, +36 fs^2/mm is the GDD/GVD of silica at wavelength of 0.8 µm, and −22 fs^2/mm at wavelength of 1.5 µm. While the zero dispersion of it is at 1.27 µm.

Phase constant (β), is a mode and frequency-dependent quantity, which is generally used instead of the wave number k to describe the light propagation in optical fibers.

Therefore, Equation 2.14, became

$$\beta(\omega) = \frac{n(\omega)\omega}{c} = \beta_0 + \beta_1(\omega - \omega_0) + \frac{1}{2}\beta_2(\omega - \omega_0)^2 + \ \ldots \qquad (2.18)$$

The pulse envelope speed is therefore ($vg = 1/\beta_1$), $\beta_2$is referred to GVD and accounts for the dispersion parameter D, by

$$\beta_2 = -\frac{\lambda^2 D}{2\pi c} \qquad (2.19)$$

2.8.2. Normal and Anomalous Dispersion Regimes

There are three regimes of dispersion, normal dispersion (positive dispersion when, $\beta_2 > 0$), anomalous dispersion (negative dispersion $\beta_2 < 0$) and zero dispersion.

The dispersion can be also related to the dispersion parameter β_2, with opposite sign,

$$D_\lambda = -\frac{2\,\pi\,c}{\lambda^2} \cdot \frac{\partial^2 k}{\partial \omega^2} \quad or = -\frac{2\,\pi\,c}{\lambda^2} \cdot \beta_2 \qquad (2.20)$$

The dispersion is accounted in (ps^2.nm^{-1}.km^{-1}).

The combination of SPM and D effects leads in the positive direction for shaping the optical pulse to be a soliton, where the pulse can propagate without distortion through the fiber.

In this thesis to calculate the total cavity dispersion and GVD, the formula below is used:

$$D_{cavity,total} = \sum_{x=1}^{last\ element} \frac{length\ of\ the\ element\ x(\ meter\ )}{1000} \cdot D_{element\ x} \qquad (2.21)$$

and cavity total group velocity dispersion is,

$$GVD_{total} = -\frac{\lambda^2{}_{(\ nm\ )} D_{cavity,total}}{2\pi c} \qquad (2.22)$$

where, the GVD is measured in the unit of $ps^2.km^{-1}$.

2.8.3. Effects of Chromatic Dispersion On Pulse Propagation

Chromatic dispersion is a sensitive concept that influence the light propagation in a pulse form, that the pulse has a limited spectral range, therefore dispersion can bring changes in the phase account to the pulse frequencies. Therefore the pulse frequency harmonics transmits with speeds. Pulse transmission through a waveguide with normal dispersion, results to a positive chirp due to slowing the speed of the envelope of higher frequency harmonics, unlike the one with anomalous dispersion which leads to negative chirps.

If an ultra-short light pulses with complex amplitudes (A) propagate through a dispersive ambient, the following change in amplitudes describes with,

$$\frac{\partial}{\partial z} A(z,\omega) = -i\,\beta(\omega)A(z,\omega) = i\left(\frac{\beta_2}{2}\,\Delta\omega^2 + \frac{\beta_3}{6}\,\Delta\omega^3 + \ \ldots\right) A(z,\omega) \tag{2.23}$$

The changing elements are replaced derivatives in the time domain:

$$\frac{\partial}{\partial z} A(z,t) = \sum_{n=1}^{\infty}(-1)^{(n+1)}\ \frac{\beta_n}{n!}\frac{\partial^n A}{\partial t^n} = \left(-i\ \frac{\beta_2}{2}\frac{\partial^2}{\partial t^2} + \ \frac{\beta_3}{6}\frac{\partial^3}{\partial t^3} + ..\right)A(z,t) \tag{2.24}$$

Originally unchirped optical pulse width will take a rise when pass through a dispersive ambient namely (*dispersive pulse broadening*). Initially unchirped Gaussian pulse has duration τ_0, will acquaintances with just second-order component of dispersion, the resulting pulse width is take a rise in a manner of

$$\tau = \ \tau_0\sqrt{1 + \left(\ 4\ ln2\,\frac{GVD}{\tau_0^2}\right)^2} \ \ \approx 4\ ln2\,\frac{GVD}{\tau_0^2} \tag{2.25}$$

This approximation is valid for GVD >> τ_0^2.

2.9. SOLITON PULSE GENERATION IN EDFRL

The combined of Kerr Nonlinearity with the dispersion can give enhancement to the formation of solitons. These combinations can leads to generate exceedingly short optical pulses with special mode-locking laser effect namely, *Soliton-Mode-locked* laser. Such a kind of laser requires very precise dispersion management over a wide wavelength range.

2.9.1. Nonlinear Kerr Effect

The changes in the refractive indices arising from electric field influences are proportionate with the square of its strength. It occurs when light propagates in glasses, crystals, and other media such as gases.

There are two sorts of Kerr effect:

The first sort is Kerr Electro-Optic-Effect (DC Kerr Effect), which happens when a slowly varying electric field (electrodes) utilized to a medium, for example, a piece of glass, can then experience a polarization-dependent change.

The phase change is

$$\Delta\varphi = \frac{2\pi}{\lambda}\Delta n = 2\pi K E^2 \quad (2.26)$$

where Δn is the difference in refractive indices between two polarization directions, K is a constant belongs to the material, L is the path length, and E is the utilized voltage strength.

The second, type is AC Kerr Effect, which happenes in account to the intensity of electric field of the incident light itself. The instantaneously change in the nonlinear response, can be described by,

$$\Delta n = n_{nl} I \quad (2.27)$$

where n_{nl}, is the nonlinear refractive index and I, is intensity of the field.

Z-scan is the technique in which $\chi^{(3)}$measured with. $\chi^{(3)}$is the third order term of the susceptibility, which is the main parameter in which the medium nonlinear refractive index n_{nl} value can be calculated. The nonlinearity index is measured in the unit of cm^2/W. For fused silica it is equal to 2.7×10^{-16} cm^2/W at 1.5 μm wavelength.

The refractive index change with time and frequency-dependency leads to SPM, Kerr lensing, as well as to cross-phase modulation (CPM).

2.9.2. Self-Phase Modulation (SPM) And Four Wave Mixing (FWM)

Due to Kerr effect, materials suffer changes in the refractive index as in Equation 2.27, proportional with the light intensity. Kerr effect of a medium causes phase shift with time dependency according to the time dependency of the transmitted light pulse intensity.

The temporal dependence of the phase shift of the nonlinear delay in the phase derives furthermore, the linear phase delay, as shown in Figure.2.11, which is explain the SPM.

When an originally unchirped pulse of light transmits through a media, it acquires chirp.

The alteration happens to a beam of light consist of Gaussian pulse, has beam diameter $2w_b$ in uniform medium of length L is described by

$$\gamma_{SPM} = (\frac{2\pi}{\lambda} n_{nl}\, L) / (\frac{\pi}{2} w_b^2) = \frac{4\, n_{nl}\, L}{\lambda\, w_b^2} \tag{2.28}$$

Figure 2.10: Self-Plase Modulation for Originally Unchirped Gaussian Pulse

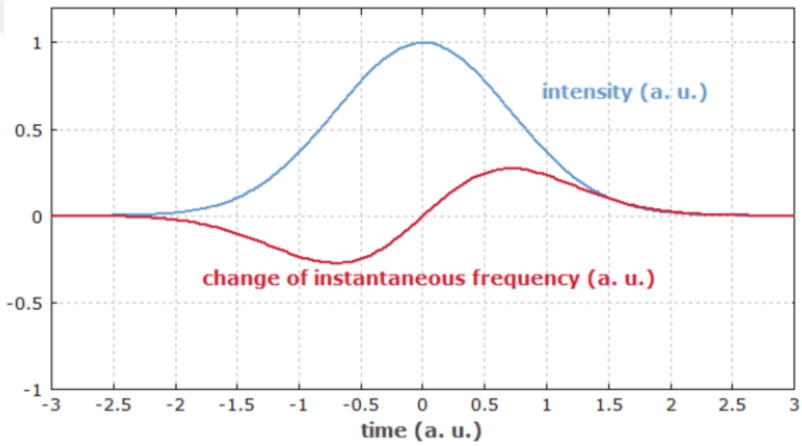

Reference: RP photonic, 2015.

When more than one optical frequency harmonics transmit simultaneously through a nonlinear medium like a fiber, a nonlinear effect due to the third-order optical nonlinearity $a_{\chi}^{(3)}$, causes Four-wave mixing.

Considering at least two frequency components ν1 and ν2 (with ν2 > ν1), another two additional frequency components, due to the refractive index modulation occurs at the difference frequency, as shown in Figure 2.11.

Two new frequency components are generated:

$$\left.\begin{aligned} &\nu_3 = \nu_1 - (\nu_2 - \nu_1) = 2\,\nu_1 - \nu_2 \\ &and \\ &\nu_4 = \nu_2 + (\nu_2 - \nu_1) = 2\,\nu_2 - \nu_1 \end{aligned}\right\} \tag{2.29}$$

As shown in Figure.2.13. (Alternatively,

$$\left.\begin{aligned} \nu_5 &= \nu_1 + (\nu_2 + \nu_1) = 2\nu_1 + \nu_2 \\ &and \\ \nu_6 &= \nu_2 + (\nu_2 + \nu_1) = \nu_1 + 2\nu_2 \end{aligned}\right\} \quad (2.30)$$

because phase matching can be difficult it is unlike to obtain, this situation.

Figure 2.11: Four-Wave Mixing For Harmonics Frequency Generation

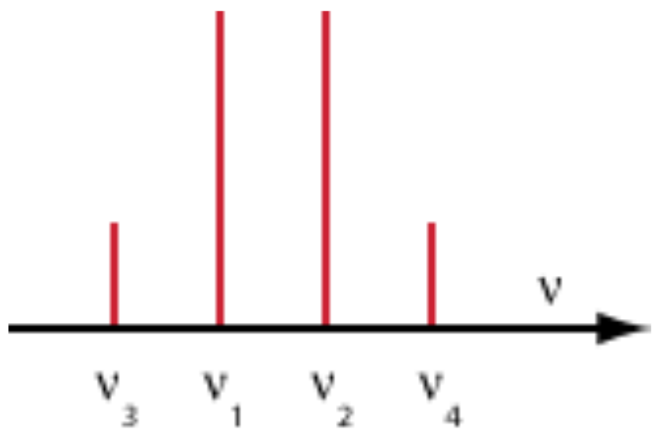

Reference: RP photonic, 2008.

2.10. MODE-LOCKING IN FIBER LASERS AND ITS IMPORTANT PARAMETERS

It is the second method for short pulses generation. With this method shorter pulse with less fluctuation with comparison with the Q-switching technique, pulse period range in between nanoseconds (10^{-9} s) to (10^{-15} s) femtoseconds. When all of the longitudinal oscillating modes in the cavity own a constant phase relation, extremely short pulses can be introduced. The higher in phase mode number the shortest the pulse can be. The laser cavity length can be a sensitive parameter not only with the laser repetition rate only, but also on the period of the pulse. The shorter the cavity the higher the repetition pulse rate and duration could be. The fixed phase relation is the cause of the name “mode-locking” or “phase-locking”. The constant phase overlap of all the modes bouncing in the cavity leads to convent the CW light into a pulse train. Numbers of longitudinal modes that can laser at the same time are relay on the gain-losses band width B and the separation frequency ν_F between modes, as in Figure 2.13.

Figure 2.12: Mode-Locked Operation Principle

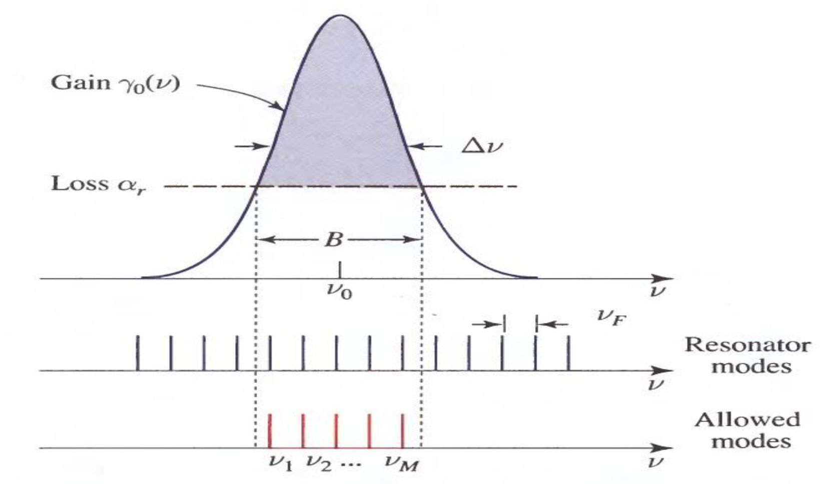

Reference: Bahaa, E., A., Saleh., Malvin, C., Teich., Richard, E., Slusher., 1991.

There are two sorts of mode-locking techniques:

The active modulator in active mode-locking, like acousto-optic modulator or any other mean is used. A passive modulator, like a semiconductor mirror or optical nonlinear material that called a saturable absorber is required for passive mode-locking. Over the last several years many solid-state and fiber lasers have been used but recently, fiber lasers are more preferred for their advantages over the solid-state lasers, that there is no need for the alignment, small size and no need for an additional source to cool the laser cavity (all fiber).

The maximum attainable number of oscillating modes, M in the cavity under sufficient laser pumping, is

$$M = \frac{\Delta v}{c/L_{optic}} = \frac{L_{optic}}{c}\Delta v \tag{2.31}$$

where c is equal to 3×10^8 m/s and $(L_{optic} = n.L)$ is the optical length of a linear cavity, L is the linear cavity physical length and Δv is the frequency difference of the gain width at full width half maximum (FWHM). The shortest attainable pulse period with given gain line width (Peter et. al., 2010) is

$$\tau_{min} = \frac{L_{optic}}{cM} = \frac{1}{\Delta v} \tag{2.32}$$

Figure 2.13: Dynamics of Passive Mode-Locking with Slow Saturable Absorber

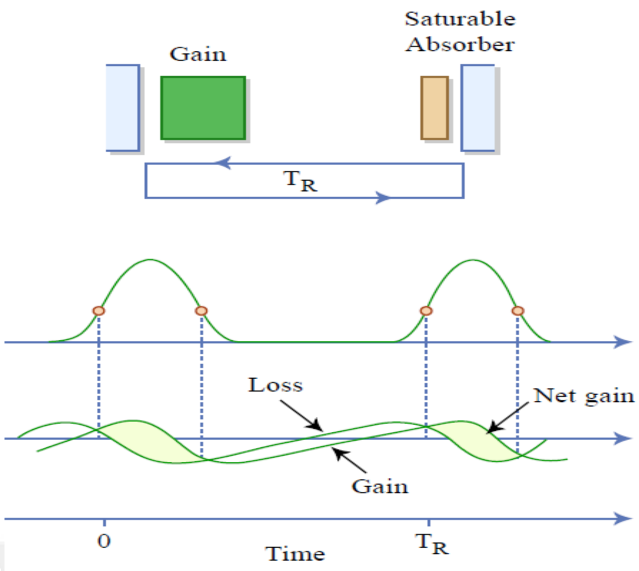

Reference: by MIT OCW, 2006.

Figure 2.13, shows the dynamic of passively mode-locked laser produces the equidistant train of pulses, where T_R the repetition time indicates the frequency of the train while pulse period is referred by τ_w.

As in Figure 2.12, phase-locked frequency's comb can be obtained with fixed mode separation, ν_F that equals $1/T_R$. The period of the pulse, τ_w, is inversely proportionate to the spectral width at FWHM, 3dB gain level $\Delta\nu$.

The pulse train repetition rate can be calculated as,

$$R.r = \frac{c}{L_{optic}} \tag{2.33}$$

and therefore the round-trip time, *is*

$$T_R = \frac{L_{optic}}{c} \tag{2.34}$$

CHAPTER THREE

BIZMUTH TELLURIDE (Bi_2Te_3) BASED SATURABLE ABSORBER

3.1. INTRODUCTION

Bismuth telluride is one of a group of materials called Topological insulators (TIs). To understand this kind of materials and why they are used as saturable absorbers (SAs), one need to know some important concepts and terms as explained bellow:

1. Phase transition is defined as the sudden change occurs in a system over a small range in a control variable (BRENT FULTZ, 2014). It occurs in different materials, such as vanadium oxides, ferroelectrics, and other dielectric materials. These materials can present noticeable changes in their electrical characteristics triggered by metaphysics fields, electric field, including temperature, stress, and light (such as laser).

2. Symmetry breaking: expresses a phenomenon in which infinitesimally small fluctuations act on a system going through a critical point that determines the fate of the system, by deciding which branch of the bifurcation is to be taken. To an outside observer unaware of volatility (or "noise"), the selection will appear random. This process is called "breaking" of symmetry, because such transformations usually move the system from a symmetric but disorganized state to one or more specific states.

This phenomenon is part of most theories of everything (Fran De Aquino, 1999). Symmetry breaking is believed to play a major role in pattern formation. Even if reductionism is true, it's opposite, construction, the idea that scientists can easily predict complex phenomena by looking at theories describing their components, is not (P.W.Anderson, 1972).

Symmetry breaking can be distinguished into two types, explicit symmetry breaking (Castellani, E., 2003, Sinha & Amaratunga, 2016) and spontaneous symmetry breaking (Miransky, Vladimir A., 1993), and is characterized by whether the equations of motion are not constant or the base case fails to be constant.

3. Pauli effect is a remarkable physical phenomenon that supposed tendency of technical equipment to encounter critical failure in the presence of certain people.

Pauli interviewed Hans Bender and Carl Jung and saw the effect as an example of the concept of synchronicity (A.I. Miller, 2009; R. Moss, 2009).

4. Fermi-Dirac distribution: is defined as a probability density functions used to depict the probability with which a specific particle can occupy a specific energy level.

5. Fermi level, it measures the energy of the least bond electrons within a solid material. It is important factor in determining the thermal, electrical and optical features of solid materials (J.-L. Bredas, 2014).

6. Dirac cones: is a property of the surface states or 2D-materials, depending on a linear dispersion relation between the two components k_x and k_y of the crystal momentum and energy (Jinying Wang, et al., 2015).

Also are known as the phenomenon that uses to describe unusual electron transport in some kind of materials in its some electronic band structures. These materials are like topological insulators and graphene. (Novoselov, K.S. & Geim, A.K., 2007, Hasan, M.Z. & Kane, C.L., 2010). At energies near the Fermi level, in these materials, the valance band (VB) and conduction band (CB) take the shape halves of a conical surface. The upper and lower halves, meet at specific points called, Dirac points.

3.2. TOPOLOGICAL INSULATORS (TIs)

Physical models of symmetry breaking were the only way to study the phase transitions in materials until a novel quantum Hall effect has been revealed. Symmetry breaking arguments could not explain the quantum Hall effect (K. Klitzing, 1986).

At the beginning there was a need to apply an extremely low temperature and external magnetic fields in order to observe Hall Effect. Many researchers have been devoted, until it crowned by discovering, the spin-Hall effect. The spin-orbit coupling effect of such heavy ions, like bismuth (Bi) and telluride (Te), induces Hall effect. The spin-orbit coupling effect can offset using an outer magnetic field for inducing spin-Hall effect (H.-J. Noh, et al., 2008).

Topological insulator (TI) is the term that refers to the materials that exhibit spin-Hall effect. HgTe quantum well is an example of 2-D materials. For three-dimensional (3D) materials Sb_2Te_3, Bi_2Se_3, and Bi_2Te_3 are three examples of TIs in their bulk states. In these materials Hall effect can be observed at room temperature. Due to this effect these materials are characterize by having gapless metallic state on their edges and surfaces, and being insulator elsewhere (M.Z. Hasan & C.L. Kane, 2010), so population inversion can be shown, as in Figure 3.1.

Figure 3.1: Band Diagram for Tis.

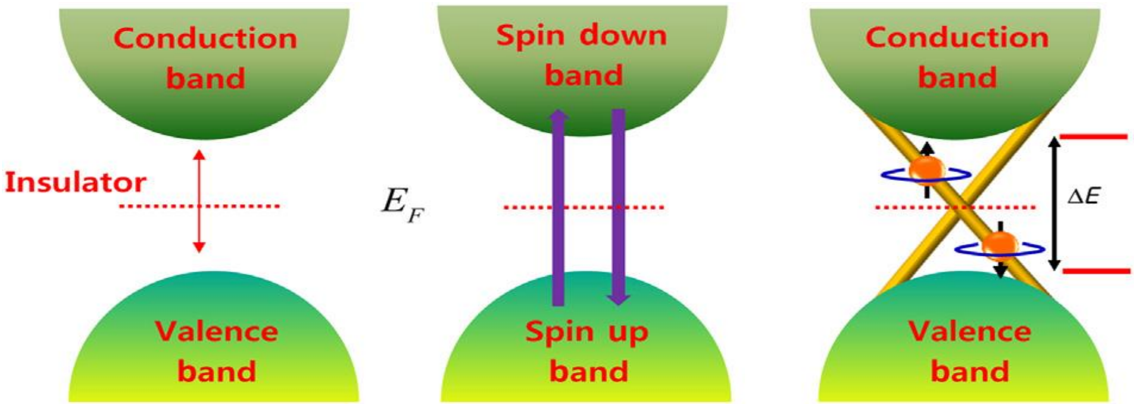

Reference: Young Min Jhon & Ju Han Lee, 2020.

Due to the larger band gap in TIs, electrons of the VB cannot pass to the CB, as shown in Figure 3.1a. But, the VB can reach the CB via strong “spin up”, while the “spin down” makes the CB arrives the VB, as in Figure 3.1b. In this way band population inversion happens as in Figure 3.1c. Therefore, electrons can pass from the VB to the CB without loss by using this path (Young Min Jhon & Ju Han Lee, 2020).

Owning to these features, TIs become target of many research Works and thereby, TIs have been widely used as base material in many fields, including, industrial applications, military, medicine, and, scientific research etc (B. Anderberg & M.L. Wolbarsht, 2013, M.D. Shirk & P.A. Molian, 1998, W.M. Steen & J. Mazumder, 2010, A. Vogel & V. Venugopalan, 2003, J. Wilson & J. Hawkes, 1987).

As explained in chapter 2, Q-switching or mode-locking technique the main methods to obtain passively pulsed fiber laser sources, which have the advantages of low price, compact and simple structure, shorter pulse duration, and reliable performance over the active counterparts (M. Brunel et al., 1999).

TIs function as a nonlinear passive optical modulator SA (J. Fleck Jr, 1970, U. Keller, 2003, M. Brunel, et al, 1999, T. Brabec, et al, 1992, J.J. Degnan, 1989, J.J. Zayhowski & C. Dill, 1994, G. Bret & F. Gires, 1964, B. Soffer, 1964) in the laser cavity in recompense the active one.

Saturable absorption is the feature of the optical nonlinear materials ONL, which is attributed to Pauli blocking effect, (J.L. Xu, et al, 2015), occurring in presence of an intense light where absorption is inversely proportional with the light intensity. Figure 3.2 shows the absorption principle in 2D layered TIs.

Figure 3.2: The Absorption Principle in 2D Layered TIs and Pauli Blocking Effect

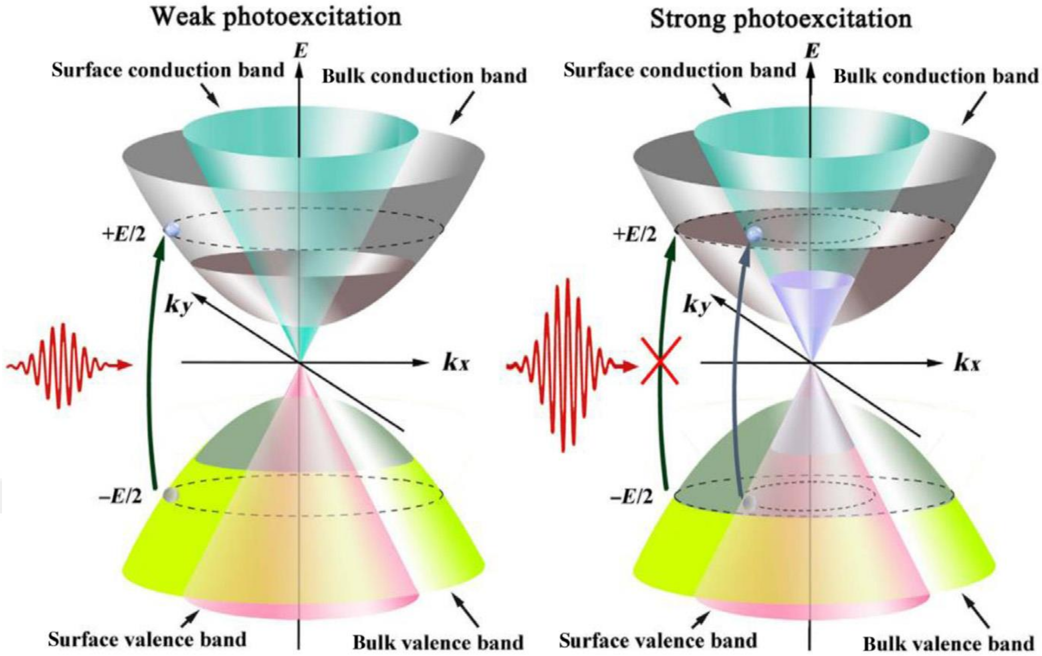

Reference: J.L. Xu, et. al, 2015.

3.3. TOPOLOGICAL INSULATOR BASED SA FABRICATION METHODS FORLASER APPLICATIONS

The manufacturing method is an important factor in determining the features, cost, and stability two dimensional layered TIs. Up-to-date two major techniques are used to synthesis two dimensional layered TIs, they are top-down and bottom-up approaches (J.L. Xu, et. al, 2015, D. Chu & E.K. Kim, 2018, Z. Lin, et. al, 2016, J. Krumrain, et. al, 2011, T. Ginley, Y. Wang & S. Law, 2016, J.E. Brom, et. al, 2012, J. Fuqiang, et. al, 2015).

The first approach is nothing but a pealing process (or exfoliation), which consists of mechanical and chemical minor types. The first minor type is scotch tape approach or mechanical exfoliation (ME) as in Figure.3.3a. In 2004 was the first demonstration of the ME by using graphene and adhesive tape. (E. Gerstner, 2010). The second minor type is the liquid phase exfoliation (LPE) approach as inFigure.3.3b, which is consist of insertion, exchanging ion and ultrasonic exfoliation. At the first demonstration they reported that more than 28% of the produced flakes were monolayred, the research material was also with using grapheme (Hernandez, Y., Nicolosi, V. & Lotya, M., 2008).

Figure 3.3: Synthesis and Transferring Approaches Used for TIs.

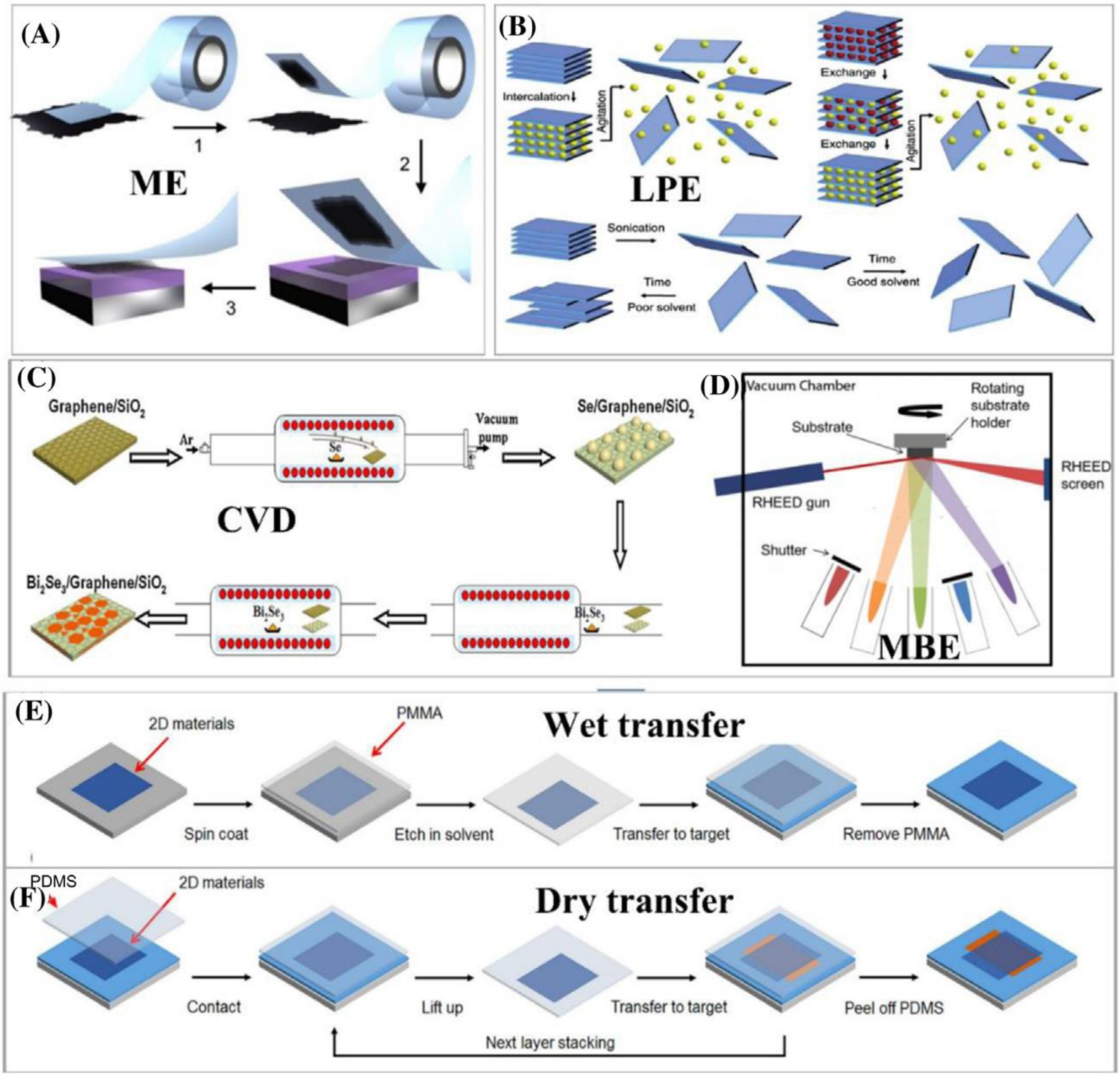

Reference: Young Min Jhon & Ju Han Lee, 2020.

The second major approach is the chemical vapor deposition (CVD), where the precursor is vaporized to be deposited on a substrate inside a CVD chamber with relatively high temperature. In this approach monolayer or few-layer two dimentional materials can be achieved, as in Figure.3.3c. The second minor approach is molecular beam epitaxial growth (MBE), which is the technique using crystal growth to growing atomic layer based on an atomic beams reaction with a heated crystalline substrate in a high vacuumed chamber, as in Figure.3.3e (Young Min Jhon & Ju Han Lee, 2020).

Transferring of the synthesized NLO two-dimensional layered material to fabricate an optoelectronic or electronic devices, the transferring method must be efficient and nondestructive. There are two famous approaches, wet and dry transfer approaches as in Figure.3.3e and Figure.3.3f.

For wet transfer approach, as in Figure.3.3f, first spin-coat a polymer material onto the two-dimensional material; secondly, peals the polymer formed layer composite film from the substrate; thirdly, transfers the formed composite film onto the target substrate and dissolve the polymer in an organic solvent.

The dry transfer approach as in Figure 3.3f is represented by first, remove the two-dimensional material from the substrate by the poly stamp; secondly, join the stamp with the two-dimensional material to another one to carry the two-dimensional layers on the stamp; thirdly, by repeating the same process more two-dimensional layers can be achieved. (Y.R. Wang, et al., 2017).

In this thesis, a new, novel, very easy, low cost, very efficient, high yield, not affected by the surrounding ambient humidity and reliable method I propose to synthesize a SA and other NLO materials based on TIs, as explained in subsection 3.4.

3.4. BISMUTH TELLURIDE (Bi_2Te_3) BASED ULTRA THIN FILM SA

Film casting is a traditional method to fabricate different film kinds. In this approach, the particles of the material are distributed among the particles of the matrix material (like PVA, PEG etc.) by mixing the mixture well using magnetic steering, subjecting the mixture to a sonication bath, and finally pouring the mixture into a Petri dish for drying in a vacuum environment under heat or at room temperature. Because of the Poly (Vinyl Alcohol) (PVA) properties represented by, biodegradability, water-solubility, non-toxicity, good film formation, good chemical and thermal stability, so it widely used in chemical and biological fields (Z.K. Heiba & M.B. Mohamed, 2020). Water and alcohols are the main analytes because they represented the enormous majority of chemical or biological solutions. (Y. Yu, X. Li, X. Hong, Y. Deng, K. Song, Y. Geng, & W.Tong, , 2010, R. Hao & G. Sun, 2015). Ethanol (C_2H_5OH) and Isopropyl alcohol (C_3H_8O) are the common fluids for use in different branches of materials science, particularly, in the field of nanoscience, they used for nanoparticle suspensions as dispersing media (Elisa Sani & Aldo Dell'Oro, 2016). Index matching gel (IMG) is a material that provides a "light bridge" to pass from one fiber end to other without passing through air gap, generally, used in mechanical splice and SA devices. In 1978 was first time IMG was used in the optical fiber industry (AEN046, 2017).

Figure 3.4: Bi_2Te_3-PVA Film Characteristics with a) Image of FESEM, b) the Raman Spectrum of Free Standing Film, c) Linear, and d) Nonlinear Transmission

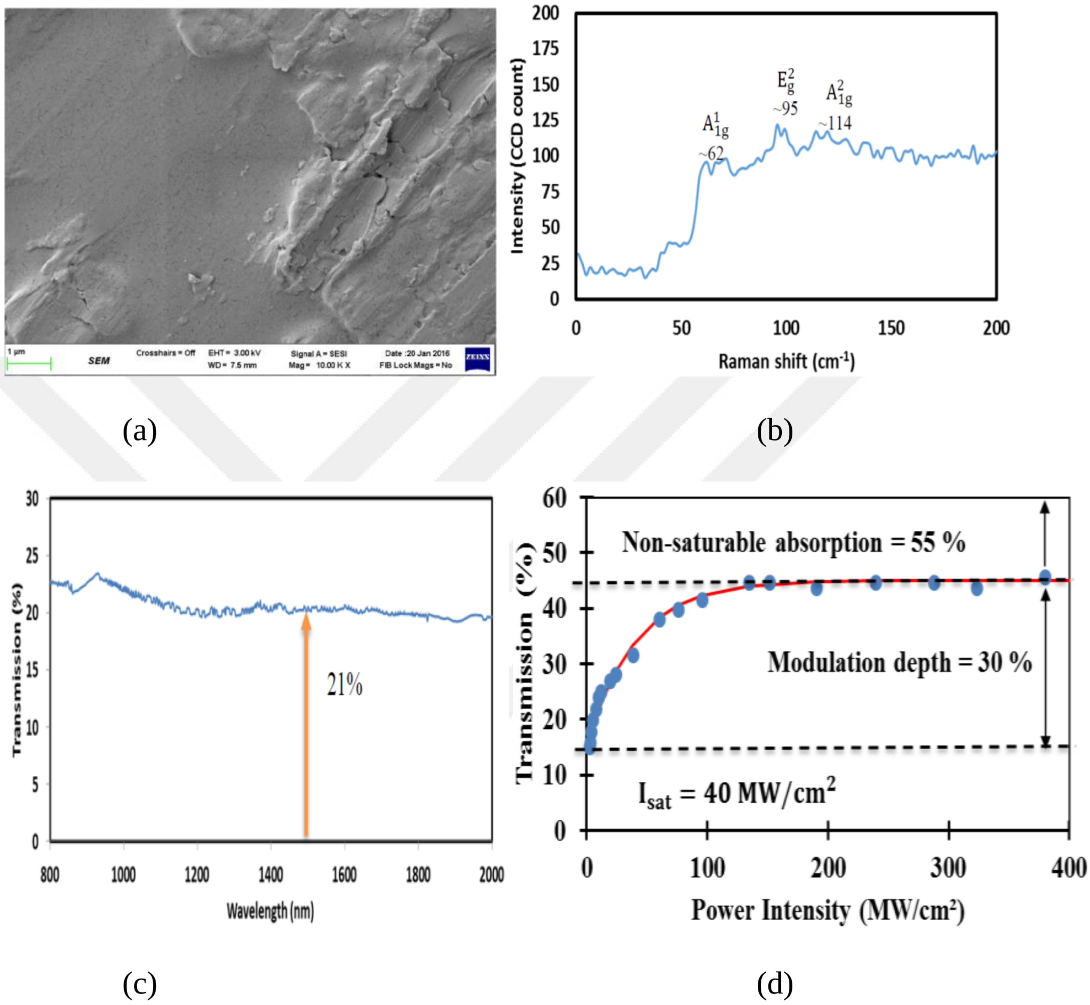

Reference: R. Z. R. R. Rosdin et. al, 2019.

The new method used to fabricate ultra thin film, is a new method I invented to fabricate a SA devices and other NLO materials using a pre casting films that used PVA as a host material, with the aid of IMG and Ethanol alcohol or Isopropyl Alcohol. The new method can be stated in five steps as bellow:

The first step, is by sandwiching the bulk film, (already fabricated thin film that has the properties shown in Figure 3.4), in between two FC/PC connector ferrules (Bi_2Te_3-PVA in this thesis) or any other substrates with adding IMG and few drops from Ethanol alcohol.

Second step, is by applying a pressure to the connectors/substrates (in this thesis the FC/PC connectors fastened very well to the optical fiber adapter).

Third step is by removing the original film that being sandwiched in step one, from the connector-adapter-connector device.

Fourth step is to cook the SA device well by applying pump power a little bit higher than the power level of threshold pump power, for about one to three hours depends on the SA kind. The cooking word, here, means to make sure the ultrathin film is being adhesive to the ferrule core hole part and the round area, in another word to the fiber faced end.

Fifth and last step is by cleaning the cooked SA connector ferrules by alcohol and a special tissue, because there is no more need to the IMG any more with using this way. So, one can deal with the new fabricated SA as a free two FC/PC connectors.

The resulted device can be suppurated into two devices by using each SA FC/PC connector alone with new FC/PC pig tailed connector and adapter. We can gate in each process two devices.

Figure 3.5: The Ultra Thin Film New Fabrication Method

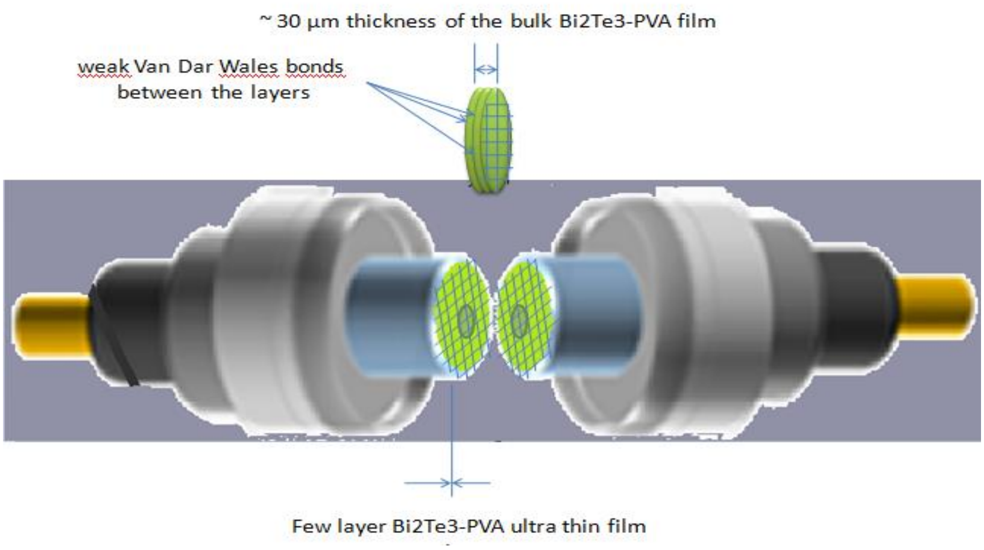

Through the experiments that I made, as shown in chapter 4 and chapter 5, the new fabrication method characterizes by high output/yield, fast, low cost, very stable laser performance, robust and not sensitive to the ambient humidity in contrast to other PVA thin films. This approach is a mix of the film preparation and film transferring methods.

The new SA is differ from the original film by the thickness, lower atomic layers referred to as a quintuple layer, lower thermal conductivity which is favorable to improve the thermoelectric performance and less band gap approximately, these indicate changes in the optical properties that the original film has (G. Zhou & D. Wang, 2015). Figure 3.5 shows the fabrication steps of the new fabrication method for ultra thin film SA device.

CHAPTER FOUR

BISMUTH TELLURIDE (Bi_2Te_3) SATURABLE ABSORBER BASED Q-SWITCHED EDFRL

4.1. INTRODUCTION

In recent years, great emphasis has been placed on the Q-switched fiber laser operating at1.5 micron wavelength range due to its ability to produce high pulse energy by modulating the optical loss in the laser cavity using active or passive modulating elements. In the active case, photoelectric modulators (EOM) (A. F. El-Sherif & T. A. King, 2003) and acoustic-optical modulators (AOM) (W. Li, H. Liu, et. al, 2016) are used. In the passive case, it uses semiconductor saturable absorber mirrors (SESAMs) (M. Wang,et.al., 2014) and microchip saturable absorber films (J. J. Zayhowski & A. L. Wilson, 2003) in addition to two-dimensional materials 2D such as saturable absorber films (N. F. Zulkipli et al., 2021) and carbon nanotubes CNTs (N. Kasim,et al., 2014), graphene (Z. Yu et al., 2014), transition metal dichalcogenides (TMDs) (B. Chen, X. Zhang et al., 2015, D. Mao et al., 2015), black phosphorous (J. Sotor, 2015, S. B. Lu et al., 2015, M. Hisyam, et al., 2017, H. Mu et al., 2015), and topological insulators (TIs) (J. Sotor, G. Sobon, and K. M. Abramski, 2014, J. Sotor, et al. 2014, Y. -H. Lin et al.,2015). 2D materials have attracted great interest due to their advantages such as simple preparation process, cost-effective fabrication and relatively wide operating bandwidth, allowing them to produce fiber lasers with tunable wavelength (Hsin-Ju Peng, et al., 2021).

The wavelength tuning of a passive Q-switched fiber laser based on 2D materials by utilizing a tunable filter constructed by a birefringent plate in an erbium-doped fiber laser has been reported from 1522.5 to 1555 nm, from 1510.9 to 1589.1 nm, and from 1519.6 to 1567.1 nm based on graphene (D. Popa, et al., 2011), Bi_2Te_3 (Y. Chen, et al., 2013), and MoS_2 (Y. Huang, et al., 2014).

TIs topological insulators have unique properties as they have a nonlinear super-wavelength optical response from visible to microwave (H. Zhang et al., 2009) due to the co-interaction between the small bulky-gap band and the zero-gap surface state as a result of the effects of spin-orbit interactions and time-reversal symmetry (X. Zhang, 2010). TIs was considered as one of the few alternative materials suitable for conventional saturable absorbers regarding the research results that showed a wide pulse range from infrared to mid-infrared (Z. Luo et al., 2013, M. Jung et al., 2014, H. Yu et al., 2013, J. Sotor et al., 2014, Y. Lin et al., 2014, H. Liu et al., 2014, P. Tang et al., 2013, J. Sotor, 2014, J. Lee et al., 2014, Z. Luo et al., 2013, Z. Yu et al., 2014).

4.2. Q-SWITCHED EDFRL OPERATING AT 1.5-MICRON REGION USING Bi_2Te_3 SA

In this subsection, passively Q-switched pulse trains are generated in an EDFRL cavity using the Bi_2Te_3 thin film SA as a passive modulator. An EDFRL is constructed to study and observe the performance of the Bi_2Te_3-PVA thin film SA. Bi_2Te_3-PVA thin film SA is used to self starting the Q-switching process for pulse generation. Bi_2Te_3-PVA thin film SA used in the experiments was fabricated in University of Malaya Photonic Research Group and had saturable intensity of 40 MW/cm^2, saturable absorption of 30%, and non-saturable absorption of 55%, respectively, as shown in Figure 4.1.

For Q-switched laser operating at 1.5-micron region with Bi_2Te_3 thin film SA the experiments has been made with the thin film Bi_2Te_3-PVA that it's nonlinear transmission properties shown in Figure.4.1.

Figure 4.1: Bi_2Te_3 Linear and Nonlinear Optical Absorption Characteristics: The Saturable Intensity Of 40 MW/cm^2, Saturable Absorption of 30%, and Non-Saturable Absorption of 55%

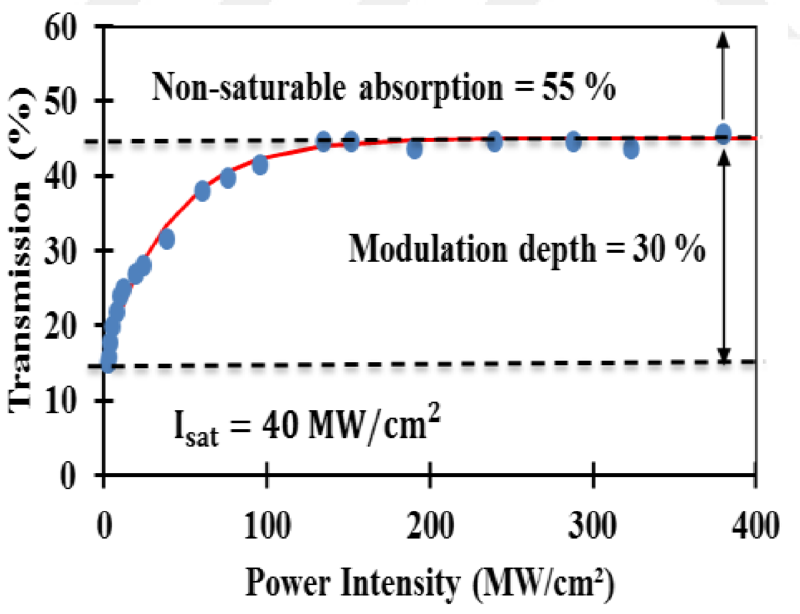

Reference: R. Z. R. R. Rosdin et al., 2019.

4.2.1. Q-Switched EDFRL Using Bidirectional Pumping Method

The experimental setup used for passively Q-switched EDFRL using bidirectional pumping method in EDFA was as shown in figure 4.2. In this setup, the output of EDFRL was taken from the 10% port of the tap coupler with a 90%-10% splitting ratio and then divided into two ports, to observe the optical spectrum of the output signal at one port using an optical spectrum analyzer (OSA Anritsu-MS9710B), and to analyze the pulse waveforms at the other port using an InGaAs 5GHz photodiode (Thorlabs-DET08CFC/M) connected to an oscilloscope (Keysight-DSOX2002A).

Figure 4.2: The Ring Laser Cavity Used in The Experiments of Passive Q-Switched EDFRL

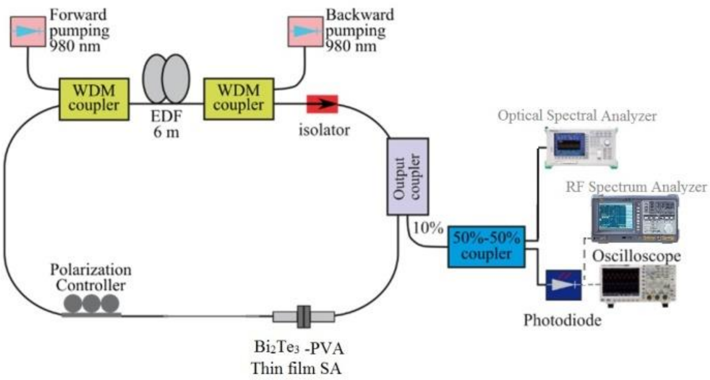

In the experimental set up a manual polarization controller (PC) was used to eliminate the unwanted polarization effects that may occur due to the polarization rotation in the ring and to keep the polarization state of the oscillating wave under control. After inserting Bi_2Te_3-PVA SA device into the cavity, a free running continuous wave laser is firstly generated in the EDFRL until the pump power reached to 73.04 mW, the EDFRL delivers a train of Q-switched microsecond laser pulses. The shortest pulse width generated in these experiments with total cavity length about 9.5 m was 3.351 µs as shown in Figure 4.3a, the related output power spectrum 1559.4 nm central wavelength, as in Figure 4.3b.Whereas Figure 4.3c shows the RF power spectrum output where the SNR was 53.64 dB and the repetition rate of 48.78 kHz.

The pulse train started to appear at threshold bidirectional pumping power of 73.5 mW with pulse width of 12.1879 µs, repetition rate of 15.679 kHz, SNR of 30 dB, output average power of 0.2 mW, pulse energy of 9.33 nJ, pulse peak power of 0.7654 mW and power conversion efficiency (laser efficiency) of 0.2116%.

Figure 4.3: a) Pulse Shape, b) Optical Output Spectrum, and c) Electrical Output Spectrum of Bi_2Te_3-PVA SA Based Q-Switched EDFRL with a Bidirectional Pumping Power of 332.1 mW in EDFA.

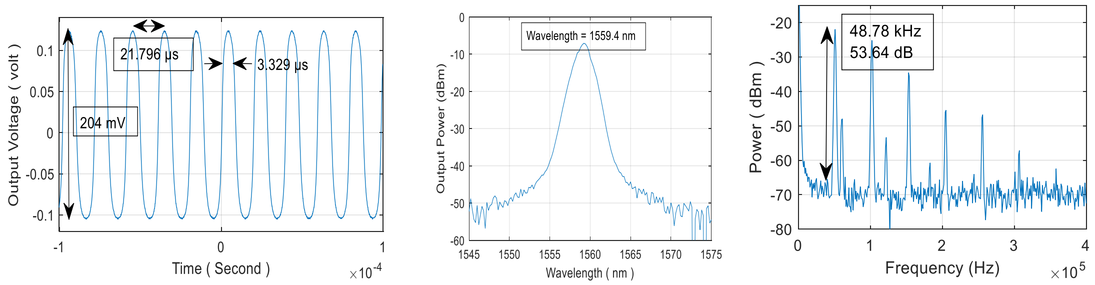

(a) (b) (c)

Figure 4.4: Q-switched Laser a) Optical Output Spectrum as a Function of the Output Wavelength and b) Output Power and Pulse Energy, c) Peak Pulse Power and Laser Efficiency, d) Pulse Width and Repetition Rate, e) Electrical Output, SNR and Pulse Amplitude of Bi_2Te_3 SA Based EDFRL as a Function of The Bidirectional Pump Power Range From 73.5 mW to 379.6 mW.

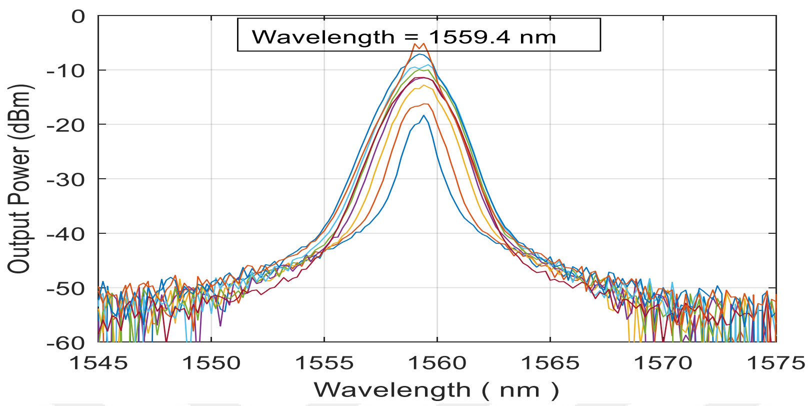

(a)

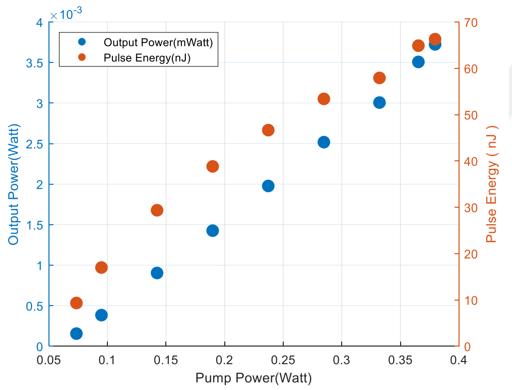

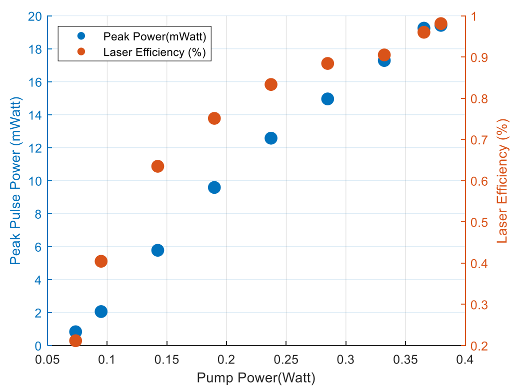

(b) (c)

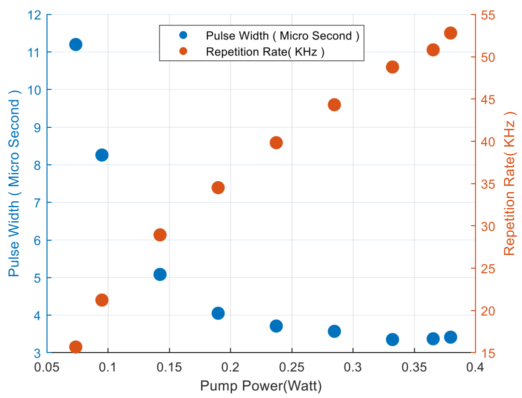

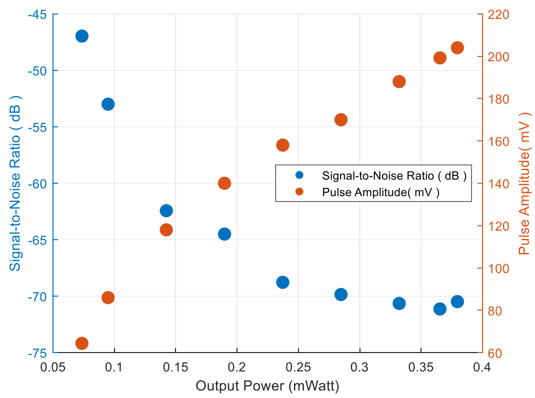

(d) (e)

Whereas, the laser worked efficiently up to the bidirectional pumping power of 379.6 mW, and at this pumping power the pulse width, the repetition rate, the output power, the pulse energy, the peak power, and the power conversion efficiency (laser efficiency) were 3.329 μs, 44.78 KHz, 3.7 mW, 66.297 nJ, 19.3772 mW, and 0.981%, respectively, as shown in Figure 4.4.

4.2.2. Q-Switched EDFRL Using Forward Pumping Method

In this experiments have been made on Bi_2Te_3-PVA SA device using forward pump configuration used in Figure 4.5.

After inserting Bi_2Te_3-PVA device into the cavity, a free running continuous wave laser is firstly generated in the EDFRL when the pump power has reached to 79.5 mW, the EDFRL start to generate a train of Q-switched microsecond laser pulses. The shortest pulse width that we have generated by this experiments with total cavity length about 9.5 m was 3.2156 μs as shown in Figure 4.6a, the corresponding output power spectrum that at around 1559.16 nm central wavelength, as in Figure 4.6b. Whereas the RF power spectrum was as in Figure 4.7c where the SNR was 52.38 dB and the repetition rate of 45.88 KHz, were respectively.

Figure 4.5: The Ring Laser Cavity Used in The Experiments of Passive Q-Switched EDFRL

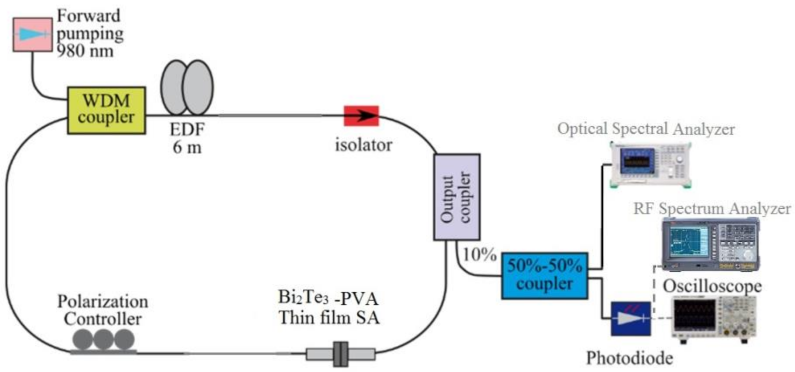

Figure 4.6: a) Pulse Shape, b) Optical Output Spectrum, and c) Electrical Output Spectrum of Bi_2Te_3-PVA SA Based Q-Switched EDFRL with Forward Pumping Power of 308.4 mW in EDFA.

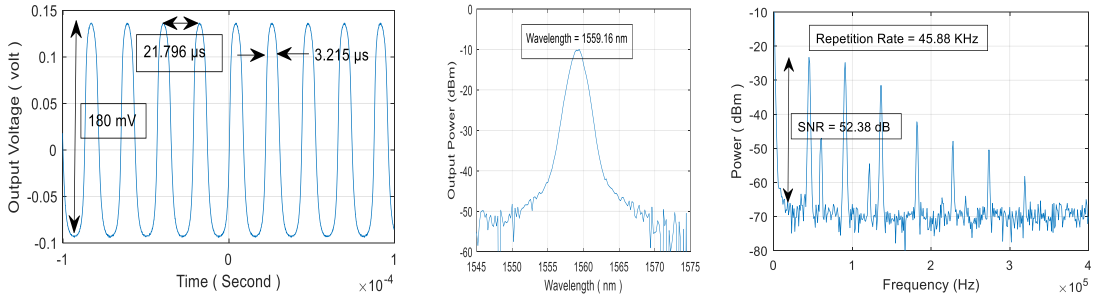

(a) (b) (c)

The pulse train started to appear at the threshold forward pumping power of 79.5 mW with pulse width of 10.64 µs, repetition rate of 23.38 kHz, SNR of -39.1 dB, output average power of 0.2 mW, pulse energy of 6.3721nJ, pulse peak power of 0.6269 mW and power conversion efficiency (laser efficiency) of 0.1993%. Whereas, the laser worked efficiently up to the forward pumping power of 308.4 mW, and at this pumping power the pulse width, the repetition rate, the output power, the pulse energy, the peak power, and the power transferring efficiency were 3.125 µs, 45.88 KHz, 1.8 mW, 36.2664 nJ, 11.2783 mW, and 0.5739%, respectively, as shown in Figure 4.7.

Figure 4.7: Q-Switched Laser a) Optical Output Spectrum as A Function of the Output Wavelength and b) Output Power and Pulse Energy, c) Peak Pulse Power and Laser Efficiency, d) Pulse Width and Repetition Rate, e) Electrical Output, SNR and Pulse Amplitude of Bi_2Te_3 SA based EDFRL as a Function of the Forward Pumping Power Range from 79.5 mW to 308.4 mW

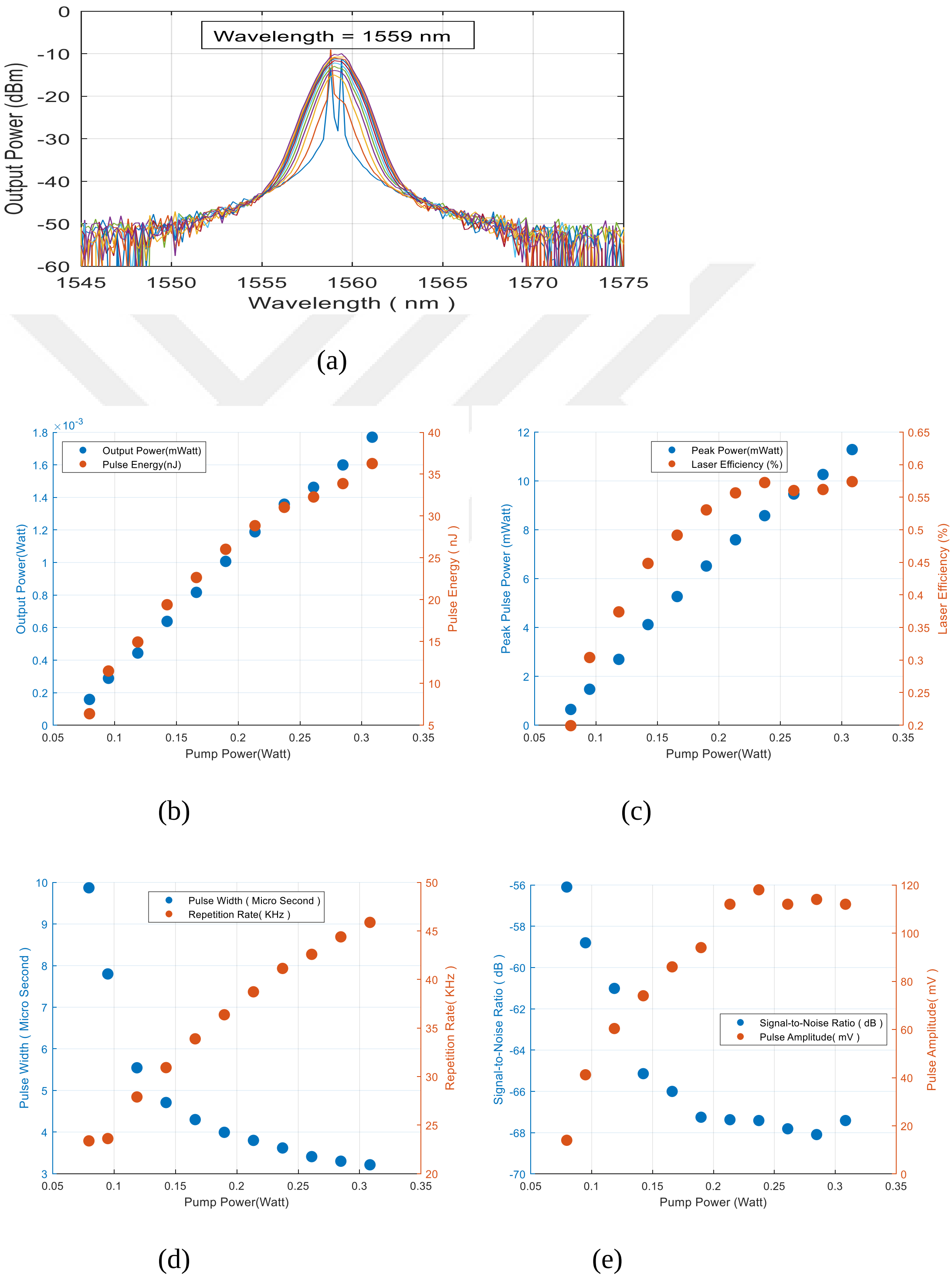

4.2.3. Q-Switched EDFRL with Ultra-Thin Film Bi_2Te_3-PVA SA

In these experiments, passively Q-switched pulse trains are generated in an EDFRL cavity using the newly fabricated Bi_2Te_3 ultra thin film SA as a passive modulator. By using the same EDFRL configuration in Figure 4.2 as the Bi_2Te_3-PVA ultra thin film was used instead of the Bi_2Te_3-PVA thin film SA, shown in Figure 4.2. Bi_2Te_3-PVA ultra thin film SA is used to self starting the Q-switching process for pulse generation. Bi_2Te_3-PVA ultra thin film SA used in the experiments was fabricated by the new fabrication method described in subsection 3.4 of Chapter 3.

When the Bi_2Te_3-PVA ultra thin film SA introduced to the cavity a free running continuous wave laser is firstly generated in the EDFRL until the pump power reached to 57.3 mW, the EDFRL was generated a train of Q-switched microsecond laser pulses. The shortest pulse width generated by this experiment with total cavity length about 9.5 m was 2.5336 μs as shown in Figure 4.8a, the corresponding output power spectrum was at 1565.23 nm central wavelength, as in Figure.4.8b. Whereas Figure 4.8c shows the RF power spectrum where the SNR of 52.76 dB and the repetition rate of 63.37 KHz, were respectively.

Figure 4.8: a) Pulse Shape, b) Optical Output Spectrum, and c) Electrical Output Spectrum of Bi_2Te_3 SA Based Q-Switched EDFRL with a Bidirectional Pumping Power of 417.6 mW in EDFA

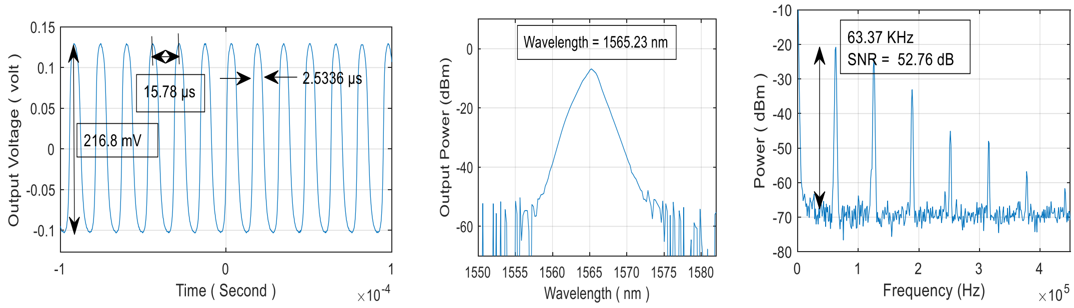

(a) (b) (c)

The pulse train started to appear at threshold bidirectional pumping power of 57.3 mW with pulse width of 22 μs, repetition rate of 6.9512 kHz, SNR of 30 dB, output average power of 0.1 mW, pulse energy of 8.7512 nJ, pulse peak power of 0.4 mW and power conversion efficiency (laser efficiency) of 0.1129%.

Whereas, the laser worked efficiently up to the bidirectional pumping power of 417.6 mW, and at this pumping power the pulse width, the repetition rate, the output power, the pulse energy, the peak power, and the power transferring efficiency were 2.5336 μs, 63.37 KHz, 3.8 mW, 56.5255 nJ, 22.3 mW, and 0.9126%, respectively, as shown in Figure.4.9.

Figure 4.9: Q-Switched Laser a) Optical Output Spectrum as A Function of the Output Wavelength and b) Output Power and Pulse Energy, c) Peak Pulse Power and Laser Efficiency, d) Pulse Width and Repetition Rate, e) Electrical Output, SNR and Pulse Amplitude of Bi_2Te_3 SA Based EDFRL as A Function of the Bidirectional Pumping Power Range from 57.3 mW to 417.6 mW.

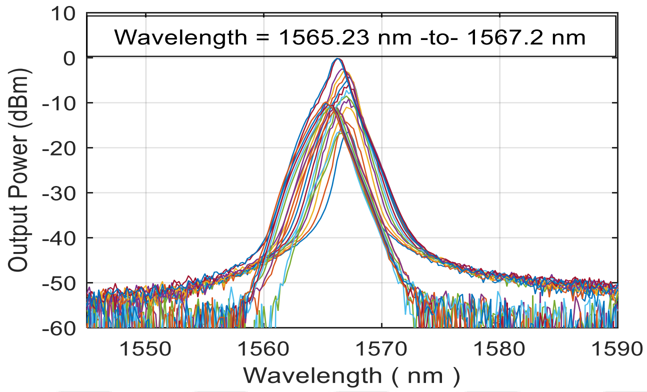

(a)

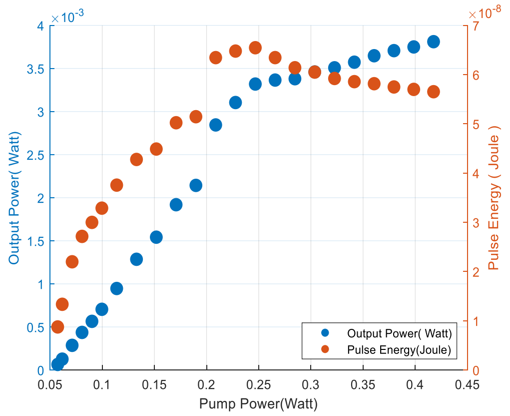

(b)

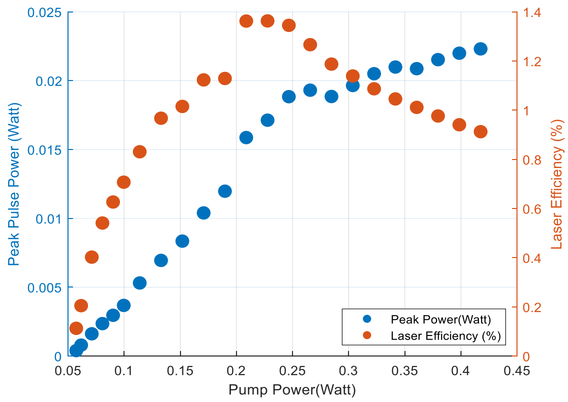

(c)

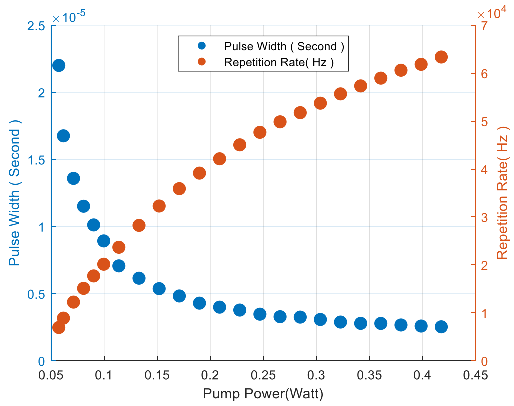

(d)

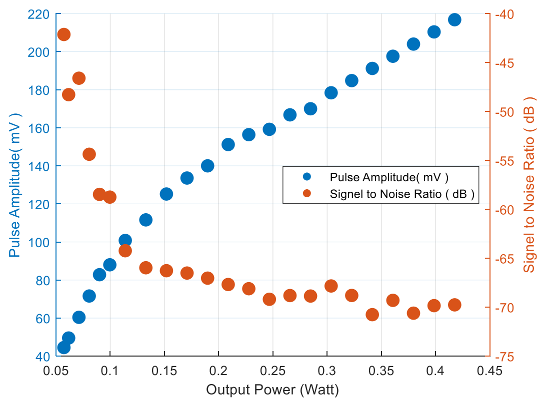

(e)

4.3. WAVELENGTH TUNABLE PASSIVELY Q-SWITCHED EDFRL OPERATING AT 1.5-MICRON REGION USING Bi_2Te_3-PVA SA

In this section, wavelength tunable passively Q-switched pulses were generated in an EDFRL cavity using Bi_2Te_3 thin film SA as a Q-switch. An EDFRL is constructed to study the spectral performance of the Bi_2Te_3-PVA thin film SAs. Bi_2Te_3-PVA thin film SA was used to initiate Q-switching process for pulse generation.

The experimental set up used in these experiments was the same given in Figure 4.2 except a Manuel optical tunable band pass filter (TBPF), Fabry-Perrot type JDS FITEL TB 1.520-1.567 micro meter, with a line width of 3 nm was added in the cavity as shown in Figure 4.10.

4.3.1. Wavelength Tunable Passively Q-switched EDFRL Operating at 1.5-Micron Region Using Thin Film Bi_2Te_3-PVA SA and Bidirectional Pumping Method

After inserting Bi_2Te_3-PVA SA device into the cavity, a free running continuous wave laser is firstly generated in the EDFRL when the bidirectional pumping power has reached to 73.04 mW, the EDFRL started to generate a train of Q-switched microsecond laser pulses.

By adding the TBPF, a tuning range of (from 1538.2 to 1571nm), a tuning range of 32 nm has been realized with bidirectional pumping power of 95 mW.

Figure 4.10: Tunable Passively Q-Switched EDFRL Cavity

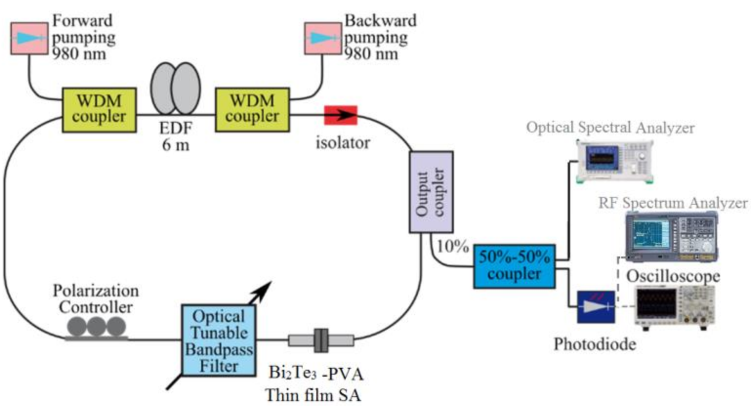

Figure 4.11: a) Pulse Shape, b) Optical Output Spectrum, and c) Electrical Output Spectrum of Bi_2Te_3 SA Based Q-Switched EDFRL with a Bidirectional Pumping Power of 95 mW in EDFA and 1542.52 nm TBPF Tuning Wavelength

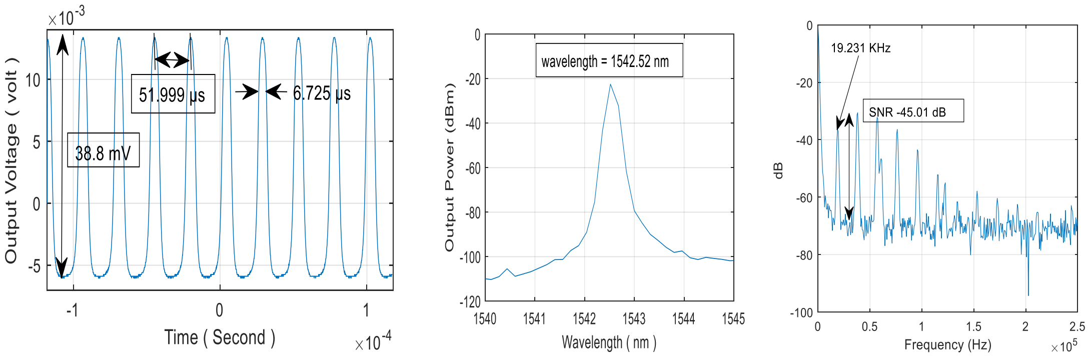

(a) (b) (c)

The shortest pulse that realized by this experiments with total cavity length about ~ 10.5 m was 6.725 µs as shown in Figure 4.11a, the related output power spectrum was around 1542.52 nm central wavelength, as in Figure 4.11b.Whereas Figure 4.11c shows the RF power spectrum output where the SNR of -62 dB and the repetition rate of 19.231 KHz.

In Figure 4.12a the output power spectrum with respect to the tuning wavelength power covers 32.8 nm (from 1538.2 to 1571 nm), Figure 4.12b the output average power and pulse energy with respect to the pump power, where, the minimum output power was 0.2685 mW and the maximum output power was 0.375 mW.

The pulse train started to appear at constant bidirectional pumping power of 95.7 mW at TBPF tuning wavelength of 1538.2 nm where the pulse width, repetition rate, SNR, output average power, pulse energy, pulse peak power, and power conversion efficiency (laser efficiency) were 6.845 µs, 19.3 kHz, -50 dB, 0.29 mW, 14.14 nJ, 2.1 mW and of 0.3036%, respectively.

Whereas, the laser worked efficiently up to TBPF tuning wavelength of 1571 nm, and at this tuning wavelength the pulse width, the repetition rate, the output power, the pulse energy, the peak power, and the power transferring efficiency were 16.458 µs, 8.946 KHz, 0.293 mW, 30.8 nJ, 1.9 mW, and 0.3064%, respectively, under constant bidirectional pumping power of 95.7 mW as shown in Figure 4.12.

Figure 4.12: Wavelength Tunable Q-Switched Laser a) Optical Output Spectrum, b) Output Power and Pulse Energy, c) Peak Pulse Power and Laser Efficiency, d) Pulse Width and Repetition Rate, e) Electrical Output, SNR and Pulse Amplitude of Bi_2Te_3 SA Based EDFRL as A Function of The TBPF Tuning Wavelength at A Constant Bidirectional Pumping Power of 95.7 mW.

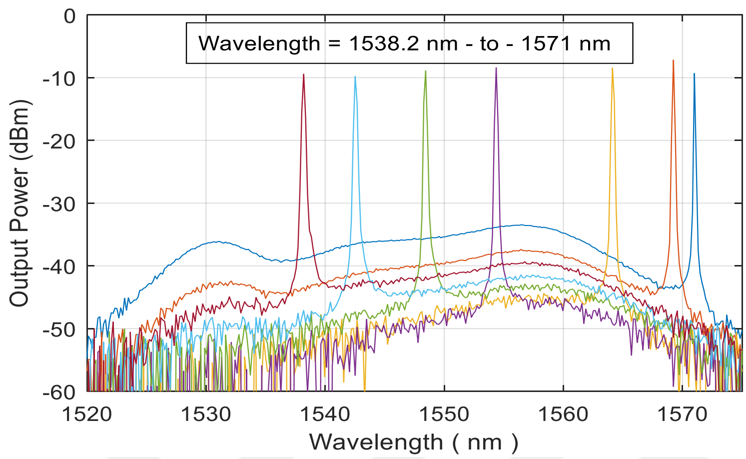

(a)

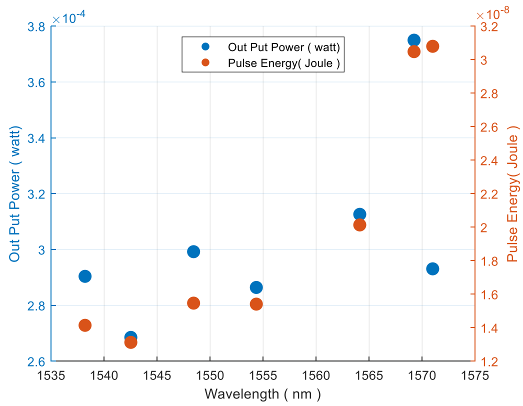

(b)

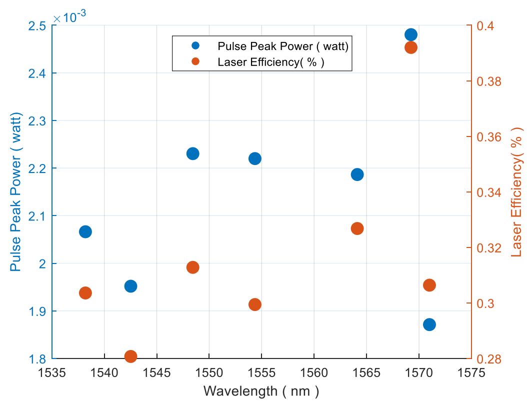

(c)

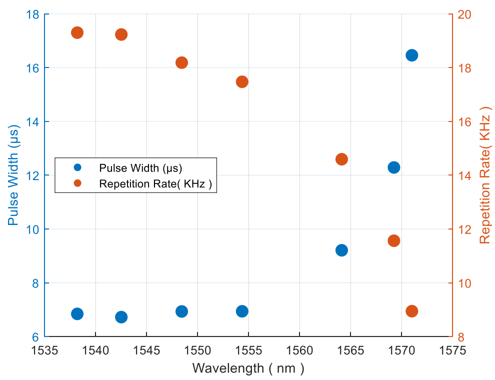

(d)

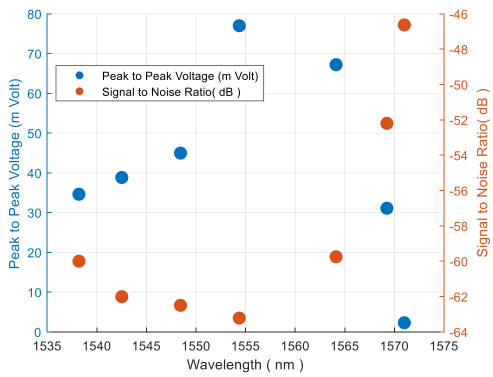

(e)

4.3.2. Wavelength Tunable Passively Q-Switched EDFRL Operating At 1.5-Micron Region Using Ultra Thin Film Bi_2Te_3-PVA SA and Bidirectional Pumping Method

In this experiment the same EDFRL cavity in Figure 4.10 was used. After inserting the ultra thin film Bi_2Te_3-PVA SA device into the cavity, a free running continuous wave laser is firstly generated in the EDFRL when the bidirectional pumping power of has reached to 57.3 mW, the EDFRL start to generate a train of Q-switched microsecond laser pulses.

First, using a forward pumping power of 99.9 mW and backward pumping power of 83.7 mW and by tuning the TBPF from 1523.9 nm to 1571nm, a tuning range of 47 nm has been realized with total pumping power of 183.6 mW.

The shortest pulse that realized by this experiments with total cavity length about ~ 10.5 m was 3.769 µs as shown in Figure 4.13a, the related output power spectrum at around 1529.45 nm central wavelength, as in Figure 4.13b.Whereas Figure 4.13c shows the RF power spectrum output where the SNR of -67 dB and the repetition rate of 49.731 KHz.

Figure 4.13: a) Pulse Shape, b) Optical Output Spectrum, and c) Electrical Output Spectrum of Bi_2Te_3 SA Based Q-Switched EDFRL with Total Pumping Power of 183.6 mW in EDFA and 1529.45 nm TBPF Tuning Wavelength

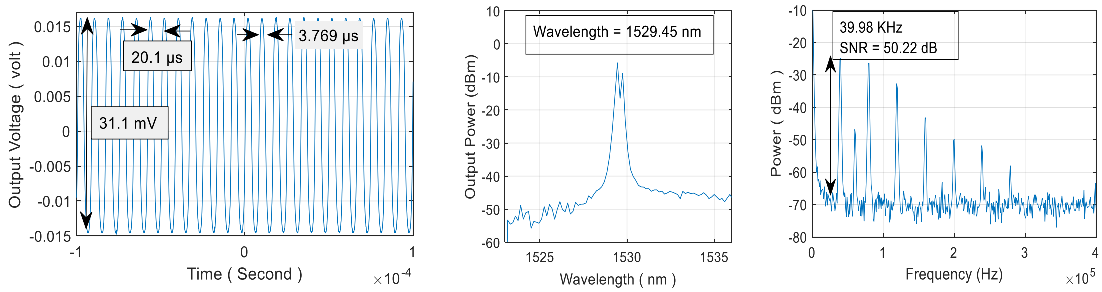

(a) (b) (c)

Figure 4.14: Wavelength Tunable Q-Switched Laser a) Optical Output Spectrum, b) Output Power and Pulse Energy, c) Peak Pulse Power and Laser Efficiency, d) Pulse Width and Repetition Rate, e) Electrical Output, SNR and Pulse Amplitude of Bi_2Te_3 SA Based EDFRL as a Function of the TBPF Tuning Wavelength at A Constant Total Pumping Power of 183.6 mW.

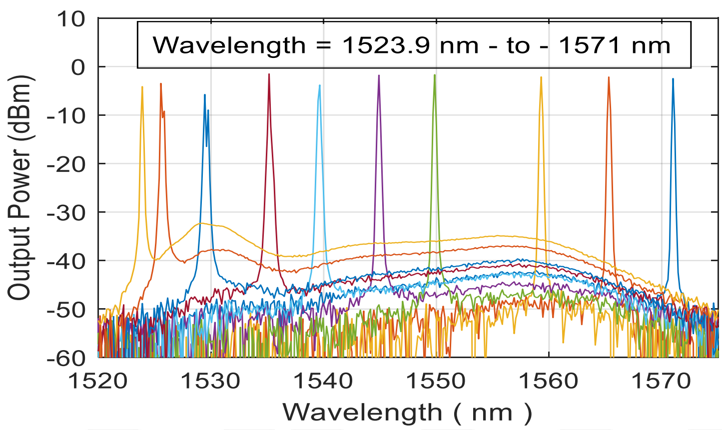

(a)

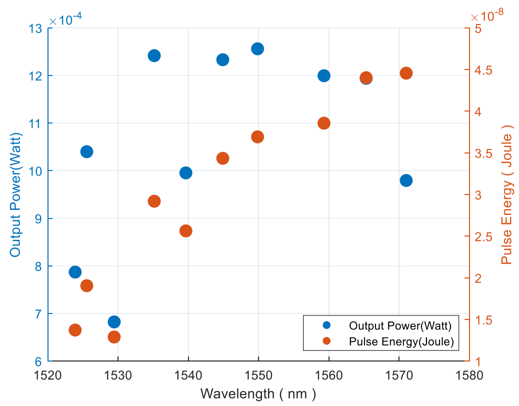

(b)

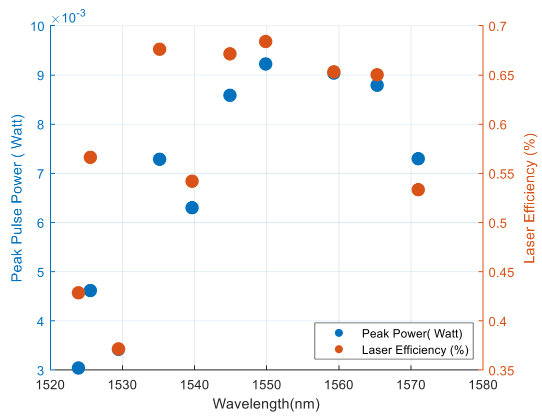

(c)

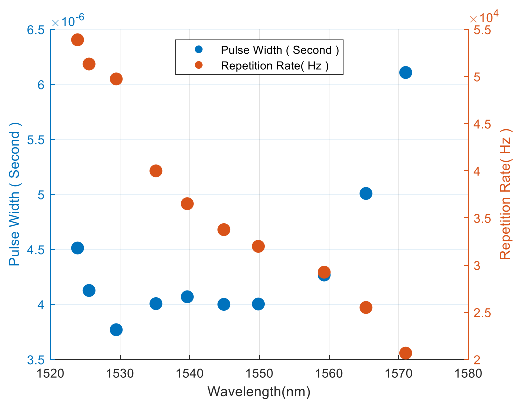

(d)

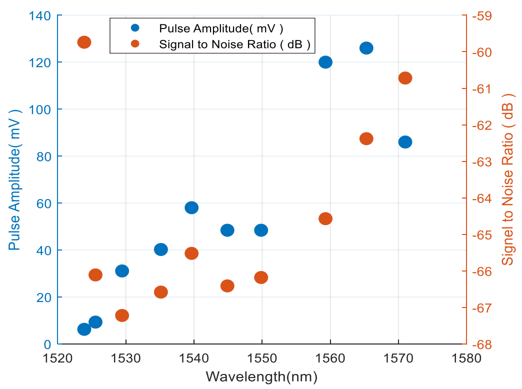

(e)

In Figure 4.14a the output power spectrum with respect to the tuning wavelength power covers 47 nm (from 1523.9 nm to 1571 nm), Figure 4.14b the output average power and pulse energy with respect to the pump power, where, the minimum output power was 0.7 mW and the maximum output power was 1.3 mW.

The pulse train started to appear at constant total pumping power of 183.6 mW at TBPF tuning wavelength of 1523.9 nm where the pulse width, repetition rate, SNR, output average power, pulse energy, pulse peak power, and power conversion efficiency (laser efficiency) were 4.511 μs, 53.88 kHz, 59 dB, 0.8 mW, 13.73 nJ, 3 mW and of 0.4286%, respectively.

Whereas, the laser worked efficiently up to TBPF tuning wavelength of 1571 nm, and at this tuning wavelength the pulse width, the repetition rate, the output power, the pulse energy, the peak power, and the power transferring efficiency were 6.1 μs, 20.661 KHz, 1.0 mW, 44.563 nJ, 7.3 mW, and 0.5334%, respectively, under constant total pumping power of 183.6 mW as shown in Figure 4.14.

Secondly, using a forward pumping power of 112 mW and backward pumping power of 67.9 mW and by tuning the TBPF from 1523.45 nm to 1571.15 nm, a tuning range of 47.7 nm has been realized with total pumping power of 179.9 mW. The shortest pulse that realized by this experiments with total cavity length about ~ 10.5 m was 3.975 μs as shown in Figure 4.15a, the related output power spectrum at around 1527.8 nm central wavelength, as in Figure 4.15b.Whereas Figure 4.15c shows the RF power spectrum output where the SNR of -67 dB and the repetition rate of 46.88 kHz.

Figure 4.15: a) Pulse Shape, b) Optical Output Spectrum, and c) Electrical Output Spectrum of Bi_2Te_3 SA Based Q-Switched EDFRL with Total Pumping Power of 179.9 mW in EDFA and 1529.45 nm TBPF Tuning Wavelength

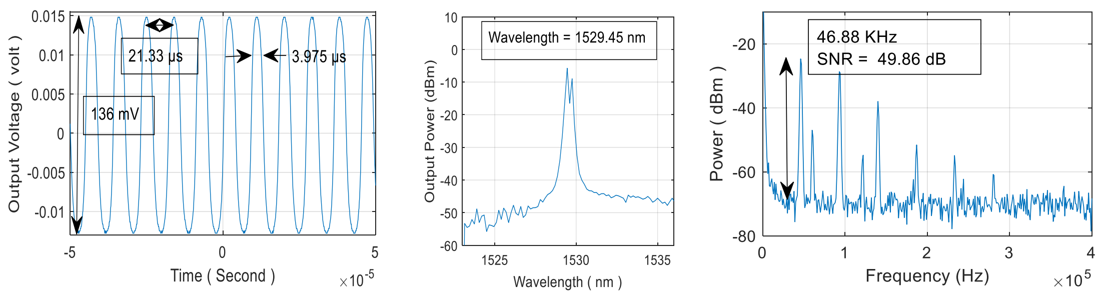

(a) (b) (c)

Figure 4.16: Wavelength Tunable Q-Switched Laser a) Optical Output Spectrum, b) Output Power and Pulse Energy, c) Peak Pulse Power and Laser Efficiency, d) Pulse Width and Repetition Rate, e) Electrical Output, SNR and Pulse Amplitude of Bi_2Te_3 SA Based EDFRL as a Function of the TBPF Tuning Wavelength at A Constant Total Pumping Power of 179.9 mW

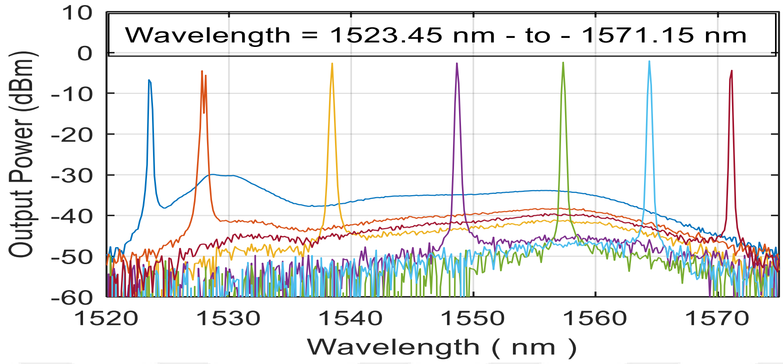

(a)

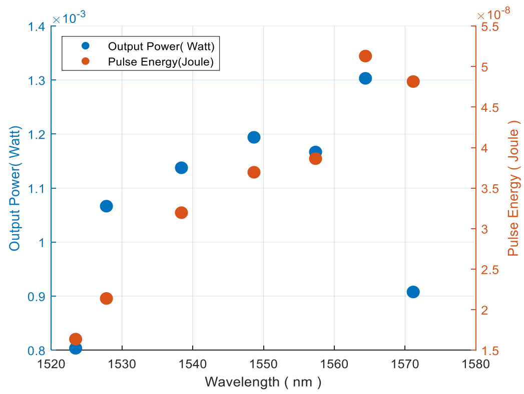

(b)

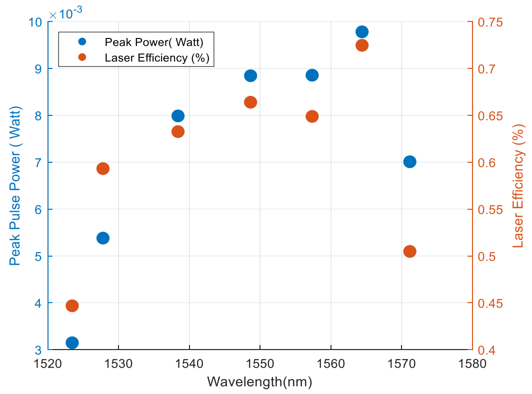

(c)

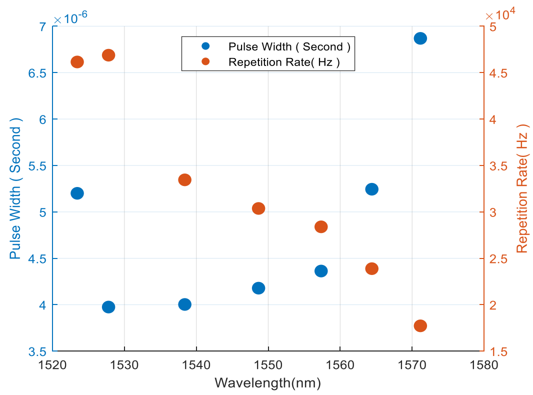

(d)

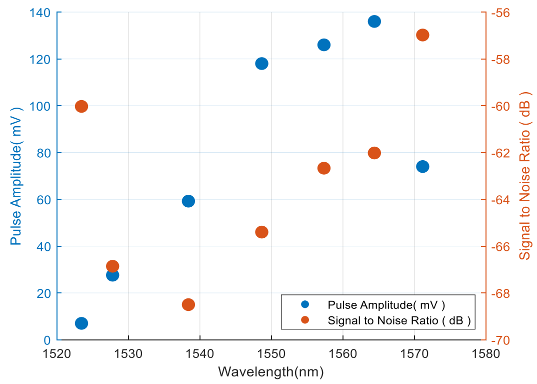

(e)

In Figure 4.16a the output power spectrum with respect to the tuning wavelength power covers 47 nm (from 1523.45 to 1571.15 nm), Figure 4.16b the output average power and pulse energy with respect to the pump power, where, the minimum output power was 0.8 mW and the maximum output power was 1.3 mW.

The pulse train started to appear at constant total pumping power of 179.9 mW at TBPF tuning wavelength of 1523.45 nm where the pulse width, repetition rate, SNR, output average power, pulse energy, pulse peak power, and power conversion efficiency (laser efficiency) were 5.2 μs, 46.15 kHz, -60 dB, 0.8 mW, 16.37 nJ, 3.1 mW and of 0.4468%, respectively.

Whereas, the laser worked efficiently up to TBPF tuning wavelength of 1571.15 nm, and at this tuning wavelength the pulse width, the repetition rate, the output power, the pulse energy, the peak power, and the power conversion efficiency (laser efficiency) were 6.8692 μs, 17.724 kHz, 0.9 mW, 48.15 nJ, 7 mW, and 0.5048%, respectively, under constant total pumping power of 179.9 mW as shown in Figure 4.16.

4.3.3. Wavelength Tunable Passively Q-Switched EDFRL Operating At 1.5-Micron Region Using Ultra Thin Film Bi_2Te_3-PVA SA And Forward Pumping Method

The EDFRL cavity in Figure 4.17 was used in this experiment. After inserting the ultra thin film Bi_2Te_3-PVA SA device into the cavity, a free running continuous wave laser is firstly generated in the EDFRL when the bidirectional pumping power of has reached to 57.3 mW, the EDFRL start to generate a train of Q-switched microsecond laser pulses.

By using a forward pumping power of 261.9 mW and tuning the TBPF from 1535.6 nm to 1571nm, a tuning range of 35 nm has been realized.

The shortest pulse that realized by this experiments with total cavity length about ~ 10.5 m was 3.719 μs as shown in Figure 4.18a, the related output power spectrum at around 1544.15 nm central wavelength, as in Figure 4.18b.Whereas Figure 4.18c shows the RF power spectrum output where the SNR of -70 dB and the repetition rate of 27.23 kHz.

In Figure 4.19a the output power spectrum with respect to the tuning wavelength power covers 35 nm (from 1535.6 to 1571 nm), Figure 4.19b the output average power and pulse energy with respect to the pump power, where, the minimum output power was 0.4 mW and the maximum output power was 2.1 mW.

Figure 4.17: Tunable Passively Q-Switched EDFRL Cavity

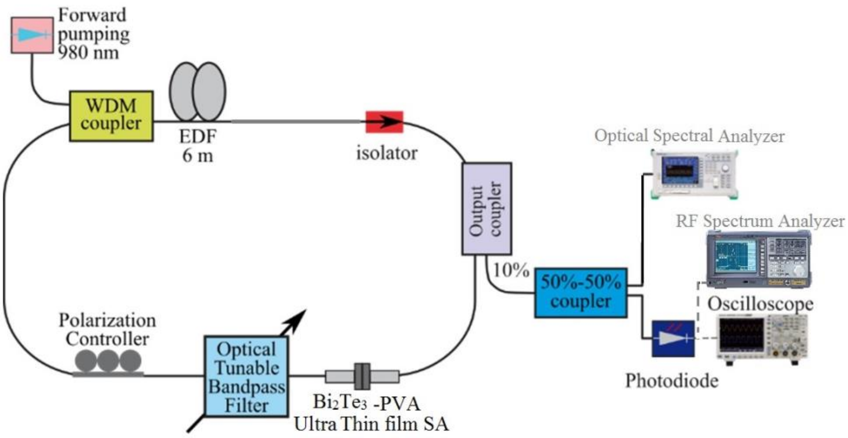

The pulse train started to appear at constant forward pumping power of 261.9 mW at TBPF tuning wavelength of 1535.6 nm where the pulse width, repetition rate, SNR, output average power, pulse energy, pulse peak power, and laser extraction efficiency were 4.5227 μs, 59.99 kHz, -66 dB, 0.4 mW, 5.8891 nJ, 1.3 mW and of 0.1435%, respectively.

Figure 4.18: a) Pulse Shape, b) Optical Output Spectrum, and c) Electrical Output Spectrum of Bi_2Te_3 SA Based Q-Switched EDFRL with Forward Pumping Power of 261.9 mW and 1544.15 nm TBPF Tuning Wavelength

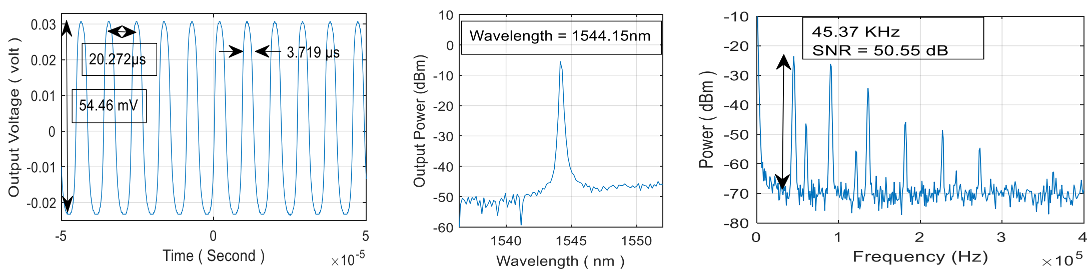

(a) (b) (c)

Figure 4.19: Wavelength Tunable Q-Switched Laser a) Optical Output Spectrum, b) Output Power and Pulse Energy, c) Peak Pulse Power and Laser Efficiency, d) Pulse Width and Repetition Rate, e) Electrical Output, SNR and Pulse Amplitude of Bi_2Te_3 SA Based EDFRL as a Function of the TBPF Tuning Wavelength at A Constant Forward Pumping Power of 261.9 mW

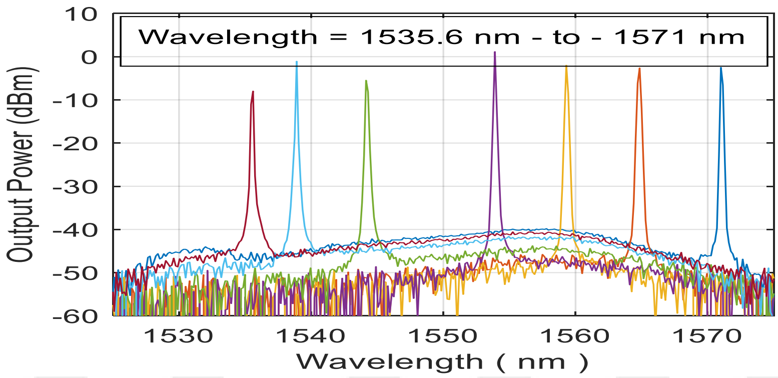

(a)

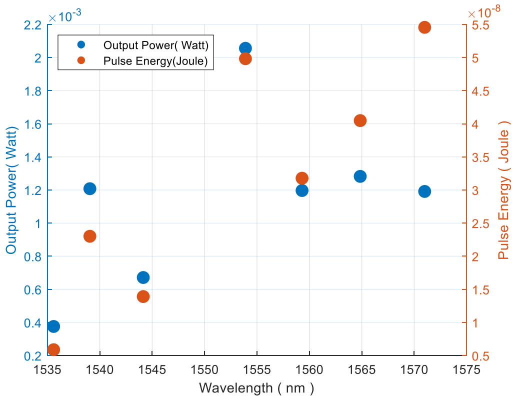

(b)

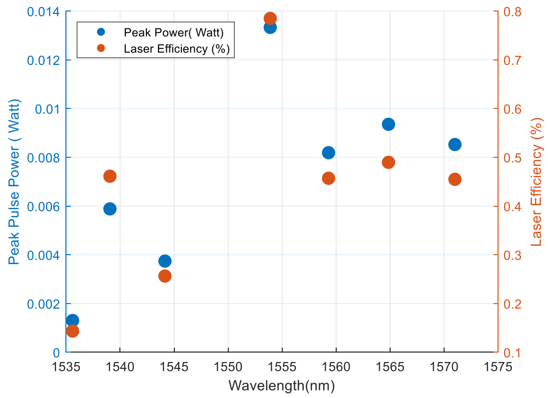

(c)

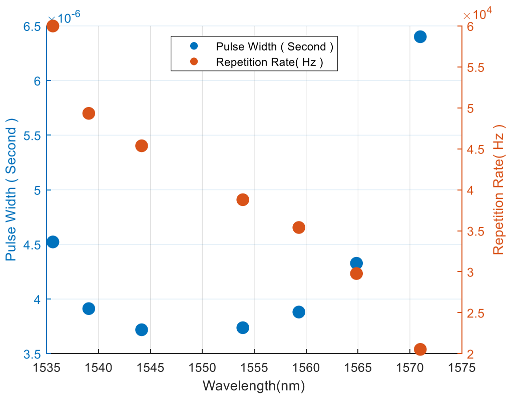

(d)

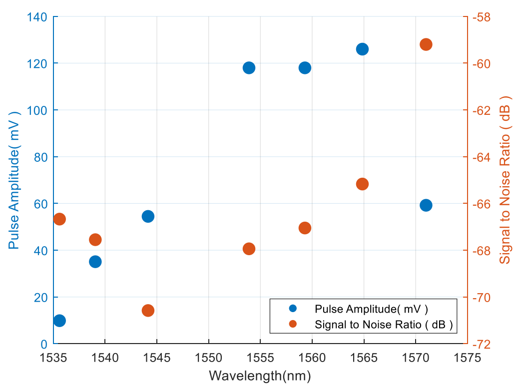

(e)

Whereas, the laser worked efficiently up to TBPF tuning wavelength of 1571 nm, and at this tuning wavelength the pulse width, the repetition rate, the output power, the pulse energy, the peak power, and the power conversion efficiency (laser efficiency) were 6.4 μs, 20.525 KHz, 1.2 mW, 54.5563 nJ, 8.5 mW, and 0.4548%, respectively, under constant total pumping power of 183.6 mW as shown in Figure 4.19.

4.4. SUMMARY

Stable and reliable passively Q-switched fiber lasers were demonstrated successfully by inserting a Bi_2Te_3 thin film SAs. First, thin film SA device for passively Q-switched EDFRL was demonstrated by using bidirectional pumping method. The laser operating at 1559.4 nm, within a frequency range of 15.679 kHz-48.78 kHz, for a pump power of 73.5 mW-379.6 mW. The highest output power and pulse energy of 3.7 mW and 66.297 nJ were attained respectively, at the maximum pump power. Also, the maximum peak power of 19.377 mW, the shortest pulse width of 3.329 μs and the highest pulse frequency of 48.78 kHz were observed at the pump power of 379.6 mW. A compact passively Q-switched EDFRL was also reported successfully by using forward pumping method with the same SA. The proposed EDFRL has a centre wavelength at 1559 nm. The pulsed laser had a stable Q-switched pulsed operation within a tunable frequency range of 23.38 kHz to 45.88 kHz throughout an input pump power range of 79.5 mW to 308.4 mW. The maximum peak power and the highest pulse energy recorded as 11.278 mW and 36.266 nJ, respectively. Besides, the shortest pulse width as 3.215 μs.

Secondly, an ultra thin film SA device fabricated with the new fabrication method for passively Q-switched EDFRL was demonstrated by using bidirectional pumping method. It was stably operating at 1565.23 nm-1567.2 nm, within wide frequency range of 6.9512 kHz-63.37 kHz, for pump power of 57.3 mW-417.6 mW. At the maximum pump power, the highest output power and pulse energy of 3.8 mW and 65.459 nJ were attained respectively. Additionally, the maximum peak power of 22.3 mW, the shortest pulse width of 2.533 μs and the highest pulse frequency of 63.37 kHz were observed at the pump power of 417.6 mW.

New and easy fabricated, Bi_2Te_3-PVA SAs ultra thin film, by new fabrication method with all-fiber connections offered robust, reliable, compact and highly thermal damage threshold and promising pulsed laser in research, medical, military, and industrial applications.

Stable and reliable wavelength tunable passively Q-switched fiber lasers were successfully demonstrated by inserting a Bi_2Te_3-PVA thin film SAs.

First, a thin film SA device for tunable passively Q-switched EDFRL was demonstrated using a total bidirectional pumping power of 95 mW. It was stably operating at a tunable wavelength range of 32 nm (from 1538.2 nm to 1571 nm). The shortest pulse width that generated by this experiment with total cavity length about ~ 10.5 m was 6.725 μs with repetition rate of 19.231 kHz, as well as, the related output power spectrum was around 1542.52 nm central wavelength with output average power, pulse energy, peak pulse power, laser efficiency and SNR of 0.2685 mW, 13.13 nJ, 2 mW, 0.2807% and -62 dB, respectively. The longest pulse with observed to be 16.458 μs with repetition rate of 8.946 kHz, as well as, the related output power spectrum was around 1571 nm central wavelength with output average power, pulse energy, peak pulse power, the power transferring efficiency and SNR of 0.2931, 30.8 nJ, 1.9 mW, 0.3064% and -70 dB, respectively.

Second, an ultra thin film SA device fabricated by the new fabrication method for tunable passively Q-switched EDFRL was demonstrated by using unequally pumping powers in both directions, with a forward pumping power of 99.9 mW and a backward pumping power of 83.7 mW. The proposed EDFRL had a tunable wavelength range of 47.1 nm (from 1523.9 nm to 1571 nm). The shortest pulse width that realized by this experiments with total cavity length about ~10.5 m was 3.769 μs with repetition rate of 49.73 kHz, as well as, the corresponding output power spectrum at around 1529.45 nm central wavelength with output average power, pulse energy, peak pulse power, the power transferring efficiency and SNR of 0.7 mW, 12.9 nJ, 3.4 mW, 0.3716% and -67 dB, respectively. The highest observed pulse was 6.106 μs with a repetition rate of 20.661 kHz, as well as, the related output power spectrum was around 1571 nm central wavelength with output average power, pulse energy, peak pulse power, power conversion efficiency and SNR of 1.0 mW, 44.56 nJ, 7.3 mW, 0.5334% and -60 dB, respectively.

A compact tunable passively Q-switched EDFRL was demonstrated by using unequal pumping powers in both directions, with a forward pumping power of 112 mW and a backward pumping power of 67.9 mW. The proposed EDFRL had tunable wavelength range 47 nm (from 1523.45 nm to 1571.15 nm). The shortest pulse width that realized by this experiment with total cavity length about ~10.5 m was 3.975 µs with repetition rate of 46.88 kHz, as well as, the related output power spectrum was around 1527.8 nm central wavelength with output average power, pulse energy, peak pulse power, power conversion efficiency and SNR of 1.1 mW, 21.39 nJ, 5.4 mW, 0.593% and -67 dB, respectively. The highest observed pulse was 6.869 µs with repetition rate of 17.724 kHz, as well as, the related output power spectrum was around 1571.15 nm central wavelength with output average power, pulse energy, peak pulse power, power conversion efficiency and SNR of 0.9 mW, 48.1467 nJ, 7 mW, 0.5048% and -57 dB, respectively.

Another wavelength tunable passively Q-switched EDFRL was demonstrated using forward pumping method with a power of 261.9 mW. The proposed EDFRL had tunable wavelength range 35 nm (from 1535.6 nm to 1571 nm). The shortest pulse width generated by this experiment with total cavity length about ~10.5 m was 3.719 µs with repetition rate of 45.37 kHz, as well as, the corresponding output power spectrum at around 1544.15 nm central wavelength with output average power, pulse energy, peak pulse power, power conversion efficiency and SNR of 0.7 mW, 13.91 nJ, 3.7 mW, 0.2563% and -70 dB, respectively. The highest observed pulse was 6.4 µs with a repetition rate of 20.525 kHz, as well as, the corresponding output power spectrum at around 1571 nm central wavelength with output average power, pulse energy, peak pulse power, power conversion efficiency and SNR of 1.2 mW, 54.56 nJ, 8.5 mW, 0.4548% and -59 dB, respectively.

Both the passively Q-switched and wavelength tunable passively Q-switched experiments have revealed that the new fabricated ultra thin film Bi_2Te_3-PVA SA has superiority over the thin film Bi_2Te_3-PVA SA that fabricated with ordinary casting method.

CHAPTER FIVE

MODE-LOCKED EDFRL OPERATING AT 1.5-MICRON REGION BASED ON Bi_2Te_3-PVA SATURABLE ABSORBER

5.1. INTRODUCTION

Passively mode-locking is the technique enabling pulsed laser operation with very short pulse durations, nanosecond, picoseconds and even femtoseconds time scales. Mode-locking is different from Q-switching principle where mode-locking depends on the interference of available modes in the cavity, by setting a fixed phase relationship of the cavity modes. Many factors play roles in mode-locking process like the cavity total dispersion, nonlinearity of the cavity and the ions doping ratio in the cavity gain medium. All these factors need to be well and carefully balanced to acquire a stable mode-locked operation. Unlike, Q-switching that depends on the Quality factor (Q-factor) switching between the high and low values. The repetition rate in mode-locking technique is equivalent to the inverse of the cavity round-trip time, which is not the only factor that influences the Q-switching laser repletion rate.

Recently, substantial research efforts have been focused on compact ultrafast fiber lasers due to their significant applications. Active modulation techniques are usually enabled ultrafast fibers by generating ultra fast pulses that have advantages such as low timing jitters and high repetition rates. These systems also have disadvantages, such as, complexity and high cost and therefore not particularly suited for deployment in compact systems or high-density networks. In additional to the higher risk of instability due to external perturbations and large super mode-noises. An alternative approaches, passive modulation techniques (use of semiconductor saturable absorber mirrors (SESAMs) or non-polarization rotation), are used to reduce these issues. However, it can be difficult to implement these techniques, such as, requiring fine adjustments to the cavity design, or incurring varying degrees of cost and complexity, thereby limiting their usage as well as rendering the development of a compact ultrafast fiber laser unfeasible. An interesting way in realizing the passively mode-locked fiber laser is by incorporating a broadband saturable absorber (SA) within the laser cavity, such that tunability can be provided over a wide wavelength range. For this purpose, passively mode-locked fiber lasers based on saturable absorbers (SAs) , such as, carbon nanotubes CNTs (N. Kasim, et al, 2014), transition metal dichalcogenides (TMDs) (B. Chen, et.al, 2015), black phosphorous (J. Sotor, et.al, 2015, S. B. Lu et al., 2015), topological insulators (TIs) and two-dimensional materials 2D (N. F. Zulkipli et al., 2021) have been utilized. Bi_2Te_3 is one of the topological insulators family which, have a conductivity shielded state on its edge and surface in addition to a large band gap (M.

Z. Hasan & C. L. Kane, 2010; G. Wang et al., 2010). TIs topological insulators have unique properties as they have a nonlinear super wavelength optical response from visible to microwave (H. Zhang et al., 2009) due to the co-interaction between the small bulky-gap band and the zero-gap surface state due to the effects of spin-orbit interactions and time-reversal symmetry (X. Zhang, 2010). TIs was considered as one of the few alternative materials suitable for conventional saturable absorbers as a result of the researches that showed a wide pulse range from infrared to mid-infrared (Z. Luo et al., 2013; M. Jung et al., 2014; H. Yu et al., 2013; J. Sotor et al., 2014; Y. Lin et al., 2014; H. Liu et al., 2014; P. Tang et al., 2013; J. Sotor, 2014; J. Lee et al., 2014; Z. Luo et al., 2013; Z. Yu et al., 2014).

In recent years, nanosecond pulsed fiber lasers draw attention due to its ability to produce high pulse energy by modulating the optical loss in the laser cavity using passive elements, SAs. As for nanosecond pulse generation, due to the short recovery time of the SA, it is generally difficult for realizing mode-locked fiber laser with the passive methods. A widely utilized method for obtaining a stable pulse train is extending the cavity length (F. S. M. Samsamnun, et al., 2019). In this work, we successfully achieved nanosecond mode-locked erbium doped fiber ring laser (EDFRL) based on ultra thin film Bi_2Te_3-PVA SA.

Ultra thin film Bi_2Te_3-PVA SA is seen as a viable alternative towards the former systems, with high potential for practical, real-world applications. Used as a saturable absorber (SA), ultra thin film Bi_2Te_3-PVA SA can generate the desired mode-locking pulses without complexity or costs.

This chapter starts with the demonstration of ultra thin film Bi_2Te_3-PVA SA based mode locked in a simple ring cavity EDFRL. Further development of the setup was made by inserting different lengths of SMF-28 into the mode-locked laser cavity to produce a tunable ultra thin film Bi_2Te_3-PVA SA based mode-locked EDFRL.

5.2. EXPERIMENTAL SET UP OF MODE-LOCKED EDFRL OPERATING AT 1.5-MICRON REGION USING ULTRA THIN FILM Bi_2Te_3-PVA SA

Figure 5.1 shows ultra thin film Bi_2Te_3-PVA SA based mode-locked EDFRL configuration operating at 1.5 micron region. The output of EDFRL was taken from the 10% port of the output coupler with a 90%-10% splitting ratio and then splitted into two ports, to observe the optical spectrum of the output signal at one port using an optical spectrum analyzer (OSA Anritsu MS9710B), and to analyze the pulse waveforms at the other port using an InGaAs 5GHz photodiode (Thorlabs-DET08CFC/M) connected to an oscilloscope (Keysight-DSOX2002A). In the experimental setup a polarization controller (PC) was used to keep the polarization state of the oscillating wave under control. Several lengths from standard single mode fiber SMF-28 has been used to have a stable self starting mode-locked operation as well as to balance the self phase modulation effect. The schematic representation for the experimental setup for bidirectional and forward pumping where the 1'st LD and 2'nd LD are both on in bidirectional pumping method and 2'nd LD was off at forward pumping method.

Figure 5.1: Mode-Locked EDFRL Cavity

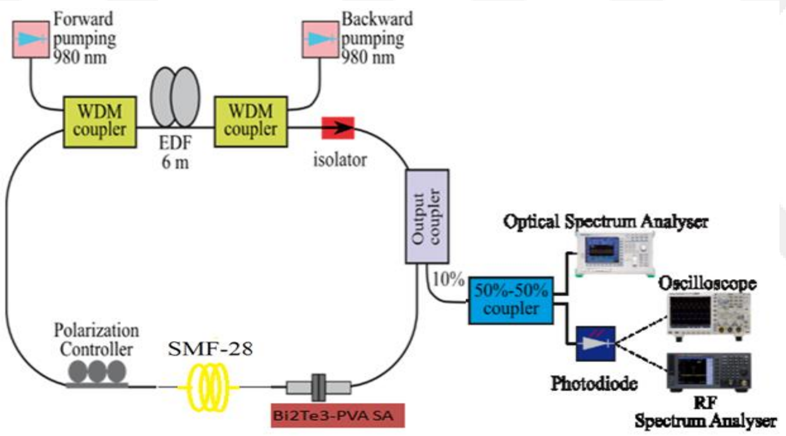

Different single mode fiber lengths used in these experiments, 171.5 m, 201.5 m, 213 m, 231.5 m, 303 m and 346 m. As a result of adding each length of SMF-28 to the EDFRL cavity, an anomalous dispersion regime and accompanying group velocity scattering (GVD) were obtained, as shown in Figure 5.2. The total cavity dispersion and GVD were calculated by considering the dispersion coefficients of each fiber types EDF (Liekki Er-30), SMF-28, and WDM HI1060 of -9.8 ps^2/(nm.km), 18.32 ps^2/(nm.km), and 7 ps^2/(nm.km), respectively, at 1560 nm and substituting their values into Equations 2.21 and 2.22.

Figure 5.2: The Total Dispersion and GVD as a Function of the Total Cavity Length in EDFRL

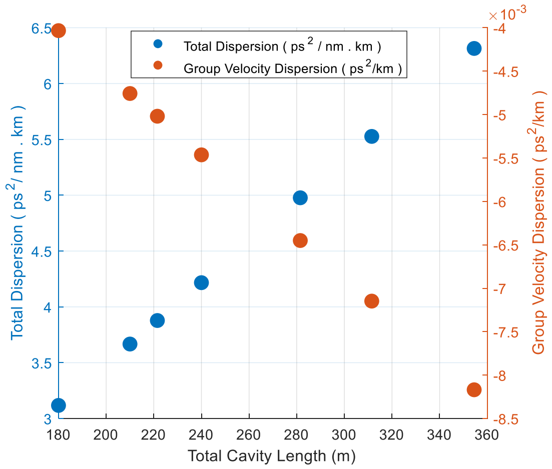

The EDFRL systems produced variety of pulse widths and frequencies as explained in details bellow:

5.3. MODE-LOCKED EDFRL OPERATING AT 1.5-MICRON REGION USING ULTRA THIN FILM Bi_2Te_3-PVA SA FOR BIDIRECTIONALY PUMPING METHOD

In the first experiment 171.5 m of SMF-28 and bidirectional pumping method was used as in mode-locked EDFRL configuration shown in Figure 5.1. The shortest pulse width generated by this experiment with total cavity length about 181 m was 554 ns as shown in Figure 5.3a, the corresponding output power spectrum at 1561.62 nm central wavelength, as in Figure 5.3b. Whereas Figure 5.3c shows the RF power spectrum where the SNR of 47.02 dB and the repetition rate of 950.1 KHz, were respectively.

The pulse train started to appear at threshold bidirectional pumping power of 161.3 mW with pulse width of 557 ns, repetition rate of 948.8 kHz, SNR of -60.7 dB, output average power of 1.2 mW, pulse energy of 1.244 nJ, pulse peak power of 2.2 mW and power conversion efficiency of 0.7316%. Whereas, the laser worked efficiently up to the bidirectional pumping power of 365.4 mW, and at this pumping power the pulse width, the repetition rate, the output power, the pulse energy, the peak power, and the power conversion efficiency were 554 ns, 950.1 kHz, 3.3 mW, 3.5178 nJ, 6.3 mW, and 0.9147%, respectively, as shown in Figure 5.4.

Figure 5.3: a) Pulse Shape, b) Optical Output Spectrum, and c) Electrical Output Spectrum of Bi_2Te_3 SA Based Mode-Locked EDFRL Measured with Bidirectional Pumping Power of 365.4 mW and S-SMF of 171.5 m.

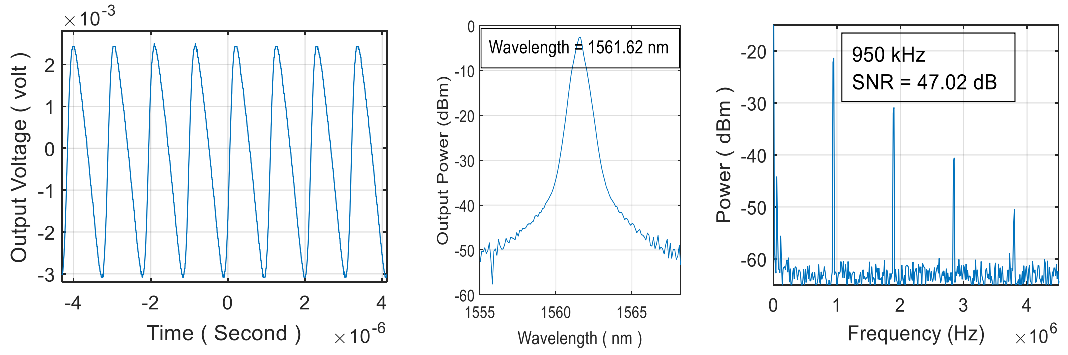

(a) (b) (c)

Figure 5.4: Mode-Locked Laser a) Output Power and Pulse Energy, b) Peak Pulse Power and Laser Efficiency, c) Pulse Width and Repetition Rate, of Bi_2Te_3 SA Based EDFRL Measured as A Function of the Bidirectional Pumping Power Range from 161.3 mW to 365.4 mW with SMF of 171.5 m.

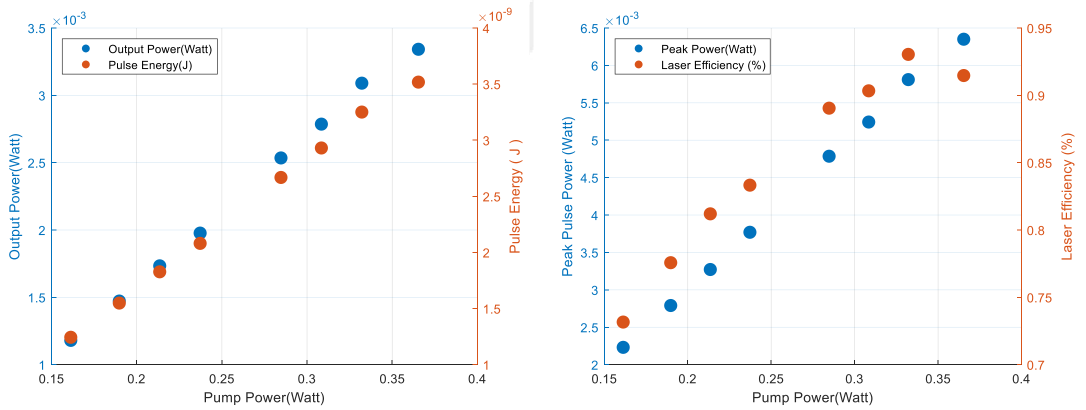

(a) (b)

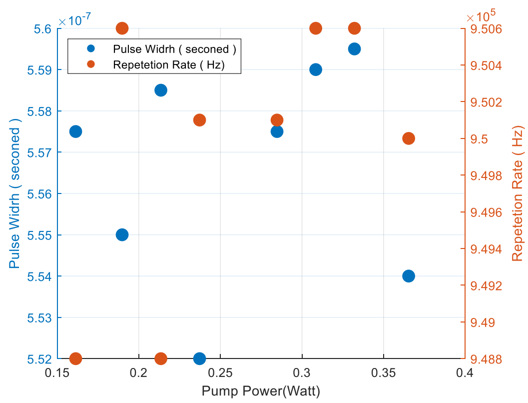

(c)

In the second experiment, 201.5 m of SMF-28 and bidirectional pumping method was used as in mode-locked EDFRL configuration shown in Figure 5.1.

The shortest pulse width generated by this experiment with total cavity length about 211 m was 638 ns as shown in Figure 5.5a, the corresponding output power spectrum at 1563.78 nm central wavelength, as in Figure 5.5b. Whereas Figure 5.5c shows the RF power spectrum where the SNR of 47.1 dB and the repetition rate of 826.5 kHz, were respectively.

The pulse train started to appear at threshold bidirectional pumping power of 84.5 mW with pulse width of 585 ns, repetition rate of 826.5 kHz, SNR of -61 dB, output average power of 0.4 mW, pulse energy of 0.4263 nJ, pulse peak power of 0.7 mW and laser extraction efficiency of 0.4172%. Whereas, the laser worked efficiently up to the bidirectional pumping power of 365.4 mW, and at this pumping power the pulse width, the repetition rate, the output power, the pulse energy, the peak power, and the laser efficiency were 638 ns, 826.5 kHz, 3.5 mW, 4.2341 nJ, 6.6 mW, and 0.9578%, respectively, as shown in Figure 5.6.

Figure 5.5: a) Pulse Shape, b) Optical Output Spectrum, and c) Electrical Output Spectrum of Bi_2Te_3 SA Based Mode-Locked EDFRL Measured with Bidirectional Pumping Power of 365.4 mW and S-SMF of 201.5 m.

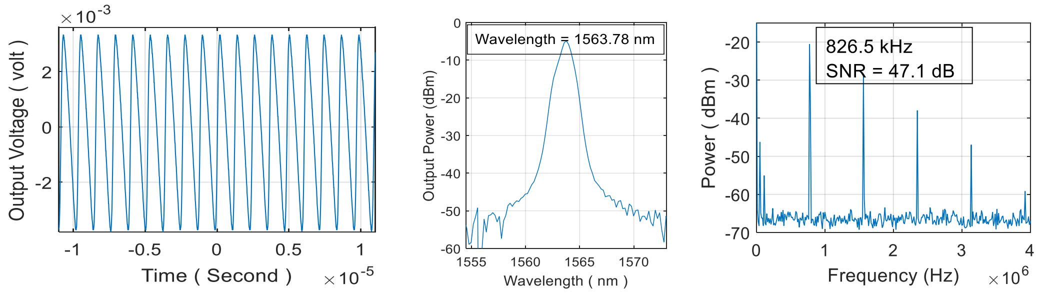

(a) (b) (c)

Figure 5.6: Mode-Locked Laser a) Output Power and Pulse Energy, b) Peak Pulse Power and Laser Efficiency, c) Pulse Width and Repetition Rate, of Bi_2Te_3 SA Based EDFRL Measured as A Function of the Bidirectional Pumping Power Range from 84.5 mW to 365.4 mW with SMF of 201.5 m.

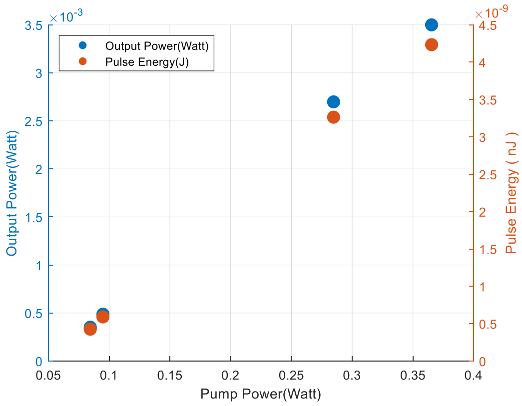

(a)

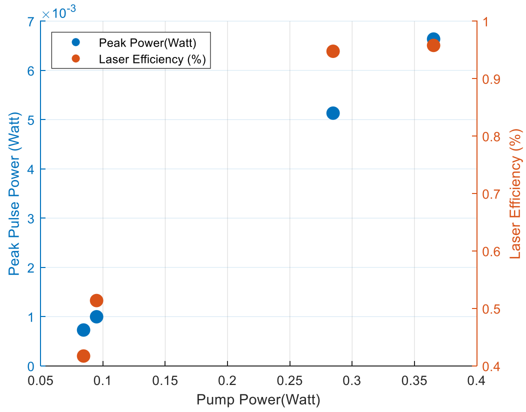

(b)

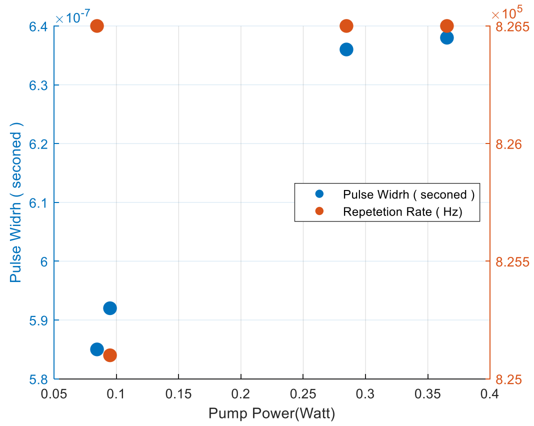

(c)

In the third experiment 213 m of SMF-28 and bidirectional pumping method was used as in mode-locked EDFRL configuration shown in Figure 5.1.

The shortest pulse width generated by this experiment with total cavity length about 222.5 m was 672 ns as shown in Figure 5.7a, the corresponding output power spectrum at 1561.98 nm central wavelength, as in Figure 5.7b. Whereas Figure 5.7c shows the RF power spectrum where the SNR of 49.95 dB and the repetition rate of 787.4 kHz, were respectively.

The pulse train started to appear at threshold bidirectional pumping power of 87.3 mW with pulse width of 567 ns, repetition rate of 784.9 kHz, SNR of -62.41 dB, output average power of 0.4 mW, pulse energy of 0.4583 nJ, pulse peak power of 0.7

mW and laser extraction efficiency of 0.4121%. Whereas, the laser worked efficiently up to the bidirectional pumping power of 365.4 mW, and at this pumping power the pulse width, the repetition rate, the output power, the pulse energy, the peak power, and the laser efficiency were 672 ns, 787.4 kHz, 3.5 mW, 4.4137 nJ, 6.6 mW, and 0.9512%, respectively, as shown in Figure 5.8.

Figure 5.7: a) Pulse Shape, b) Optical Output Spectrum, and c) Electrical Output Spectrum of Bi_2Te_3 SA Based Mode-Locked EDFRL Measured with Bidirectional Pumping Power of 365.4 mW and S-SMF of 213 m.

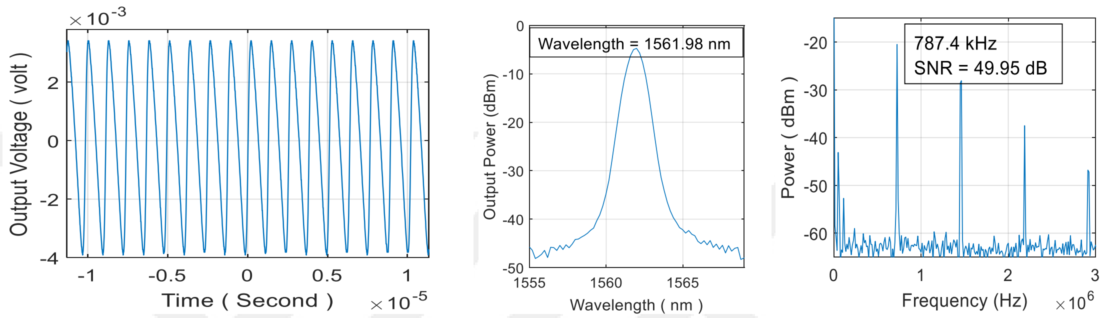

(a) (b) (c)

Figure 5.8: Mode-Locked Laser a) Output Power and Pulse Energy, b) Peak Pulse Power and Laser Efficiency, c) Pulse Width and Repetition Rate, of Bi_2Te_3 SA Based EDFRL Measured as A Function of the Bidirectional Pumping Power Range from 87.3 mW to 365.4 mW with SMF of 213 m.

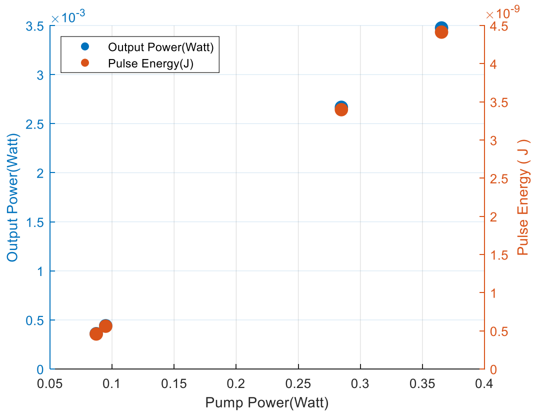

(a)

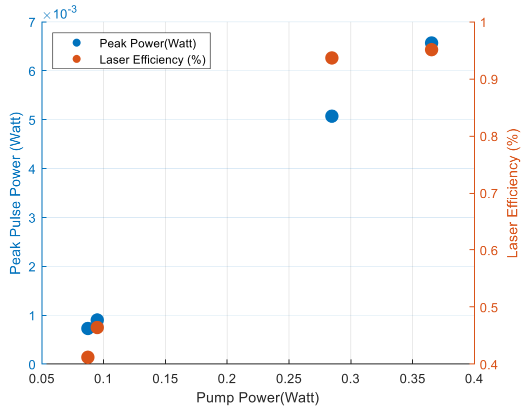

(b)

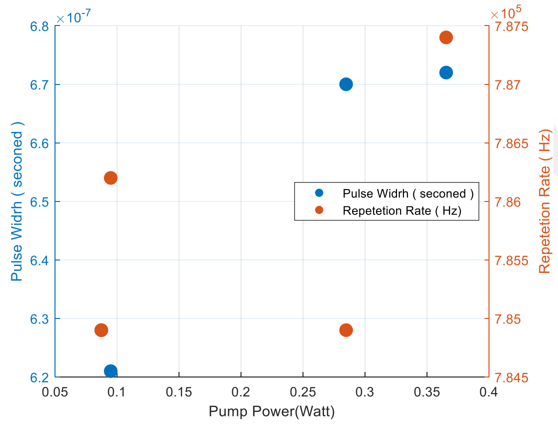

(c)

In the fourth experiment 231.5 m of SMF-28 and bidirectional pumping method was used as in mode-locked EDFRL configuration shown in Figure 5.1.

The shortest pulse width generated by this experiment with total cavity length about 241 m was 772 ns as shown in Figure 5.9a, the corresponding output power spectrum at 1562.82 nm central wavelength, as in Figure 5.9b. Whereas Figure 5.9c shows the RF power spectrum where the SNR of 48.5 dB and the repetition rate of 732.9 kHz, were respectively.

Figure 5.9: a) Pulse Shape, b) Optical Output Spectrum, and c) Electrical Output Spectrum of Bi_2Te_3 SA Based Mode-Locked EDFRL Measured with Bidirectional Pumping Power of 365.4 mW and S-SMF of 231.5 m.

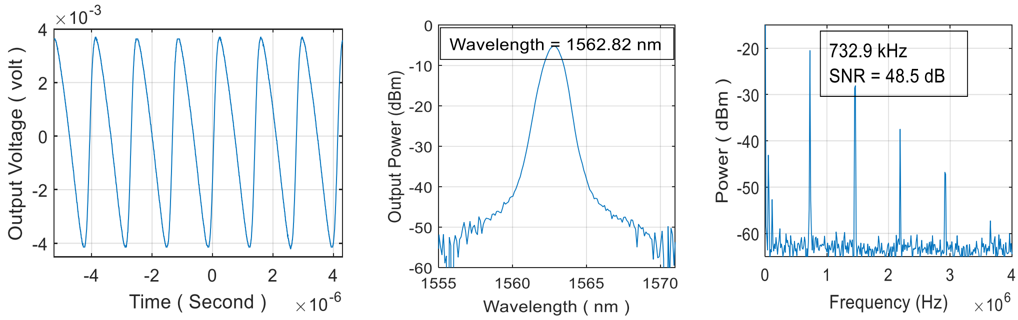

(a) (b) (c)

The pulse train started to appear at threshold bidirectional pumping power of 90.2 mW with pulse width of 677.5 ns, repetition rate of 730.2 kHz, SNR of -6.58 dB, output average power of 0.4 mW, pulse energy of 0.5553 nJ, pulse peak power of 0.8 mW and laser extraction efficiency of 0.4498%. Whereas, the laser worked efficiently up to the bidirectional pumping power of 365.4 mW, and at this pumping power the pulse width, the repetition rate, the output power, the pulse energy, the peak power, and the laser efficiency were 772 ns, 732.9 kHz, 3.5 mW, 4.7529 nJ, 6.6 mW, and 0.9534%, respectively, as shown in Figure 5.10.

Figure 5.10: Mode-Locked Laser a) Output Power and Pulse Energy, b) Peak Pulse Power and Laser Efficiency, c) Pulse Width and Repetition Rate, of Bi_2Te_3 SA Based EDFRL Measured as a Function of the Bidirectional Pumping Power Range from 90.2 mW to 365.4 mW with SMF of 231.5 m.

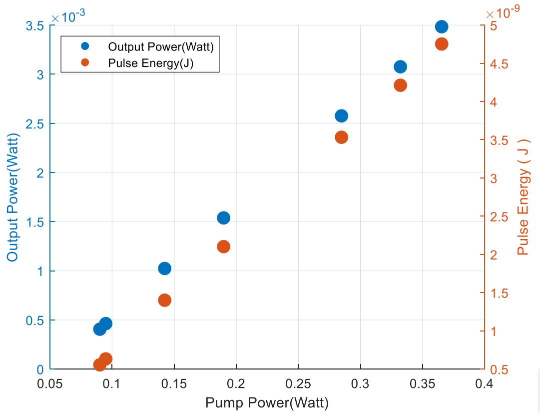

(a)

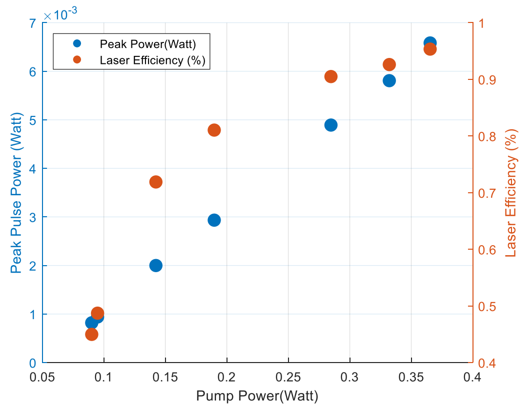

(b)

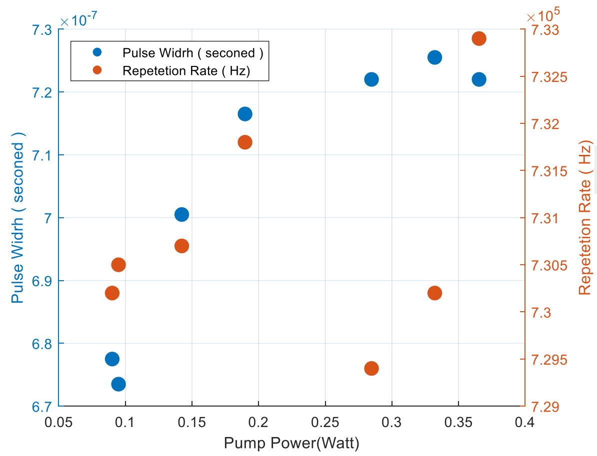

(c)

In the fifth experiment 303 m of SMF-28 and bidirectional pumping method was used as in mode-locked EDFRL configuration shown in Figure 5.1.

The shortest pulse width generated by this experiment with total cavity length about 312.5 m was 951 ns as shown in Figure 5.11a, the corresponding output power spectrum at 1561.38 nm central wavelength, as in Figure 5.11b. Whereas Figure 5.11c shows the RF power spectrum where the SNR of 45.58 dB and the repetition rate of 564 kHz, were respectively.

Figure 5.11: a) Pulse Shape, b) Optical Output Spectrum, and c) Electrical Output Spectrum of Bi_2Te_3 SA Based Mode-Locked EDFRL Measured with Bidirectional Pumping Power of 365.4 mW and S-SMF of 303 m.

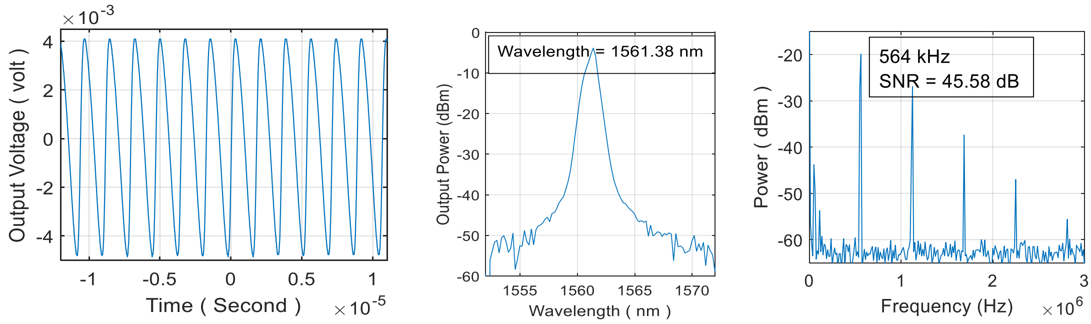

(a) (b) (c)

The pulse train started to appear at threshold bidirectional pumping power of 83.5 mW with pulse width of 796 ns, repetition rate of 563.4 kHz, SNR of -61 dB, output average power of 0.3 mW, pulse energy of 0.5464 nJ, pulse peak power of 0.7 mW and power conversion efficiency of 0.3683%. Whereas, the laser worked efficiently up to the bidirectional pumping power of 365.4 mW, and at this pumping power the pulse width, the repetition rate, the output power, the pulse energy, the peak power, and the laser efficiency were 796 ns, 563.4 kHz, 3.2 mW, 5.6457 nJ, 5.9 mW, and 0.8715%, respectively, as shown in Figure 5.12.

Figure 5.12: Mode-Locked Laser a) Output Power and Pulse Energy, b) Peak Pulse Power and Laser Efficiency, c) Pulse Width and Repetition Rate, of Bi_2Te_3 SA Based EDFRL Measured as A Function of the Bidirectional Pumping Power Range from 83.5 mW to 365.4 mW with SMF of 303 m.

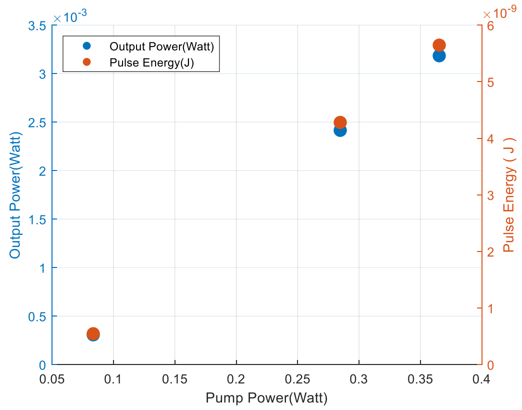

(a)

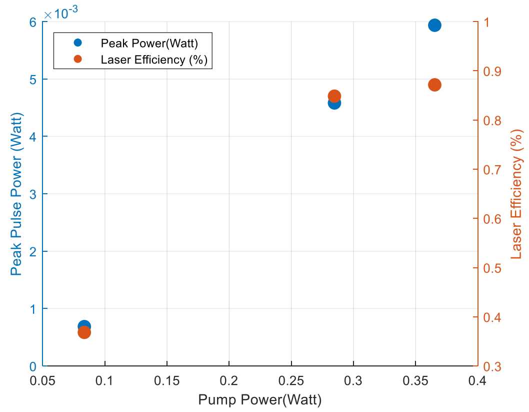

(b)

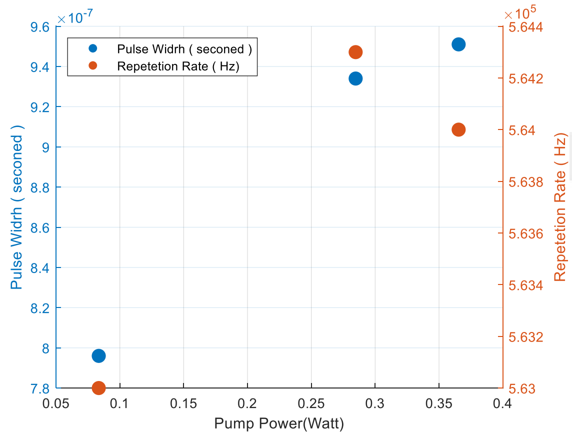

(c)

In the sixth experiment 346 m of SMF-28 and bidirectional pumping method was used as in mode-locked EDFRL configuration shown in Figure 5.1.

The shortest pulse width generated by this experiment with total cavity length about 355.5 m was 1051 ns as shown in Figure 5.13a, the corresponding output power spectrum at 1561.58 nm central wavelength, as in Figure 5.13b. Whereas Figure 5.13c shows the RF power spectrum where the SNR of 50.62 dB and the repetition rate of 503 kHz, were respectively.

Figure 5.13: a) Pulse Shape, b) Optical Output Spectrum, and c) Electrical Output Spectrum of Bi_2Te_3 SA Based Mode-Locked EDFRL Measured with Bidirectional Pumping Power of 365.4 mW and S-SMF of 346 m.

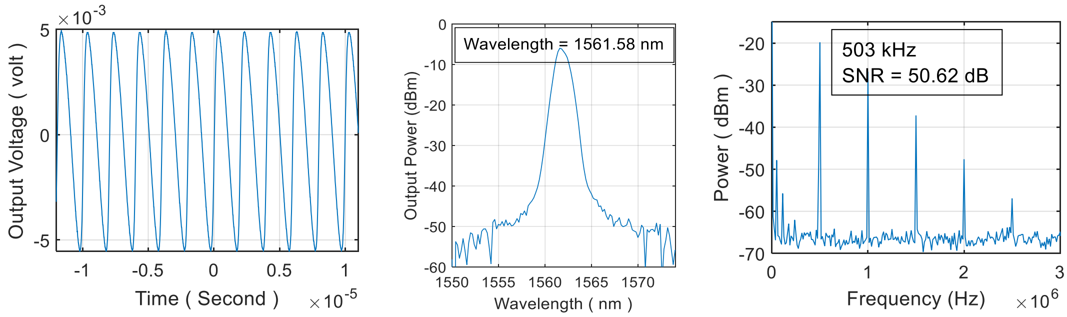

(a) (b) (c)

The pulse train started to appear at threshold bidirectional pumping power of 76.9 mW with pulse width of 831 ns, repetition rate of 501 kHz, SNR of -62.52 dB, output average power of 0.3 mW, pulse energy of 0.57 nJ, pulse peak power of 0.7 mW and power conversion efficiency of 0.3718%. Whereas, the laser worked efficiently up to the bidirectional pumping power of 365.4 mW, and at this pumping power the pulse width, the repetition rate, the output power, the pulse energy, the peak power, and the laser efficiency were 1051 ns, 503 kHz, 3.5 mW, 6.9093 nJ, 6.6 mW, and 0.9512%, respectively, as shown in Figure 5.14.

Figure 5.14: Mode-Locked Laser a) Output Power and Pulse Energy, b) Peak Pulse Power and Laser Efficiency, c) Pulse Width and Repetition Rate, of Bi_2Te_3 SA Based EDFRL Measured as A Function of the Bidirectional Pumping Power Range from 76.9 mW to 365.4 mW with SMF of 346 m.

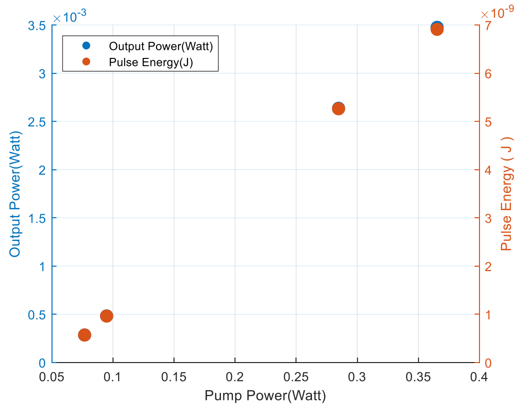

(a)

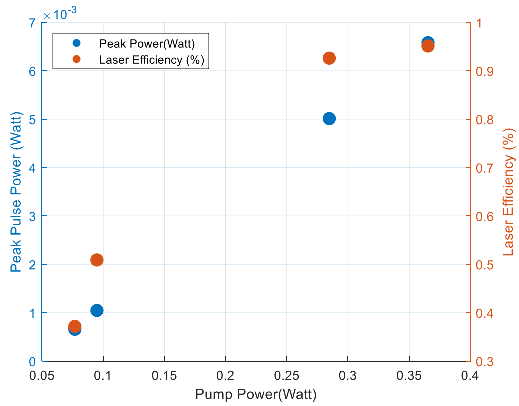

(b)

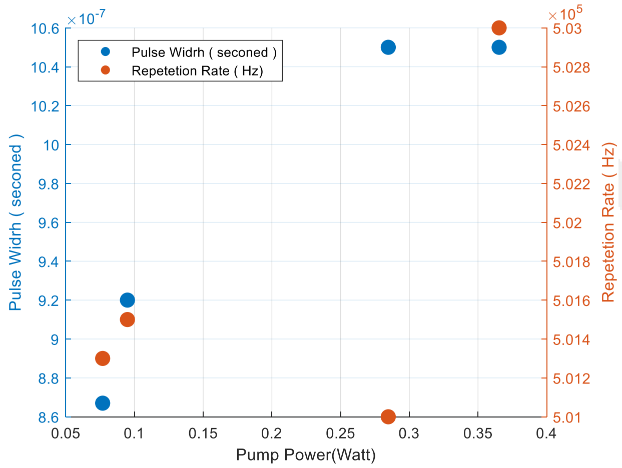

(c)

5.4. MODE-LOCKED EDFRL OPERATING AT 1.5-MICRON REGION USING ULTRA THIN FILM Bi_2Te_3-PVA SA FOR FORWARD PUMPING METHOD

In the first experiment 171.5 m of SMF-28 and forward pumping method was used as in mode-locked EDFRL configuration shown in Figure 5.1. The forward pumping method indicates as mentioned before that the1'st LD was on and the other LD was off.

The shortest pulse width generated by this experiment with total cavity length about 181 m was 558.5 ns as shown in Figure 5.15a, the corresponding output power spectrum at 1562.4 nm central wavelength, as in Figure 5.15b. Whereas Figure 5.15c shows the RF power spectrum where the SNR of 45.33 dB and the repetition rate of 950.1 kHz, were respectively.

The pulse train started to appear at threshold forward pumping power of 168.3 mW with pulse width of 559.5 ns, repetition rate of 949.7 kHz, SNR of -60 dB, output average power of 1.0 mW, pulse energy of 1.001 nJ, pulse peak power of 1.8 mW and power conversion efficiency of 0.5648%. Whereas, the laser worked efficiently up to the forward pumping power of 284.7 mW, and at this pumping power the pulse width, the repetition rate, the output power, the pulse energy, the peak power, and the laser efficiency were 558.5 ns, 950.1 kHz, 1.8 mW, 1.8674 nJ, 3.3 mW, and 0.6232%, respectively, as shown in Figure 5.16.

Figure 5.15: a) Pulse Shape, b) Optical Output Spectrum, and c) Electrical Output Spectrum of Bi_2Te_3 SA Based Mode-Locked EDFRL Measured with Forward Pumping Power of 284.7 mW and S-SMF of 171.5 m.

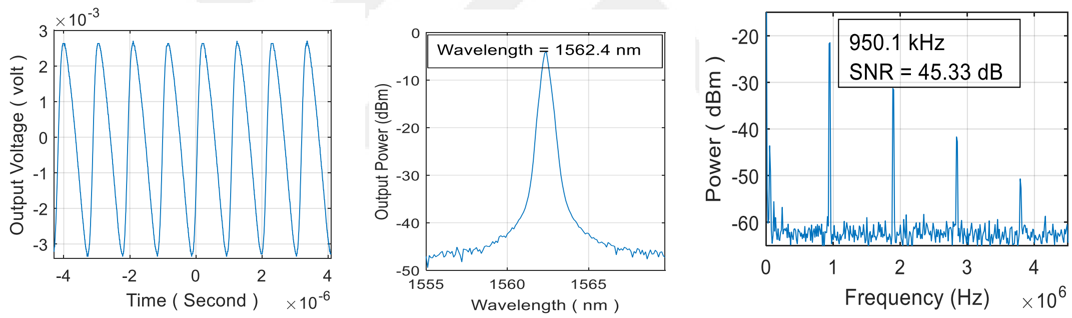

(a) (b) (c)

Figure 5.16: Mode-Locked Laser a) Output Power and Pulse Energy, b) Peak Pulse Power and Laser Efficiency, c) Pulse Width and Repetition Rate, of Bi_2Te_3 SA Based EDFRL Measured as A Function of the Forward Pumping Power Range From 168.3 mW to 284.7 mW with SMF of 171.5 m.

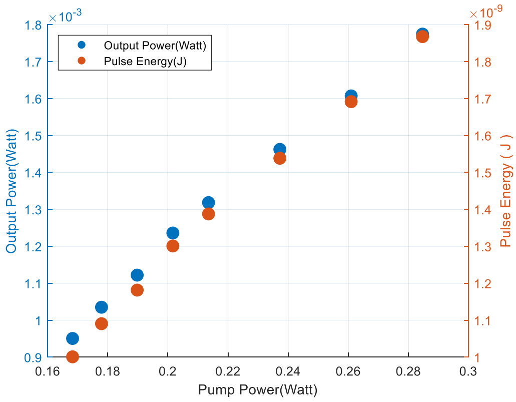

(a)

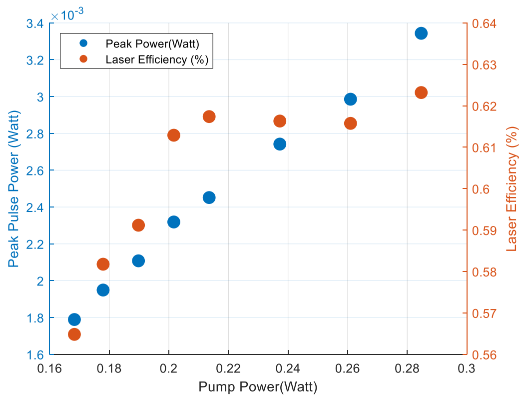

(b)

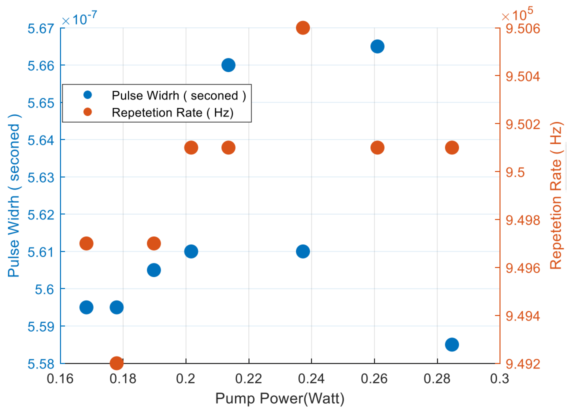

(c)

In the second experiment 201.5 m of SMF-28 and forward pumping method was used as in mode-locked EDFRL configuration shown in Figure 5.1. The forward pumping method indicates as mentioned before that the1'st LD was on and the other LD was off.

The shortest pulse width generated by this experiment with total cavity length about 211 m was 636 ns as shown in Figure 5.17a, the corresponding output power spectrum at 1564.98 nm central wavelength, as in Figure 5.17b. Whereas Figure 5.17c shows the RF power spectrum where the SNR of 46.04 dB and the repetition rate of 827.1 kHz, were respectively.

The pulse train started to appear at threshold forward pumping power of 68.8 mW with pulse width of 542 ns, repetition rate of 825.8 kHz, SNR of -57.66 dB, output average power of 0.2 mW, pulse energy of 0.235 nJ, pulse peak power of 0.4336 mW and power conversion efficiency of 0.2821%. Whereas, the laser worked efficiently up to the forward pumping power of 261 mW, and at this pumping power the pulse width, the repetition rate, the output power, the pulse energy, the peak power, and the laser efficiency were 636 ns,827.1 kHz, 1.7 mW, 2.1011 nJ, 3.3298 mW, and 0.6659%, respectively, as shown in Figure 5.18.

Figure 5.17: a) Pulse Shape, b) Optical Output Spectrum, and c) Electrical Output Spectrum of Bi_2Te_3 SA Based Mode-Locked EDFRL Measured with Forward Pumping Power of 261 mW and S-SMF of 201.5 m.

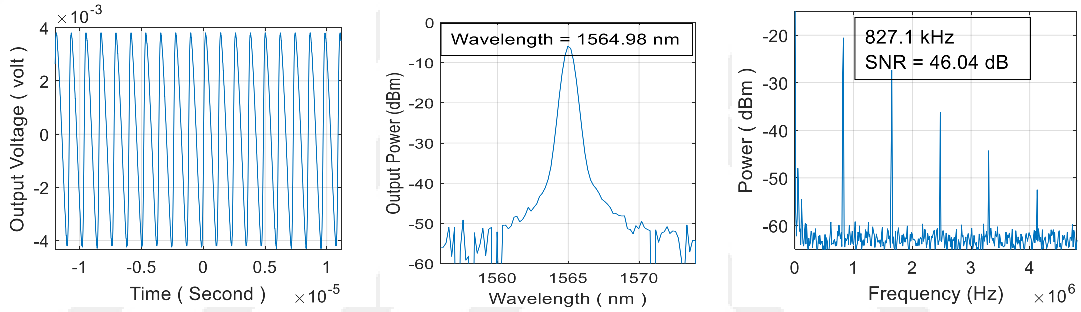

(a) (b) (c)

Figure 5.18: Mode-Locked Laser a) Output Power and Pulse Energy, b) Peak Pulse Power and Laser Efficiency, c) Pulse Width and Repetition Rate, of Bi_2Te_3 SA Based EDFRL Measured as A Function of the Forward Pumping Power Range from 68.8 mW to 261 mW with SMF of 201.5 m.

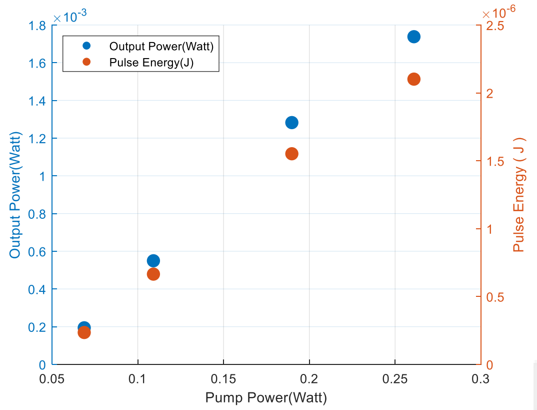

(a)

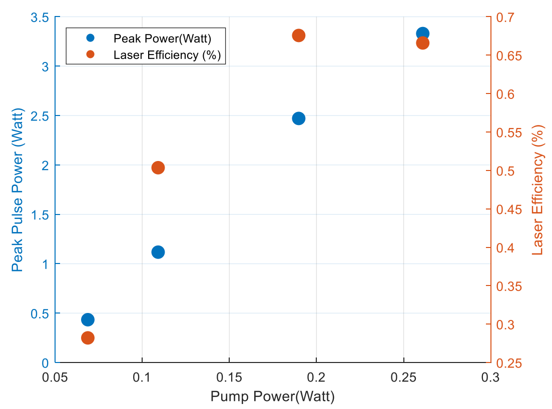

(b)

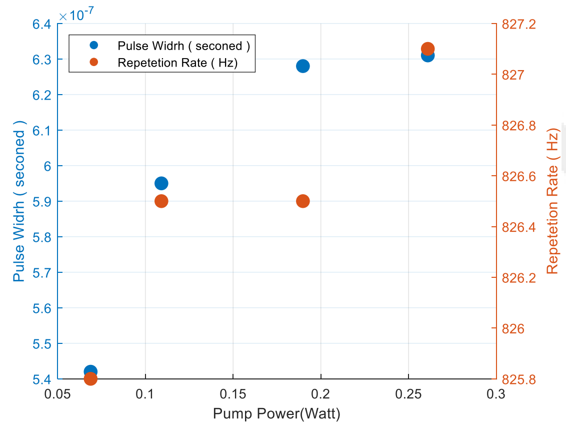

(c)

In the third experiment 213 m of SMF-28 and forward pumping method was used as in mode-locked EDFRL configuration shown in Figure 5.1. The forward pumping method indicates as mentioned before that the1'st LD was on and the other LD was off.

The shortest pulse width generated by this experiment with total cavity length about 222.5 m was 633 ns as shown in Figure 5.19a, the corresponding output power spectrum at 1562.58 nm central wavelength, as in Figure 5.19b. Whereas Figure 5.19c shows the RF power spectrum where the SNR of 46.65 dB and the repetition rate of 786.8 kHz, were respectively.

Figure 5.19: a) Pulse Shape, b) Optical Output Spectrum, and c) Electrical Output Spectrum of Bi_2Te_3 SA Based Mode-Locked EDFRL Measured with Forward Pumping Power of 261 mW and S-SMF of 213 m.

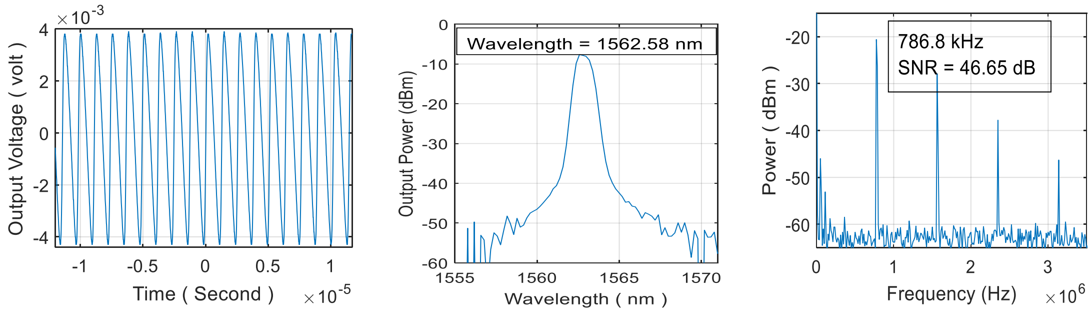

(a) (b) (c)

The pulse train started to appear at threshold forward pumping power of 78.3 mW with pulse width of 567 ns, repetition rate of 784.9 kHz, SNR of -60 dB, output average power of 0.2 mW, pulse energy of 0.3171 nJ, pulse peak power of 0.6 mW and power conversion efficiency of 0.3179%. Whereas, the laser worked efficiently up to the forward pumping power of 261 mW, and at this pumping power the pulse width, the repetition rate, the output power, the pulse energy, the peak power, and the laser efficiency were 633 ns, 786.8 kHz, 1.7 mW, 2.1684 nJ, 3.3 mW, and 0.6537%, respectively, as shown in Figure 5.20.

Figure 5.20: Mode-Locked Laser a) Output Power and Pulse Energy, b) Peak Pulse Power and Laser Efficiency, c) Pulse Width and Repetition Rate, of Bi_2Te_3 SA Based EDFRL Measured as A Function of the Forward Pumping Power Range from 78.3 mW to 261 mW with SMF of 213 m.

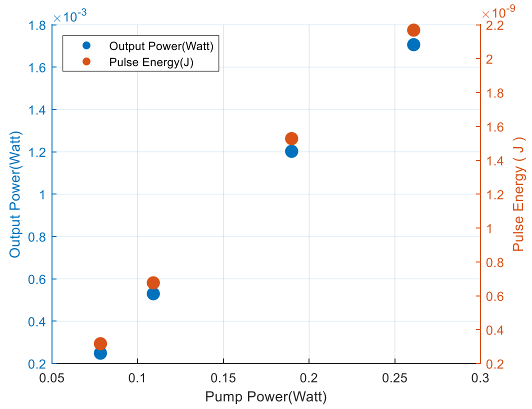

(a)

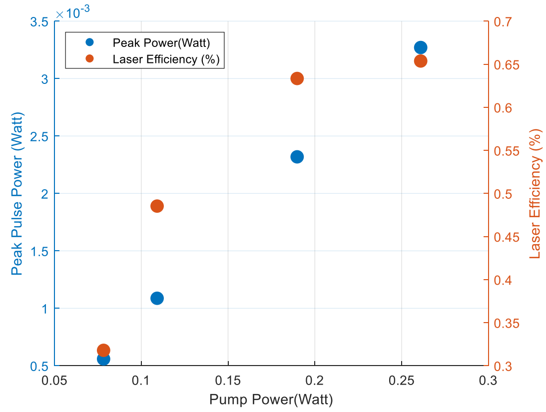

(b)

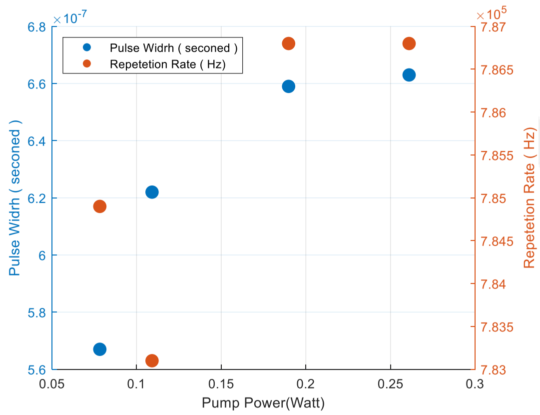

(c)

In the fourth experiment 231.5 m of SMF-28 and forward pumping method was used as in mode-locked EDFRL configuration shown in Figure 5.1. The forward pumping method indicates as mentioned before that the1’st LD was on and the other LD was off.

The shortest pulse width generated by this experiment with total cavity length about 241 m was 725 ns as shown in Figure 5.21a, the corresponding output power spectrum at 1562.02 nm central wavelength, as in Figure 5.21b. Whereas Figure 5.21c shows the RF power spectrum where the SNR of 46.33 dB and the repetition rate of 730.7 kHz, were respectively.

Figure 5.21: a) Pulse Shape, b) Optical Output Spectrum, and c) Electrical Output Spectrum of Bi_2Te_3 SA Based Mode-Locked EDFRL Measured with Forward Pumping Power of 284.7 mW and S-SMF of 231.5 m.

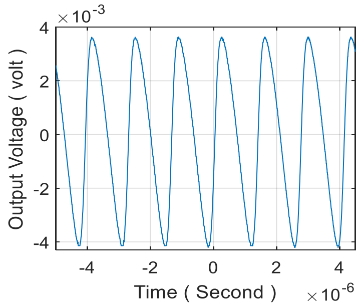

(a)

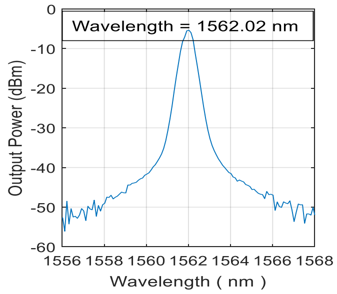

(b)

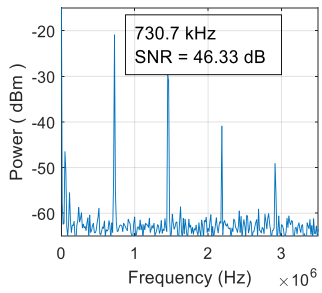

(c)

Figure 5.22: Mode-Locked Laser a) Output Power and Pulse Energy, b) Peak Pulse Power and Laser Efficiency, c) Pulse Width and Repetition Rate, of Bi_2Te_3 SA Based EDFRL Measured as A Function of the Forward Pumping Power Range from 122.1 mW to 284.7 mW with SMF of 231.5 m.

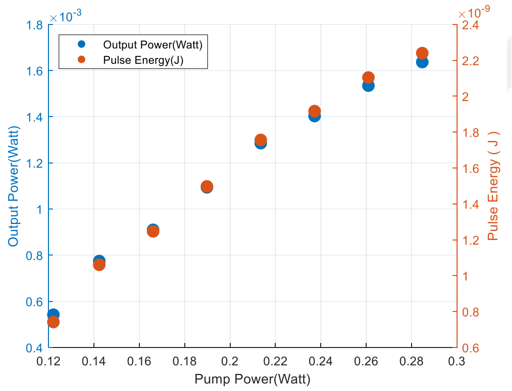

(a)

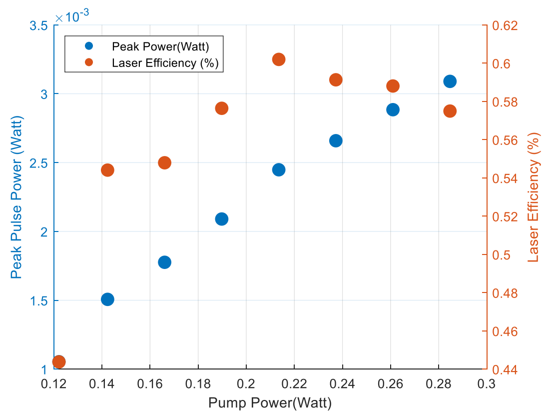

(b)

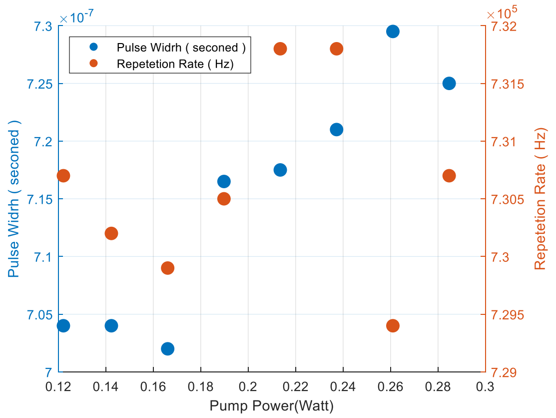

(c)

The pulse train started to appear at threshold forward pumping power of 122.1 mW with pulse width of 704 ns, repetition rate of 730.7 kHz, SNR of -65.5 dB, output average power of 0.5 mW, pulse energy of 0.7418 nJ, pulse peak power of 1.1 mW and power conversion efficiency of 0.4438%. Whereas, the laser worked efficiently up to the forward pumping power of 284.7 mW, and at this pumping power the pulse width, the repetition rate, the output power, the pulse energy, the peak power, and the laser efficiency were 725 ns, 730.7 kHz, 1.6 mW, 2.2401 nJ, 3.3 mW, and 0.5749%, respectively, as shown in Figure 5.22

In the fifth experiment 303 m of SMF-28 and forward pumping method was used as in mode-locked EDFRL configuration shown in Figure 5.1. The forward pumping method indicates as mentioned before that the1'st LD was on and the other LD was off.

The shortest pulse width generated by this experiment with total cavity length about 241 m was 895 ns as shown in Figure 5.23a, the corresponding output power spectrum at 1563.38 nm central wavelength, as in Figure 5.23b. Whereas Figure 5.23c shows the RF power spectrum where the SNR of 47.27 dB and the repetition rate of 730.7 kHz, were respectively.

Figure 5.23: a) Pulse Shape, b) Optical Output Spectrum, and c) Electrical Output Spectrum of Bi_2Te_3 SA Based Mode-Locked EDFRL Measured with Forward Pumping Power of 261 mW and S-SMF of 303 m.

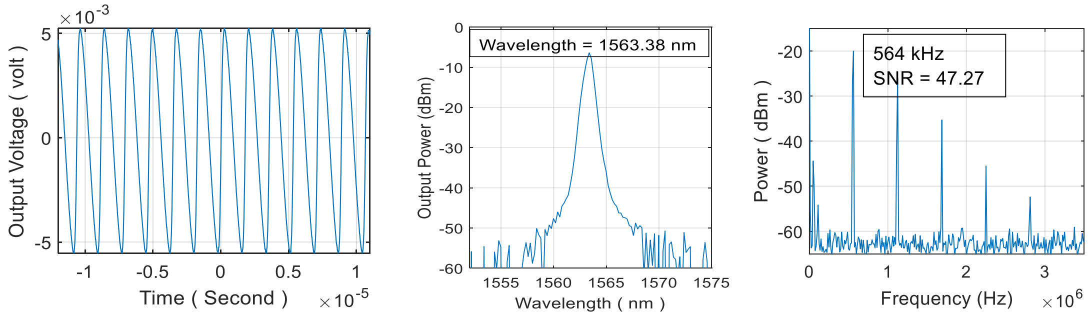

(a) (b) (c)

Figure 5.24: Mode-Locked Laser a) Output Power and Pulse Energy, b) Peak Pulse Power and Laser Efficiency, c) Pulse Width and Repetition Rate, of Bi_2Te_3 SA Based EDFRL Measured as A Function of the Forward Pumping Power Range from 66 mW to 261 mW with SMF of 303 m.

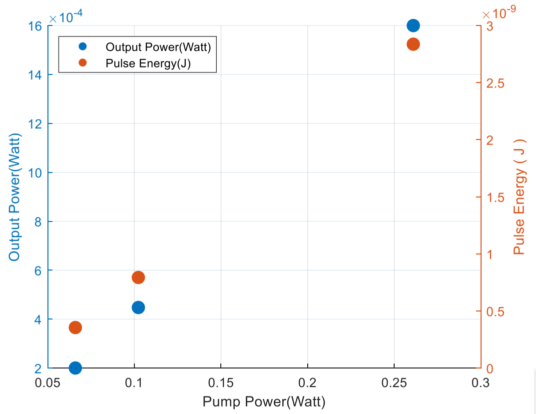

(a)

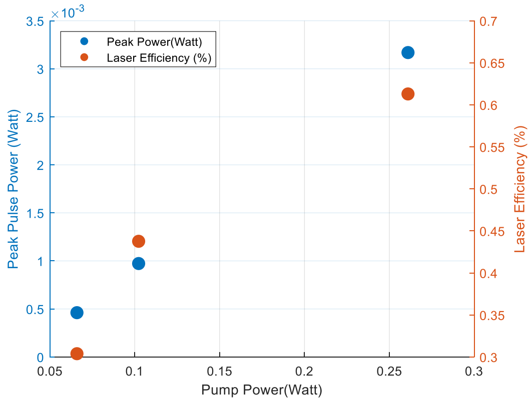

(b)

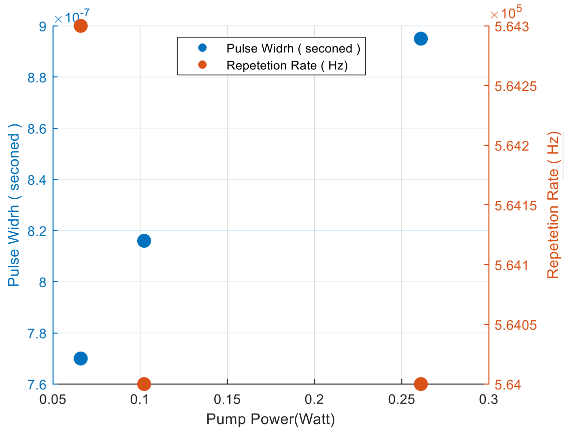

(c)

The pulse train started to appear at threshold forward pumping power of 66 mW with pulse width of 770 ns, repetition rate of 564 kHz, SNR of -60 dB, output average power of 0.2 mW, pulse energy of 0.3552 nJ, pulse peak power of 0.5 mW and power conversion efficiency of 0.3039%. Whereas, the laser worked efficiently up to the forward pumping power of 261 mW, and at this pumping power the pulse width, the repetition rate, the output power, the pulse energy, the peak power, and the laser efficiency were 895 ns, 564 kHz, 1.6 mW, 2.8361 nJ, 3.2 mW, and 0.6129%, respectively, as shown in Figure 5.24.

In the sixth experiment 346 m of SMF-28 and forward pumping method was used as in mode-locked EDFRL configuration shown in Figure 5.1. The forward pumping method indicates as mentioned before that the1'st LD was on and the other LD was off.

The shortest pulse width generated by this experiment with total cavity length about 355.5 m was 996 ns as shown in Figure 5.25a, the corresponding output power spectrum at 1562.38 nm central wavelength, as in Figure 5.25b. Whereas Figure 5.25c shows the RF power spectrum where the SNR of 52 dB and the repetition rate of 502 kHz, were respectively

Figure 5.25: a) Pulse Shape, b) Optical Output Spectrum, and c) Electrical Output Spectrum of Bi_2Te_3 SA Based Mode-Locked EDFRL Measured with Forward Pumping Power of 261 mW and S-SMF of 346 m.

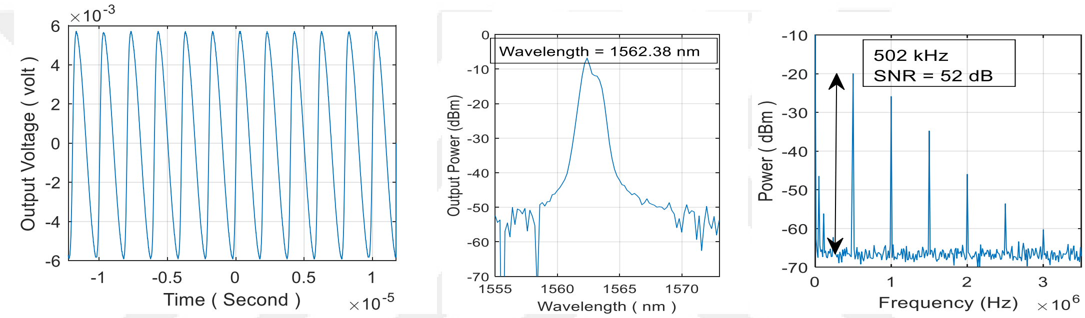

(a) (b) (c)

The pulse train started to appear at threshold forward pumping power of 62.6 mW with pulse width of 831 ns, repetition rate of 501 kHz, SNR of -58.57 dB, output average power of 0.2 mW, pulse energy of 0.3874 nJ, pulse peak power of 0.5 mW and power conversion efficiency of 0.3099%. Whereas, the laser worked efficiently up to the forward pumping power of 261 mW, and at this pumping power the pulse width, the repetition rate, the output power, the pulse energy, the peak power, and the laser efficiency were 996 ns, 502 kHz, 1.7 mW, 3.4143 nJ, 3.4 mW, and 0.7224%, respectively, as shown in Figure 5.26.

Figure 5.26: Mode-Locked Laser a) Output Power and Pulse Energy, b) Peak Pulse Power and Laser Efficiency, c) Pulse Width and Repetition Rate, of Bi_2Te_3 SA Based EDFRL Measured as A Function of the Forward Pumping Power Range From 62.6 mW to 261 mW with SMF of 346 m.

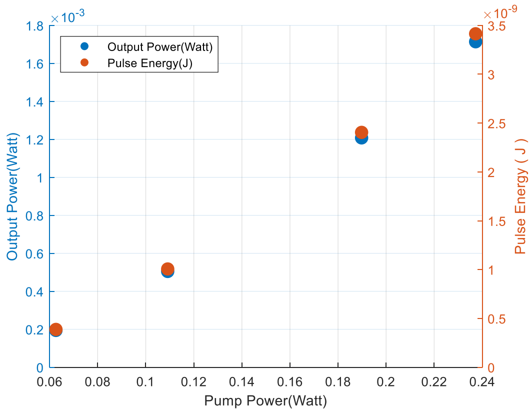

(a)

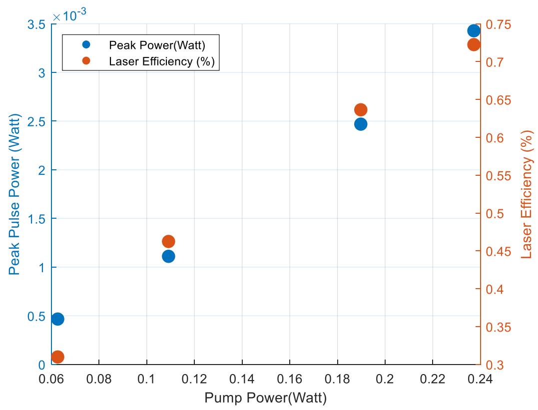

(b)

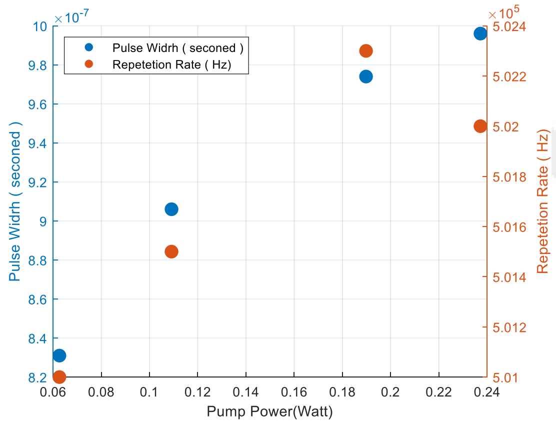

(c)

From the all mode-locked experiments made with using bidirectional and forward pumping methods one can notice the pulse width and the repetition rates are varying as a function of the SMF-28 length with using the same pump power. Figure 5.27a, shows the mode-locked EDFRLs output pulse width and repetition rates as a function to the SMF-28 fiber lengths at stable bidirectional pumping power of 365.4 mW, Figure.5.27b, shows the mode-locked EDFRLs output pulse width and repetition rates as a function to the SMF-28 fiber lengths at stable forward pumping power of 261 mW.

Figure 5.27: a) The Mode-Locked EDFRLs Output Pulse Width and Repetition Rates at Maximum Bidirectional Pumping Power of 365.4 mW and b) The Mode-Locked Edfrls Output Pulse Width and Repetition Rates at Forward Pumping Power of 261 mW, all as a Function to the SMF-28 Fiber Lengths

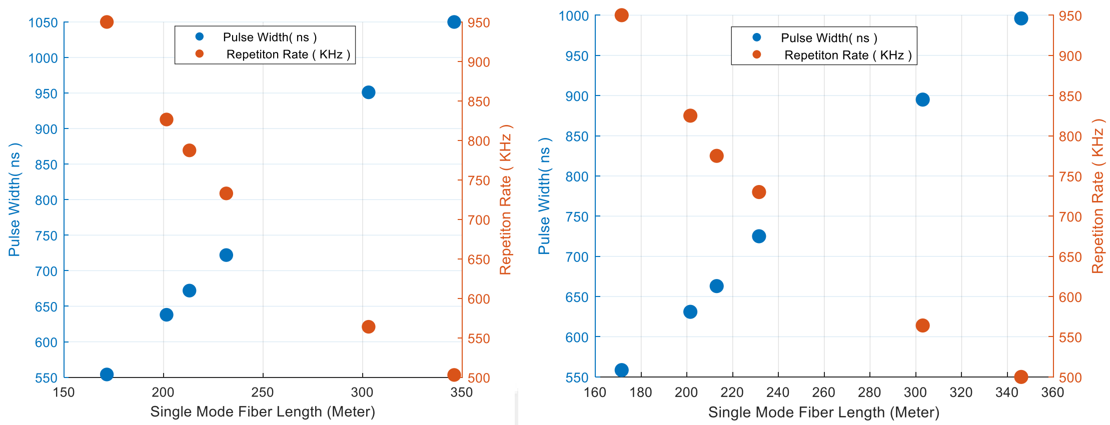

(a) (b)

5.5. SUMMARY

Stable and reliable passively mode locked EDFRLs were successfully demonstrated by integrating ultra thin film Bi_2Te_3 SA device, fabricated by the new fabrication method for passively mode-locked EDFRL, were demonstrated by adding various single mode fiber SMF-28 lengths with both bidirectional pumping and forward pumping methods.

When the ultra thin film Bi_2Te_3 SA device integrated inside the ring cavity of the EDFRL as a SA, nanosecond pulsed laser output is achieved at 1550 nm region, and a minimum pulse width of 554 ns, and a repetition rate of 0.950 MHz is observed with a 171.5 m SMF-28. The highest output power, peak power, pulse energy and peak laser efficiency were 3.3 mW, 6.3 mW, 3.5178 nJ, 6.3mW and 0.9147 maximum pump power for this length was 365.4 mW. The mode-locked EDFRLs output pulse width and repetition rates variations measured as a function of the SMF-28 fiber lengths at both stable bidirectional and forward pumping powers. These results indicate that the ultra thin Bi_2Te_3 SA has a promising application as SA for generating nanosecond mode locked EDFRL. Further studies are being focused on to achieve picoseconds pulses with ultra-thin film SA based EDFRLs.

CHAPTER SIX

CONCLUSION AND FUTURE WORK

6.1. CONCLUSION

In this thesis, novel saturable absorber device based on bismuth telluride was studied for developing Q-switched and mode-locked EDFRLs at 1.5 μm region. These lasers could facilitate a broad range of applications, including laser material processing, telecommunications, and medical diagnostics. The main achievements and findings of the present work can be summarized as follows:

1. Successful fabrication of a new kind ultra-thin film passive Bi_2Te_3 SA from already fabricated thin film SA.

2. Successful demonstration of various Q-switched EDFRLs based on ultra-thin film Bi_2Te_3 SA in 1.5-micron region.

3. Successful demonstration of various wavelength tunable Q-switched EDFRLs based on ultra-thin film Bi_2Te_3 SA in 1.5-micron region.

4. Successful demonstration of various mode-locked EDFRLs based on the ultra-thin film Bi_2Te_3 SA.

Stable and reliable passively Q-switched EDFRLs were successfully demonstrated by integrating a thin film Bi_2Te_3-PVA SA and an ultra-thin film Bi_2Te_3 SA. Specifically, very stable and reliable passively Q-switched, wavelength tunable passively Q-switched and passively mode-locked EDFRLs were proposed using an ultra-thin film Bi_2Te_3 SA.

Firstly, an ultra-thin film Bi_2Te_3 SA based passively Q-switched EDFRL was demonstrated using bidirectional pumping method. It was stably operating between 1565.23 nm and 1567.2 nm, with a wide repetition rate change from 6.9512 kHz to 63.37 kHz for a pump power range from 57.3 mW to 417.6 mW. At the maximum pump power, the highest output power and pulse energy of 3.8 mW and 65.459 nJ were obtained, respectively. Additionally, the maximum peak power of 22.3 mW, the lowest pulse width of 2.533 μs and the highest pulse repetition rate of 63.37 kHz were observed at the pump power of 417.6 mW.

Secondly, an ultra-thin film Bi_2Te_3 SA based wavelength tunable passively Q-switched EDFRL was demonstrated using unequally pumping powers in both directions, with a forward pumping power of 99.9 mW and a backward pumping power of 83.7 mW. The proposed EDFRL had a tunable wavelength range of 47.1 nm from

1523.9 nm to 1571 nm. The lowest pulse width observed in these experiments with a total cavity length of ~10.5 m was 3.769 μs with a repetition rate of 49.73 kHz. The corresponding output power spectrum was around 1529.45 nm with an output average power, pulse energy, peak pulse power, laser extraction efficiency and SNR of 0.7 mW, 12.9 nJ, 3.4 mW, 0.3716% and 67 dB, respectively. The highest observed pulse width was 6.106 μs with a repetition rate of 20.661 kHz. The corresponding output power spectrum was around 1571 nm with an output average power, pulse energy, peak pulse power, power conversion efficiency and SNR of 1.0 mW, 44.56 nJ, 7.3 mW, 0.5334% and 60 dB, respectively.

In addition, a wavelength tunable passively Q-switched EDFRL was demonstrated using unequal pumping powers in both directions with a forward pumping power of 112 mW and a backward pumping power of 67.9 mW. The proposed EDFRL had a tunable wavelength range of 47 nm from 1523.45 nm to 1571.15 nm. The lowest pulse width observed in this experiment for a total cavity length of ~10.5 m was 3.975 μs with a repetition rate of 46.88 kHz. The corresponding output power spectrum was around 1527.8 nm with an output average power, pulse energy, peak pulse power, power conversion efficiency and SNR of 1.1 mW, 21.39 nJ, 5.4 mW, 0.593% and 67 dB, respectively. The highest observed pulse width was 6.869 μs with a repetition rate of 17.724 kHz. The corresponding output power spectrum was around 1571.15 nm with an output average power, pulse energy, peak pulse power, laser extraction efficiency and SNR of 0.9 mW, 48.1467 nJ, 7 mW, 0.5048% and 57 dB, respectively.

Another wavelength tunable passively Q-switched EDFRL result was demonstrated using forward pumping method with a power of 261.9 mW. The proposed EDFRL had a tunable wavelength range of 35 nm from 1535.6 nm to 1571 nm. The lowest pulse width generated in this experiment for a total cavity length of ~10.5 m was 3.719 μs with a repetition rate of 45.37 kHz. The corresponding output power spectrum was around 1544.15 nm with an output average power, pulse energy, peak pulse power, power conversion efficiency and SNR of 0.7 mW, 13.91 nJ, 3.7 mW, 0.2563% and 70 dB, respectively. The highest observed pulse width was 6.4 μs with a repetition rate of 20.525 kHz. The corresponding output power spectrum was around 1571 nm with an output average power, pulse energy, peak pulse power, power conversion efficiency and SNR of 1.2 mW, 54.56 nJ, 8.5 mW, 0.4548% and 59 dB, respectively.

Thirdly, an ultra-thin film Bi_2Te_3 SA device fabricated with the newly method for passively mode-locked EDFRL was demonstrated by adding a 171.5 m SMF-28 standard fiber within the Q-switched EDFRL cavity and using a bidirectional pumping power range from 161.3 mW to 365.4 mW. The obtained results in these measurements were a pulse width range from 559.5 ns to 554 ns, a repetition rate range from 948.8 kHz to 950.6 kHz, an output average power range from 1.2 mW to 3.3 mW, a pulse energy range from 1.244 nJ to 3.5178 nJ, a pulse peak power range from 2.2 mW to 6.3 mW. Using the same length of SMF-28 fiber and a forward pumping power range from 168.3 mW to 284.7 mW, the obtained results in these measurements were a pulse width range from 831 ns to 996 ns, a repetition rate range from 501 kHz to 502.3 kHz, an output average power range from 1.0 mW to 1.8 mW, a pulse energy range from 1.001 nJ to 1.8674 nJ, a pulse peak power range from 1.8 mW to 3.3 mW and a laser extraction efficiency range from 0.5648% to 0.6232%.

The obtained results for ultra-thin film Bi_2Te_3 SA based passively mode-locked EDFRL with 201.5 m S-SMF and a bidirectional pumping power range from161.3 mW to 365.4 mW were the output pulse width, repetition rate, output average power, pulse energy, pulse peak power, and laser extraction efficiency of varying between (585 ns-638 ns), (825.1 kHz-826.5 kHz), (0.4 mW-3.5 mW), (0.4263 nJ-4.2341 nJ), (0.7 mW-6.6 mW) and (0.4172%-0.9578), respectively.

The obtained results for ultra-thin film Bi_2Te_3 SA based passively mode-locked EDFRL with 201.5 m S-SMF and a forward pumping power range from 68.8 mW to 261 mW were the output pulse width, repetition rate, output average power, pulse energy, pulse peak power, and laser extraction efficiency of varying between (542 ns–631 ns), (825.8 kHz–827.1 kHz), (0.2 mW-1.7 mW), (0.235 nJ–2.1011 nJ), (0.4336 mW-3.3298 mW) and (0.282%-0.6659%), respectively.

The obtained results for ultra-thin film Bi_2Te_3 SA based passively mode-locked EDFRL with 213m S-SMF and a bidirectional pumping power range from 87.3 mW to 365.4 mW were the output pulse width, repetition rate, output average power, pulse energy, pulse peak power, and laser extraction efficiency of varying between (621 ns-672 ns), (784.9 kHz-787.4 kHz), (0.4 mW-3.5 mW), (0.4583 nJ-4.4137 nJ), (0.7 mW-6.6 mW) and (0.4121%-0.9512%), respectively.

The obtained results for ultra-thin film Bi_2Te_3 SA based passively mode-locked EDFRL with 213m S-SMF and a forward pumping power range from 78.3 mW to 261 mW were the output pulse width, repetition rate, output average power, pulse energy, pulse peak power, and laser extraction efficiency of varying between (567 ns-663 ns), (783.1 kHz-786.8 kHz), (0.2 mW-1.7 mW), (0.3171 nJ-2.1684 nJ), (0.6 mW-3.3 mW) and (0.3179%-0.6537%), respectively.

The obtained results for ultra-thin film Bi_2Te_3 SA based passively mode-locked EDFRL with 231.5 m S-SMF and a bidirectional pumping power range from90.2 mW to 365.4 mW were the output pulse width, repetition rate, output average power, pulse energy, pulse peak power, and laser extraction efficiency of varying between (673.5 ns-725.5 ns), (729.4 kHz-732.9 kHz), (0.4 mW-3.5 mW), (0.5553 nJ-4.7529 nJ), (0.8 mW-6.6 mW) and (0.4498%-0.9534), respectively.

The obtained results for ultra-thin film Bi_2Te_3 SA based passively mode-locked EDFRL with 231.5 m S-SMF and a forward pumping power range from 122.1 mW to 284.7 mW were the output pulse width, repetition rate, output average power, pulse energy, pulse peak power, and laser extraction efficiency of varying between (702 ns-729.5 ns), (729.4 kHz-731.8 kHz), (0.5 mW-1.6 mW), (0.7418 nJ-2.2401 nJ), (1.1 mW-3.1 mW) and (0.4438%-0.5749%), respectively.

The obtained results for ultra-thin film Bi_2Te_3 SA based passively mode-locked EDFRL with 303 m S-SMF and a bidirectional pumping power range from 83.5 mW to 365.4 mW were the output pulse width, repetition rate, output average power, pulse energy, pulse peak power, and laser extraction efficiency of varying between (796 ns-951 ns), (563.4 kHz-564.3 kHz), (0.3 mW-3.2 mW), (0.5464 nJ-5.6457 nJ), (0.7 mW-5.9 mW) and (0.3683%-0.8715%), respectively.

The obtained results for ultra-thin film Bi_2Te_3 SA based passively mode-locked EDFRL with303 m S-SMF and a forward pumping power range from 66 mW to 261 mW were the output pulse width, repetition rate, output average power, pulse energy, pulse peak power, and laser extraction efficiency of varying between (770 ns-895 ns), (563.9 kHz-564 kHz), (0.2 mW-1.6 mW), (0.3552 nJ-2.8361 nJ), (0.5 mW-3.2 mW) and (0.3039% - 0.6129%), respectively.

The obtained results for ultra-thin film Bi_2Te_3 SA based passively mode-locked EDFRL with 346 m S-SMF and a bidirectional pumping power range from 76.9 mW to

365.4 mW were the output pulse width, repetition rate, output average power, pulse energy, pulse peak power, and laser extraction efficiency of varying between (867 ns-1051 ns), (501 kHz-503 kHz), (0.3 mW-3.5 mW), (0.57 nJ-6.9093 nJ), (0.7 mW-6.6 mW) and (0.3718%-0.9512), respectively.

The obtained results for ultra-thin film Bi_2Te_3 SA based passively mode-locked EDFRL with 346 m S-SMF and forward pumping power range from 62.6 mW to 237.2 mW were the output pulse width, repetition rate, output average power, pulse energy, pulse peak power, and laser extraction efficiency of varying between (831 ns-996 ns), (501 kHz-502.3 kHz), (0.2 mW-1.7 mW), (0.3874 nJ-3.4143 nJ), (0.5 mW-3.4 mW) and (0.3099%- 0.7224%), respectively.

As a result, ultra-thin film Bi_2Te_3 SAs have offered a robust, reliable, compact with a high thermal damage threshold operation for both passively Q-switched and tunable passively Q-switched EDFRL.

6.2. FUTURE WORK

Future work should be devoted to enhancing the performance of the proposed Q-switched and mode-locked EDFRL structures for decreasing the pulse width as well as increasing the repetition rate, output power and pulse energy. This can be achieved by addressing a shorter cavity length and enhanced gain medium. Additionally, a future work should focus on exploring the developed ultra-thin film SA at other wavelength regions such as 1µm, 2 µm and 3 µm using Ytterbium-doped fiber (YDF), Thulium-doped fiber (TDF) and ZBLAN-EDF as the gain medium, respectively.

APPENDEX

Lu2O3 İnce Film Tabanlı Doyurulabilen Soğurucu ile Pasif Mod Kilitli Halka Tipi Fiber Lazer Tasarımı
Passively Mode-Locked Fiber Ring Laser using Lu2O3 Thin Film Based Saturable Absorber

2022 30th Signal Processing and Communications Applications Conference (SIU) | 978-1-6654-5092-8/22/$31.00 ©2022 IEEE | DOI: 10.1109/SIU55565.2022.9864845

Thoalfeqar Ali Razaq Alyasiri
Photonic Tech. App.and Research Center
Kütahya Dumlupınar University
Kütahya, Turkey

Serif Ali Sadik
Photonic Tech. App.and Research Center
Kütahya Dumlupınar University
Kütahya, Turkey

Firat Ertac Durak
Photonic Tech. App.and Research Center
Kütahya Dumlupınar University
Kütahya, Turkey

Nur Farhanah Zulkipli
Dept. of Physics, Faculty of Sci. and Tech.
Airlangga University
Surabaya, Indonesia

Ahmet Altuncu
Photonic Tech. App.and Research Center
Kütahya Dumlupınar University
Kütahya, Turkey

Sulaiman Wadi Harun
Dept. of Electrical Eng., Faculty of Eng.
University of Malaya
Kuala Lumpur, Malaysia

***Özetçe* —Bu çalışmada 1560.78 nm dalgaboyunda ışıma yapan, lutetiyum oksit (Lu2O3) ince film doyurulabilir soğurucu (SA) tabanlı, kararlı ve kompakt yapıda bir erbiyum katkılı halka tipi fiber lazer önerilmiştir. Halka tipi fiber kavite içerisinde Lu2O3 SA ve 231.5 m tek modlu fiber (SMF) kullanılarak, ileri ve geri yönlü iki pompa lazeri ile toplam 597.9 mW pompa gücü ile, 0.7315 MHz tekrarlama frekansına ve 735 ns darbe genişliğine sahip mod kilitli lazer darbeleri elde edilmiştir. 597.9 mW toplam pompa gücü ile, mod kilitli çıkış darbelerinin ortalama gücü -6.46 dBm olarak ölçülmüştür. RF spektrum analizörde EDFRL çıkış darbelerinin 0.7315 MHz temel frekansta 47.73 dB sinyal gürültü oranına sahip olduğu gözlemlenmiştir. Tasarlanan Lu2O3 SA tabanlı mod kilitli darbeli EDFRL'nin performansı, 1550 nm bölgesinde çalışan nanosaniye darbeli uygulamalarda kullanılabileceğini göstermiştir.**

Anahtar Kelimeler—fiber lazer, lutetiyum oksit, mod kilitli, doyurulabilir soğurucu.

***Abstract*—In this study, a stable and compact mode-locked erbium doped fiber ring laser (EDFRL) operating at 1560.78 nm is proposed based on lutetium oxide (Lu2O3) based saturable absorber (SA) thin film. By incorporating the Lu2O3 based SA film together with a 231.5 m long single-mode fiber (SMF) into an EDFL cavity, mode-locked laser pulses with a repetition rate of 0.7315 MHz and a pulse width of 735 ns were obtained at total forward and backward pumping power of 597.9 mW. The mean output power of the mode-locked pulses were measured as -6.46 dBm at 597.9 mW total pump power. It was observed that the mode-locked EDFRL output pulses have a signal-to-noise ratio (SNR) of 47.73 dB for the 0.7315 MHz fundamental frequency obtained with an RF spectrum analyzer. The performance of the developed mode-locked pulsed EDFRL shows that it can be used for nanosecond pulse generation applications in the 1550 nm region using a Lu2O3 based SA.**

978-1-6654-5092-8/22/$31.00 ©2022 IEEE

Keywords—fiber laser, lutetium oxide, mod-locked, saturable absorber

I. Introduction

In recent years, great importance has been attached to the development of high-speed passive pulsed fiber lasers operating around 1550 nm wavelength. By modulating optical loss in the laser cavity with a passive SA, such fiber lasers can generate stable Q-switched or mode-locked pulses depending on the cavity dispersion and nonlinearity, with great flexibility and simplicity. In contrast to the electronic active switching method using electro-optical modulators (EOM) [1] and acousto-optical modulators (AOM) [2] and carbon nanotubes (CNT) [3], semiconductor saturable absorber mirrors (SESAM) [4] and microchip saturable absorber films [5], graphene [6], transition metal dichalcogenides (TMDS) [7], [8], black phosphorus [9]–[12] and topological insulators (TI) [13]–[15] can be used.

In this study, a stable mode-locked pulsed EDFRL operating at 1560.78 nm with 0.7315 MHz pulse repetition rate and 735 ns pulse width at the pump power of 379.6 mW to 597.6 mW in total was designed. The approximately 30 μm thick Lu_2O_3-PVA SA thin film used in the cavity of the fiber ring laser was produced by a group of researchers at the University of Malaya, by suitably embedding the element Lu_2O_3 in polyvinyl alcohol (PVA) to have a sufficient optical nonlinear absorption in 1500 nm wavelength range [16].

II. Experimental Setup

In the pulsed erbium-doped fiber ring laser (EDFRL) design used in this study, a 6 m long Liekki Er-30 erbium doped fiber (EDF) was pumped in the forward and backward directions with equal pump powers at 980 nm wavelength. The EDF length was chosen based on our previous results to obtain a broadband EDFRL operation [17]. An optical isolator is used to provide unidirectional optical signal circulation in the cavity, and a manual polarization controller (PC) is used to eliminate the unwanted polarization effects that may occur due to the polarization rotation in the ring and to keep the polarization state of the lasing signal under control. A Lu_2O_3-PVA based saturable absorber was used for nanosecond pulse generation by initiating self mode-locked operation in the fiber ring and a total length of 231.5 m S-SMF was used to optimize the total cavity dispersion. As shown in Figure 1, the saturation power of the hand made SA used was 100 MW/cm^2, the unsaturated absorption and modulation depth were 58% and 10% at 1550 nm, respectively. The optical output pulses from the EDFRL were taken from the 10% port of a 10/90 splitter and then further was split into two output ports with a 50/50 splitter. The peak power, laser wavelength, and spectral width of the pulsed output signal for the mode-locked operation were measured using an optical spectrum analyzer (Anritsu MS9710B OSA) connected to the first output port. The optical pulse train was converted to electrical pulse train with an 5 GHz InGaAs-based photodiode (Thorlabs-DET08CFC/M) connected to the second port, and then the repetition rate and pulse width were measured by observing the pulse train with a digital oscilloscope (Keysight-DSOX2002A). In addition, by connecting the same signal in the second port to an 3 GHz RF spectrum analyzer (ED-PSA-3000), the output RF spectrum was obtained; the repetition rate measured in oscilloscope was also verified via RF spectrum measurements and the SNR value of the fundamental harmonics was also obtained. The schematic representation of the experimental setup used for the proposed passive Lu_2O_3-PVA saturable absorber based mode-locked EDFRL operation and characterization is given in Figure 2.

A long S-SMF fiber was added to the cavity to aid stable, self-starting mode-locked laser operation by providing an adequate amount of anomalous dispersion and also nonlinear absorption using the Lu_2O_3-PVA SA film within the cavity. With the added 231.5 m length of S-SMF, $2 \times 1\ m$ WDM pigtail fiber, and 6 m EDF, the total length of the cavity is approximately 240 m. The group velocity dispersion of S-SMF, WDM fiber, and EDF are -21.7 ps^2/km, -7 ps^2/km, and 7.65 ps^2/km, respectively. It has been understood that the EDFRL cavity operates in the anomalous dispersion regime with a group velocity dispersion (GVD) of $\sim$ -20.905 ps^2/km and a calculated total net dispersion of $\sim$-5.0172 ps^2.

III. Mode-Locked Laser Performances

A stable self-starting mode-locking operation in our pulsed EDFRL setup was observed, starting at a total threshold pump power of 379.6 mW. Mode-locked laser output pulses remained stable until total pumping power was increased to 597.9 mW. The nonlinear characteristics of the saturable absorber film create some loss inside the cavity such that it is relatively large for low intensity, however, it is fairly small for high intensity. Hence, a short pulse creates a loss modulation due to high intensity at the peak level of the pulse which saturates the absorber more strongly than its low-intensity wings.

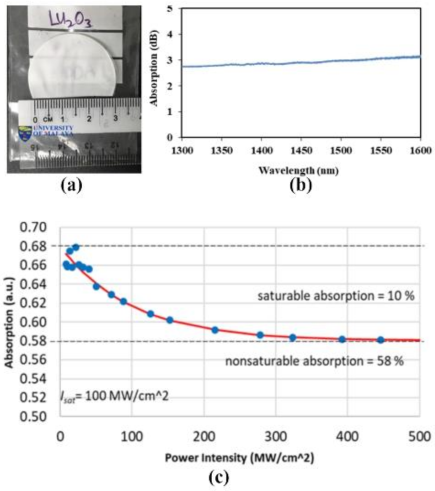

Figure 1: The characteristics of Lu_2O_3-PVA based thin film SA : (a) Physical image (b), linear absorption and (c) nonlinear absorption profiles [2]

Fig. 3 shows the significant characteristics of the mode-locked EDFRL pumped at the total pumping power of 597.9 mW using 980 nm uncooled type pump lasers. Fig. 3 (a) shows the mode-locked output pulse train waveform, repetition rate, and pulse width measured on the oscilloscope. The output waveform was sufficiently stable with almost a constant repetition rate of 0.7315 MHz, a pulse width of 735 ns and a p.p. output voltage of 158 mV. Fig. 3(b), illustrates the optical spectrum of the mode-locked EDFRL measured on the OSA. The pulsed EDFRL output spectrum at the mode-locked operation had a central lasing wavelength of 1560.78 nm, a mean power of -6.64 dBm and a total spectrum power of 3.29 dBm. It should be noted that, the actual output power is 3-dB higher than the measured value due to the 3 dB coupler connected at the output port of the EDFRL. The 3 dB optical bandwidth of the mode-locked pulse train was 1.3 nm. The total dispersion in the EDFRL cavity was calculated as -5.0172 ps2 which is consistent with obtaining narrow

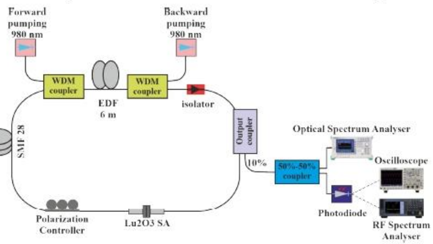

Figure 2: The proposed mode-locked EDFRL experimental setup.

(a)

(b)

(c)

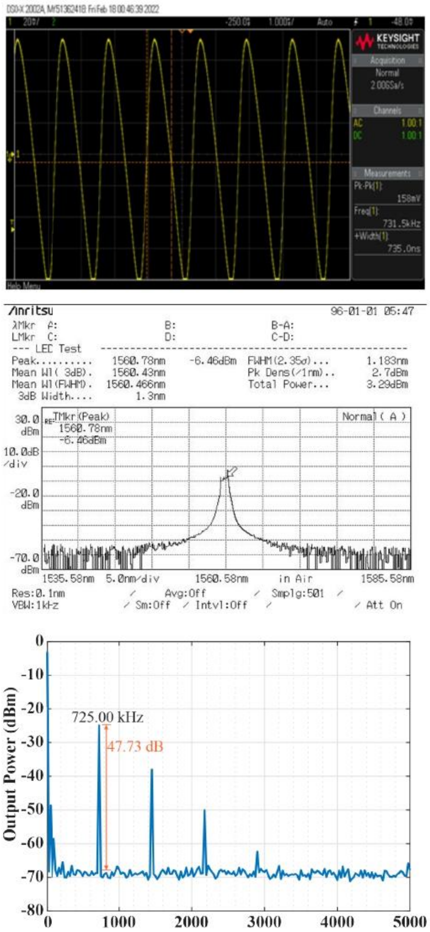

Figure 3: The experimental results of the proposed mode-locked EDFRL configuration using a total pumping power of 597.9 mW. (a) The output signal waveform, repetition rate, and pulse width measured on the oscilloscope. (b) EDFRL pulsed output signal wavelength spectrum measured on OSA. (c) Output RF spectrum measured on the RF spectrum analyzer with a 5 MHz span.

mode-locked pulses at the EDFRL output. Fig. 3(c) depicts the radio frequency (RF) spectrum of the mode-locked laser in the span of 5 MHz and taken at a resolution bandwidth (RBW) of 1 kHz. As shown in Fig. 3(c), the signal to noise ratio (SNR) is sufficiently high being around 47.73 dB to be used as an optical pulsed source in telecommunication systems and sensor applications, which affirms the noiseless of the mode-locked pulse repetition rate. As seen in Figure 3(c), the repetition rate of the fundamental harmonic obtained in the RF spectrum measurements was obtained as 0.725 MHz, slightly different from the repetition rate measurement performed in the digital oscilloscope. This small difference is mainly a result of insufficient reproducibility due to the fact that the characteristics of handcrafted SA thin films, whose properties vary with temperature, are affected by ambient temperatures and optical fibers that are not completely fixed in the experimental setup. In a commercial device design, it is considered that all these sources of uncertainty will not exist.

The long-term stability of the mode-locked operation was examined using the proposed setup for 1 h duration at room temperature for each measurement case. The observation of the laser output has shown no significant fluctuations regarding the optical output spectrum, pulse repetition rate, and pulse amplitude. Thus, this has validated the long-term stability of the designed passively mode-locked EDFRL system. This also suggests that the SA was still in good condition at very high pump levels which indicates that the SA has a significantly high thermal damage threshold than the measured maximum laser output power.

It has been well known that the repetition rate and pulse-width of a ring laser are directly related with the total length and net chromatic dispersion of the lasing ring cavity. Therefore, finally, the repetition rate and pulse width of the passively mode-locked EDFRL output signal were measured for different S-SMF lengths inserted in the cavity. The S-SMFs inserted in the ring cavity were SMF28 fiber types with lengths of 171.5 m, 201.5 m, 231.5 m, 273 m, 303 m, and 346 m. The measurement results are shown in Fig. 4. As shown in this figure, the repetition rate decreased smoothly from 1.225 MHz to 0.5 MHz for increasing S-SMF fiber lengths from 171.5 m to 346 m. Although the reduction in the repetition rate is not linear, it is quite smooth. However, the pulse width of the mode-locked output pulse train increased from 412 ns to 1111.5 ns in an almost linear fashion with increasing lengths of the S-SMF from 171.5 m to 346 m placed in the ring cavity. The results obtained have shown that they can be used to optimize the required cavity length for the desired repetition rate and pulse width values in a given practical application.

IV. Conclusion

In this study, the operation of a pulsed fiber ring laser capable of producing stable and reliable mode-locked pulses by integrating a Lu_2O_3-PVA based thin film saturable absorber into the EDFRL cavity has successfully been demonstrated. The developed pulsed laser output signal had 1560.78 nm peak wavelength and 1.3 nm 3-dB linewidth, 0.7315 MHz repetition rate, and 735 ns pulse width values, and could operate stably at a total pumping power of 597.9 mW. In this study, the average optical output power was obtained as -6.64 dBm. In addition, while the pulse width was 735 ns, a very high signal-to-noise ratio of 47.73 dB was obtained from the electrical output measurements with the RF spectrum analyzer. The proposed pulsed EDFRL performance shows that the Lu_2O_3-PVA based SA is a good candidate for passive mode-locked fiber ring laser applications operating in the 1550 nm region. In addition, the effect of S-SMF length added to the ring cavity to shift the net chromatic dispersion in the cavity to the anomalous regime for soliton-like pulse generation, on the

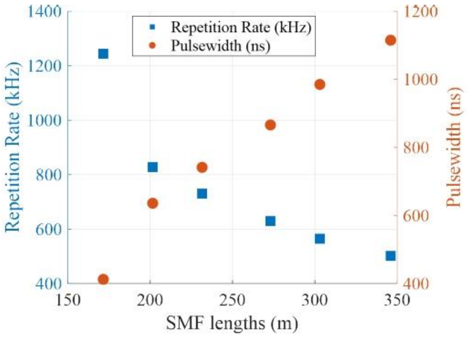

Figure 4: The repetition rate and pulse width of the passively mode-locked EDFRL output signal measured with increasing S-SMF length used in the cavity

repetition frequency and pulse width performance of passively mode-locked EDFRL was also investigated in this study. To the best of our knowledge, this study is presented for the first time in the literature. This study has shown that the repetition rate of the optical output pulse train of the mode-locked EDFRL decreases with increasing S-SMF length nonlinearly, while the pulse width increases linearly. These results can be used to optimize the mode-locked fiber ring laser cavity length for a repetition rate and pulse width value required in a particular telecommunication and sensor system application.

ACKNOWLEDGEMENT

This project was funded by Kütahya Dumlupınar University (Project No.DPU.2020-20).

REFERENCES

[1] A. F. El-Sherif and T. A. King, "High-energy, high-brightness q-switched tm3+-doped fiber laser using an electro-optic modulator," *Optics communications*, vol. 218, no. 4-6, pp. 337–344, 2003.

[2] N. F. Zulkipli, A. H. Rosol, S. A. Sadik, F. E. Durak, A. Altuncu, M. Yasin, and S. W. Harun, "Q-switched pulse generation in a bidirectionally pumped edfl utilizing lu2o3 as saturable absorber," *Optoelectronics Letters*, vol. 17, no. 9, pp. 529–533, 2021.

[3] N. Kasim, A. Al-Masoodi, F. Ahmad, Y. Munajat, H. Ahmad, and S. Harun, "Q-switched ytterbium doped fiber laser using multi-walled carbon nanotubes saturable absorber," *Chinese optics letters*, vol. 12, no. 3, p. 031403, 2014.

[4] M. Wang, C. Chen, C. Huang, and H. Chen, "Passively q-switched er-doped fiber laser using a semiconductor saturable absorber mirror," *Optik*, vol. 125, no. 9, pp. 2154–2156, 2014.

[5] J. J. Zayhowski and A. L. Wilson, "Pump-induced bleaching of the saturable absorber in short-pulse nd: Yag/cr/sup 4+: Yag passively q-switched microchip lasers," *IEEE journal of quantum electronics*, vol. 39, no. 12, pp. 1588–1593, 2003.

[6] Z. Yu, Y. Song, J. Tian, Z. Dou, H. Guoyu, K. Li, H. Li, and X. Zhang, "High-repetition-rate q-switched fiber laser with high quality topological insulator bi 2 se 3 film," *Optics express*, vol. 22, no. 10, pp. 11 508–11 515, 2014.

[7] B. Chen, X. Zhang, K. Wu, H. Wang, J. Wang, and J. Chen, "Q-switched fiber laser based on transition metal dichalcogenides mos 2, mose 2, ws 2, and wse 2," *Optics express*, vol. 23, no. 20, pp. 26 723–26 737, 2015.

[8] D. Mao, S. Zhang, Y. Wang, X. Gan, W. Zhang, T. Mei, Y. Wang, Y. Wang, H. Zeng, and J. Zhao, "Ws 2 saturable absorber for dissipative soliton mode locking at 1.06 and 1.55 μm," *Optics express*, vol. 23, no. 21, pp. 27 509–27 519, 2015.

[9] J. Sotor, G. Sobon, M. Kowalczyk, W. Macherzynski, P. Paletko, and K. M. Abramski, "Ultrafast thulium-doped fiber laser mode locked with black phosphorus," *Optics letters*, vol. 40, no. 16, pp. 3885–3888, 2015.

[10] S. Lu, L. Miao, Z. Guo, X. Qi, C. Zhao, H. Zhang, S. Wen, D. Tang, and D. Fan, "Broadband nonlinear optical response in multi-layer black phosphorus: an emerging infrared and mid-infrared optical material," *Optics express*, vol. 23, no. 9, pp. 11 183–11 194, 2015.

[11] M. B. Hisyam, M. F. M. Rusdi, A. A. Latiff, and S. W. Harun, "Generation of mode-locked ytterbium doped fiber ring laser using few-layer black phosphorus as a saturable absorber," *IEEE Journal of Selected Topics in Quantum Electronics*, vol. 23, no. 1, pp. 39–43, 2016.

[12] H. Mu, S. Lin, Z. Wang, S. Xiao, P. Li, Y. Chen, H. Zhang, H. Bao, S. P. Lau, C. Pan *et al.*, "Black phosphorus–polymer composites for pulsed lasers," *Advanced Optical Materials*, vol. 3, no. 10, pp. 1447–1453, 2015.

[13] J. Sotor, G. Sobon, and K. M. Abramski, "Sub-130 fs mode-locked er-doped fiber laser based on topological insulator," *Optics express*, vol. 22, no. 11, pp. 13 244–13 249, 2014.

[14] J. Sotor, G. Sobon, K. Grodecki, and K. Abramski, "Mode-locked erbium-doped fiber laser based on evanescent field interaction with sb2te3 topological insulator," *Applied Physics Letters*, vol. 104, no. 25, p. 251112, 2014.

[15] Y.-H. Lin, S.-F. Lin, Y.-C. Chi, C.-L. Wu, C.-H. Cheng, W.-H. Tseng, J.-H. He, C.-I. Wu, C.-K. Lee, and G.-R. Lin, "Using n-and p-type bi2te3 topological insulator nanoparticles to enable controlled femtosecond mode-locking of fiber lasers," *Acs Photonics*, vol. 2, no. 4, pp. 481–490, 2015.

[16] M. Baharom, M. Rahman, A. Latiff, P. Wang, and S. Harun, "Lutetium (iii) oxide film as passive mode locker device for erbium-doped fibre laser cavity," *Optics Communications*, vol. 446, pp. 51–55, 2019.

[17] S. A. Sadik, F. E. Durak, and A. Altuncu, "Widely tunable erbium doped fiber ring laser based on loop and double-pass edfa design," *Optics & Laser Technology*, vol. 124, p. 105979, 2020.

2022 IEEE 9th International Conference on Photonics (ICP)

Nanosecond Mode-Locked Erbium Doped Fiber Laser Based on Few Layer Bismuth Telluride Ultra Thin Film Saturable Absorber

Thoalfeqar Ali Razaq Alyasiri[1,*], Serif Ali Sadik[1], Firat Ertac Durak[1], Nur Farhanah Zulkipli[2], Ahmet Altuncu[1] and Sulaiman Wadi Harun[3]
[1]*Photonic Technologies Application and Research Center*, Kütahya Dumlupınar University, 43100 Kütahya, Turkey.
[2]*Department of Physics, Faculty of Science and Technology*, Airlangga University, Surabaya, Indonesia.
[3]*Photonics Engineering Lab., Dept. of Electrical Engineering, Faculty of Eng.*,
University of Malaya, Kuala Lumpur, Malaysia

***Abstract*—In this work, we obtained a nanosecond modelocked fiber laser that works with a pulse width of 552 - 1050 ns, and a repetition rate of 0.500 - 0.950 MHz repetition rate in 1.55 μm region. The highest output power, peak power, pulse energy and peak laser efficiency were 3.5 mW, 6.6 mW, 6.9093 nJ, and 0.9512%, respectively, with total cavity length of 354.5 m, total dispersion -7.5018 ps^2, and group velocity dispersion -21.1618 ps^2/km, at bidirectional pump power of 365.4 mW. The threshold pump power for this length was 76.9 mW. The results show that the saturable absorber derived from Bi_2Te_3 is capable of producing nanosecond mode locked fiber laser for possible applications that require high pulse energy and medium output power.**

***Index Terms*—Fiber lasers, Mode locking, Bi_2Te_3, saturable absorber, erbium doped fiber lasers**

I. Introduction

In recent years, nanosecond pulsed fiber lasers draw attention due to its ability to produce high pulse energy by modulating the optical loss in the laser cavity using passive modulating elements, such as, two-dimensional materials 2D such as Saturable Absorber (SA) films [1] and carbon nanotubes (CNTs) [2], Transition Metal Dichalcogenides (TMDs) [3], black phosphorous [4], [5]. Bi_2Te_3 is one of the topological insulators which, in addition to a large bandgap, has a conductivity shielded state on its edge or surface and have a non-linear super-wavelength optical response from visible to microwave due to the co-interaction between the small bulky-gap band and the zero-gap surface state due to the effects of spin-orbit interactions and time-reversal symmetry [6], [7]. However, besides the mentioned advantages, the topological insulators suffer from high nonsaturable losses and low laser efficiency.

As for nanosecond pulse generation, due to the short recovery time of the SA, it is generally difficult for realizing mode-locked fiber laser with the passive methods. A widely utilized method for obtaining a stable pulse train is extending the cavity length [8]. In this work, we successfully achieved nanosecond pulsed Erbium Doped Fiber Laser (EDFL) based on Bi_2Te_3 thin film SA, with a minimum pulse width of 552 ns and maximum repetition rate of 0.950 MHz.

II. Experimental Setup

We fabricated a thin film of Bi_2Te_3 [9] and sandwiched between two fiber ferrules with adding matching index gel and alcohol, then we applied a pressure by close the two connectors very well. Then we removed the original film. a very thin few layers of the film has been printed on the ferrule surfaces. As a last step we reclosed the two connectors and got our new passive saturable absorber. The original Bi_2Te_3 SA film properties of intensity of 20 Mw/cm^2, saturable absorption of 30%, and non-saturable intensity of 55% [9].

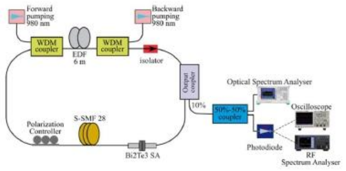

Fig. 1. Experimental setup of the mode-locked erbium doped fiber laser

In the EDFRL design, two laser diodes with operating wavelength of 980 nm were used as forward and backward pumping to provide higher pump power to the 6 m Liekki Er-30 erbium doped fiber (EDF). The optical output powers of the pump lasers were set to 150 mW. An optical isolator is used to provide unidirectional optical signal circulation in the ring. A thin film of Bi_2Te_3 based SA is used as saturable absorber to initiate Q-switching process for pulse generation. The laser cavity setup is shown in Figure 1. To observe the effect of the cavity length to mode-locking performance, single mode fibers (SMF) with different lengths are added to the cavity. A polarization controller is used in cavity to ensure that the polarization state of the light is properly controlled. The output of the laser is analysed by using an optical spectrum analyser

2022 IEEE 9th International Conference on Photonics (ICP) | 978-1-6654-2766-1/22/$31.00 ©2022 IEEE | DOI: 10.1109/ICP53600.2022.9912495

(OSA - Anritsu MS9710B). The optical pulse train was converted to electrical pulse train with an 5 GHz InGaAs-based photodiode (Thorlabs-DET08CFC/M), and then the repetition rate and pulse width were measured by observing the pulse train with a digital oscilloscope (Keysight-DSOX2002A). In addition, with a 3 GHz RF spectrum analyzer (ED-PSA-3000), the output RF spectrum was obtained.

III. Results and Discussion

We used multiple single-mode fiber lengths (171.5 m, 201.5 m, 213 m, 231.5 m, 303 m, and 346 m) to have an anomalous total cavity dispersion of -3.7152 to -7.5018 ps^2, and total group velocity dispersion (GVD) of -20.64 to -21.1618 ps^2/km respectively (Figure 2(a)). The highest pulse energy we got was with total cavity length of 354.5 m.

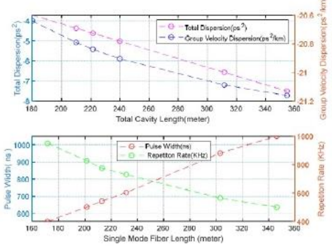

Fig. 2. a) EDFL cavity length vs Total dispersion and GVD , b) S-SMF length vs pulse width and Repetition rate at 365.4 mW bidirectional pump power

The output power, peak pulse power, and pulse energy were 0.3 mW, 0.7 mW, and 0.57 nJ at bidirectional pump power of 76.9 mW. The maximum output power, peak pulse power, pulse energy and laser efficiency were 3.5 mW, 6.6 mW, 6.9093 nJ, and 0.9512%, respectively, at bidirectional pump power of 365.4 mW. The pulse width and the repetition rate that we got with all cavity lengths at maximum bidirectional pump power of 365.4 mW are shown in Figure 2(b). One can see that the narrowest pulse width and the maximum repetition rate are achieved as 552 ns, and 0.950 MHz, respectively for an SMF length of 171.5 m.

Figure 3 shows the RF spectrum, optical spectrum and pulse train of the proposed mode-locked EDFL. The observed signal to noise ratio (SNR) is 51.64 dB. The period of the pulse train is measured as 2 μs.

IV. Conclusions

A passively nanosecond mode locked EDFL has been successfully demonstrated using a Bi_2Te_3 PVA film as a SA. As the fabricated Bi_2Te_3 PVA film is integrated inside the ring cavity of the EDFL as a SA, nanosecond pulsed laser output is achieved at 1550 nm region, and a minimum pulse width of 552 ns, and a repetition rate of 0.950 MHz is observed with a 171.5 m SMF. The highest output power, peak power, pulse energy and peak laser efficiency were 3.5 mW, 6.6 mW,

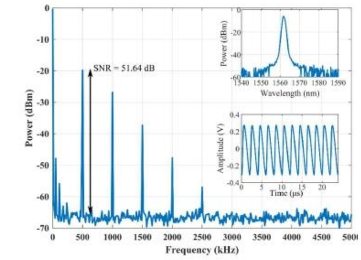

Fig. 3. RF spectrum, optical spectrum (top inset) and the pulse train (bottom inset) of the laser output for a threshold pump power of 76.9 mW

6.9093 nJ, and 0.9512% , respectively , with total cavity length of 354.5 m and bidirectional pump power of 365.4 mW. The threshold pump power for this length was 76.9 mW. These results indicate that the printed Bi_2Te_3 SA based film has a promising application as SA for generating nanosecond mode locked EDFL. Further studies are being focused on to achieve picosecond pulses with ultra-thin film SA based EDFLs.

Acknowledgment

This project was funded by Kütahya Dumlupınar University (Project No.DPU.2020-20).

References

[1] N. F. Zulkipli, A. H. A. Rosol, S. A. Sadik, F. E. Durak, A. Altuncu, M. Yasin, and S. W. Harun, "Erratum to: Q-switched pulse generation in a bidirectionally pumped EDFL utilizing lu2o3 as saturable absorber."

[2] N. K. N. Kasim, A. H. H. A.-M. A. H. H. Al-Masoodi, F. A. F. Ahmad, Y. M. Y. Munajat, H. A. H. Ahmad, and S. W. H. S. W. Harun, "Q-switched ytterbium doped fiber laser using multi-walled carbon nanotubes saturable absorber," vol. 12, no. 3, pp. 031 403–31 406.

[3] B. Chen, X. Zhang, K. Wu, H. Wang, J. Wang, and J. Chen, "Q-switched fiber laser based on transition metal dichalcogenides MoS_2, $MoSe_2$, WS_2, and WSe_2," vol. 23, no. 20, p. 26723.

[4] J. Sotor, G. Sobon, M. Kowalczyk, W. Macherzynski, P. Paletko, and K. M. Abramski, "Ultrafast thulium-doped fiber laser mode locked with black phosphorus," vol. 40, no. 16, p. 3885.

[5] S. B. Lu, L. L. Miao, Z. N. Guo, X. Qi, C. J. Zhao, H. Zhang, S. C. Wen, D. Y. Tang, and D. Y. Fan, "Broadband nonlinear optical response in multi-layer black phosphorus: an emerging infrared and mid-infrared optical material," vol. 23, no. 9, p. 11183.

[6] Y.-H. Lin, S.-F. Lin, Y.-C. Chi, C.-L. Wu, C.-H. Cheng, W.-H. Tseng, J.-H. He, C.-I. Wu, C.-K. Lee, and G.-R. Lin, "Using n- and p-type bi_2te_3 topological insulator nanoparticles to enable controlled femtosecond mode-locking of fiber lasers," vol. 2, no. 4, pp. 481–490.

[7] H. Zhang, C.-X. Liu, X.-L. Qi, X. Dai, Z. Fang, and S.-C. Zhang, "Topological insulators in bi_2se_3, bi_2te_3 and sb_2te_3 with a single dirac cone on the surface," vol. 5, no. 6, pp. 438–442.

[8] F. S. M. Samsamnun, N. F. Zulkipli, M. I. M. A. Khudus, A. S. A. Bakar, W. H. A. Majid, and S. W. Harun, "Nanosecond pulse generation with a gallium nitride saturable absorber," vol. 2, no. 1, p. 134.

[9] N. H. M. Apandi, F. Ahmad, S. N. F. Zuikafly, M. H. Ibrahim, and S. W. Harun, "Bismuth (III) telluride (bi2te3) topological insulator embed in PVA as passive q-switcher at 2 micron region," vol. 8, no. 4, p. 101.

Kütahya Dumlupınar University
Institute of Graduate Studies

Journal of Scientific
Reports-A
E-ISSN: 2687-6167
Number 51, December 2022

RESEARCH ARTICLE

WAVELENGTH TUNABLE PASSIVELY Q-SWITCHED FIBER RING LASER USING GALLIUM ARSENIDE BASED MICROCHIP SATURABLE ABSORBER

Thoalfeqar Ali Razaq ALYASIRI[1], Aşkınnur AŞKIN[2], Bünyamin KAYA[3], Şerif Ali SADIK[4*], Fırat Ertaç DURAK[5], Ahmet ALTUNCU[6]

Receive Date:31.08.2022 *Accepted Date: 05.10.2022*

ABSTRACT

The work presented in this study is focused on developing a widely wavelength tunable Q-switched pulsed erbium doped fiber ring laser (EDFRL) source operating in microsecond regime in Telecom wavelength spectrum of 1.55 μm (C and L bands). A commercial Gallium arsenide (GaAs) based microchip saturable absorber (SA) is used in the proposed EDFRL configuration to passively initiate Q-switching for stable pulse generation. Unless low damage threshold of the commercial GaAs based SA and non-optimized cavity length and losses, sufficiently stable pulse trains were obtained for a wide wavelength tuning range of 50 nm from 1520 nm to 1570 nm with high repeatability and long-term stability. The Q-switched output pulses of the proposed EDFRL have output average powers varying from +0.65 dBm to +1.53 dBm, the pulse widths varying from 4.27 μs to 7.16 μs and the repetition rates varying from 51.51 kHz to 31.42 kHz for different tuning wavelengths.

Keywords: *fiber laser, saturable absorber, Q-switched, wavelength tunable*

1. INTRODUCTION

Q-switched fiber lasers can generate high-energy pulses by modulating optical losses in the laser cavity using active or passive modulation elements. Therefore, studies on Q-switched fiber lasers have increased recently. Many modulators such as electro-optic modulators (EOM) [1], acousto-optic modulators (AOM) [2], semiconductor saturable absorber mirrors (SESAMs) [3], microchip saturable absorbers [4], and film saturable absorbers [5], carbon nanotubes [6], topological insulators (TIs) [7],

JSR A
Journal of Scientific Reports

Sadık, et all., Journal of Scientific Reports-A, Number 51, 73-80, December 2022.

graphene [8], transition metal dichalcogenides (TMDs) [9] have been utilized to achieve Q-switching pulses. In contrast with the mode-locked ones, Q-switched fiber lasers have the ability to generate much higher pulse energy with microsecond or nanosecond pulses. Also, it is necessary to balance the dispersion and control the non-linear effects in the mode-locking process, which requires precise calculations and are not needed in the Q-switching process. Therefore, Q-switched fiber lasers have the advantages of efficiency, low cost, and ease of construction. The Q-switched lasers have many potential applications in various fields, such as sensing applications [10, 11], medicine [12] and material processing [13] owing to their advantages such as fast recovery time and low saturation intensity.

Passively Q-switched microchip lasers have many advantages, simplicity of implementation, pulse generation with a well-defined energy and duration, highly stable operation and easier to obtain single-frequency operation in a passively Q-switched laser than in an actively Q-switched device. The pulse duration from a Q-switched laser generally decreases with decreasing cavity length [14] and its central lasing wavelength can be passively tuned over a wide spectrum in C and L bands as soon as providing a positive gain spectrum using a wideband erbium doped fiber amplifier inside the cavity.

In this work, we demonstrate a widely tunable Q-switched erbium doped fiber ring laser with a gallium arsenide (GaAs) based saturable absorber (SA) as a passive Q-switching element, and an optical tunable band pass filter (OTBPF) as a wavelength tuning element. Stable Q-switched pulses are obtained in a 50 nm wide wavelength tuning range, which can be tuned from 1520 nm to 1570 nm. The obtained pulses have pulse widths ranging from 4.27 μs to 7.16 μs and repetition rates from 51.51 to 31.42 kHz.

2. EXPERIMENTAL DESIGN

In the experimental design utilized in this work, one backward pump laser diode and one forward pump laser diode with operating wavelengths of 980 nm were used to provide high pump power (Optical output power of the both of the laser diodes were set to 150 mW). An active fiber (Liekki Er-30) with the length of 6 m was utilized in the experimental setup. The length of the erbium doped fiber (EDF) was chosen to obtain a wideband CW operation in EDFRL using our previous results [15]. An isolator was utilized inside the ring cavity to ensure unidirectional lasing operation. To select the lasing wavelength of EDFRL, a MEMS-based C+L band OTBPF (TF1C100) was used in the cavity. A commercial GaAs microchip based SA is used as saturable absorber medium for pulse generation. The commercial SA used was 150 μm in thickness and had an absorbance of 58%, modulation depth of 35% and saturation fluence of 300μJ/cm2 at 1550 nm. The output of EDFRL was taken from the 10% port of the tap coupler with a 90% - 10% splitting ratio and then split into two ports, to observe the optical spectrum of the output signal and the electrical pulse forms simultaneously. The optical signal was analyzed at the optical spectrum analyzer (OSA Anritsu MS9710B). At the other port of the coupler, the optical signal was detected via an InGaAs 5 GHz photodiode (Thorlabs-DET08CFC/M), and the pulse waveforms were analyzed with an oscilloscope (Keysight-DSOX2002A). In the experimental setup, a manual polarization controller (PC) was used to optimize the polarization state of the light in the ring cavity, to eliminate the unwanted polarization effects. The schematic representation of the experimental setup was given in Fig.1.

JSR A
Journal of Scientific Reports

Sadık, et all., Journal of Scientific Reports-A, Number 51, 73-80, December 2022.

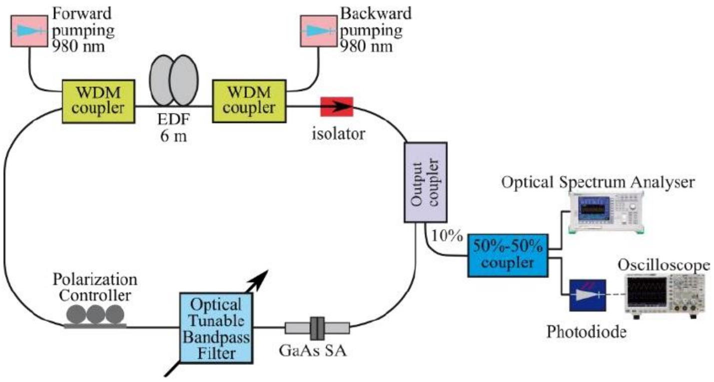

Figure 1. The proposed Q-switched EDFRL cavity used in experiments.

3. EXPERIMENTAL RESULTS

In the first experiment, the gain spectrum of the EDFA used in the setup was characterized using a commercial widely tunable (1520 nm-1607 nm) laser source (TLS) as the input light source. In these measurements, the forward and backward pump laser powers were set to 140 mW and the center wavelength of the TLS was tuned in the range of 1520-1607 nm. The gain spectrum of the bidirectional pumped EDFA is shown in Fig.2, which shows sufficient positive gains for a Q switched operation in our EDFRL design.

JSR A
Journal of Scientific Reports

Sadık, et all., Journal of Scientific Reports-A, Number 51, 73-80, December 2022.

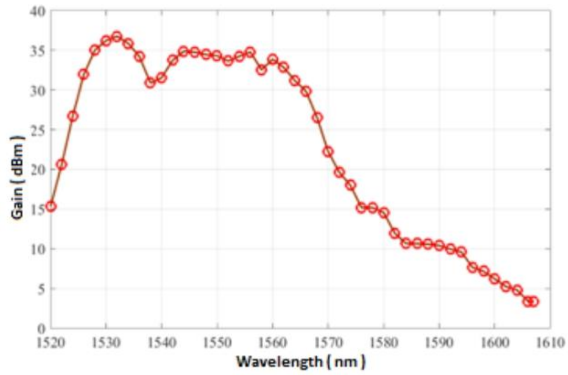

Figure 2. Gain spectrum of EDFA designed with 6 m EDF.

In the second experiment, passively Q switched EDFRL configuration has been set up as seen in Fig.1 using a GaAs based microchip saturable absorber. In Table 1, the optical output power, repetition rate and pulse width values obtained at the output of the Q switched wavelength tunable fiber ring laser designed across the entire spectrum are given. It should be noted that the output average power values measured in OSA were taken from one of the output ports of the 50%-50% splitter added to the assembly at the EDFRL output. It means that the power values given in Table 1 correspond to half the actual output power of the designed Q switched wavelength tunable EDFRL.

Table 1. The repetition rate, pulse width and output power of Q-switched wavelength tunable fiber ring laser.

Wavelength (nm)	Repetition Rate (kHz)	Pulse width (μs)	Output Peak Power (dBm)
1520	47.010	4.35	- 2.65
1530	51.516	4.274	- 2.63
1535	45.446	4.676	- 2.33
1540	38.459	4.982	- 1.74
1545	38.026	5.11	- 1.97
1550	39.435	5.334	- 1.58
1555	36.813	5.234	- 1.58
1560	33.928	5.554	- 1.54
1565	33.562	6.494	-2.03
1570	31.421	7.166	-1.53

JSR A
Journal of Scientific Reports

Sadık, et all., Journal of Scientific Reports-A, Number 51, 73-80, December 2022.

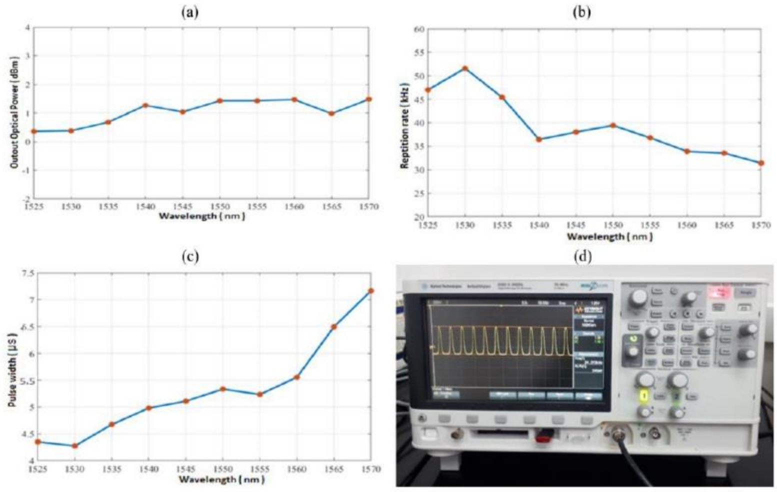

Figure 3. (a) Optical output power **(b)** Repetition rate and **(c)** Pulse width of the Q switched EDFRL as a function of tuning wavelength **(d)** A typical output waveform of the designed GaAs-SA based Q-switched wavelength tunable fiber laser.

With the Q-switched pulsed EDFRL design, highly stable pulses could be obtained for the lasing wavelength range of 1520-1570 nm having clearly measurable repetition rate, pulse width and output power values. The Optical output power, repetition rate and pulse width values measured through a 50 nm tunable wavelength range are given in Figure 3 (a), (b) and (c). The output average power measured in OSA at one port of the output splitter was changing between 0.65 dBm to 1.5 dBm depending on the lasing wavelength which correspond to the repetition rates varying between 31.42 kHz and 51.51 kHz and pulse widths varying between 4.35 µs and 7.16 µs.

JSR A
Journal of Scientific Reports

Sadık, et all., Journal of Scientific Reports-A, Number 51, 73-80, December 2022.

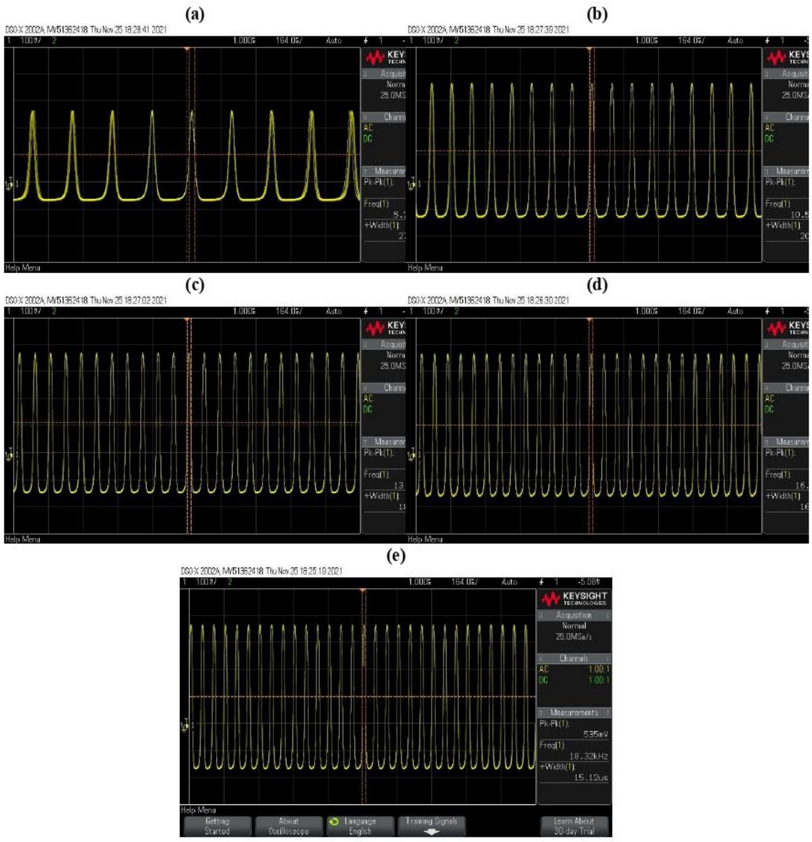

Figure 4. The Q-switched EDFRL output pulse trains at the lasing wavelength of 1567 nm obtained without using a OTBPF in the cavity at the following pump currents of **(a)** 60 mA, **(b)** 70 mA, **(c)** 80 mA, **(d)** 90 mA, **(e)** 100 mA.

A self-starting and stable Q-switched fiber laser operation using GaAs SA without OTBPF was achieved after the threshold pump currents of 60 mA. The lasing oscillation was centered at a

JSR A
Journal of Scientific Reports

Sadık, et all., Journal of Scientific Reports-A, Number 51, 73-80, December 2022.

wavelength of 1567 nm. The Q-switched lasing operation remained stable as the pump laser currents were raised up to 100 mA. Fig.4 shows the increment of the repetition rate from 5.27 kHz to 18.32 kHz and the decreasement of the pulse with from 27.64 µs to 15.12 µs as the pump laser currents were increased from 60 mA to 100 mA.

4. CONCLUSION

In this study, highly stable Q-switched output pulses have been obtained in a bidirectionally pumped EDFRL configuration for a tunable wavelength range of 50 nm from 1520 nm to 1570 nm with an output average power of between +0.65 dBm and +1.53 dBm, the pulse width of 4.27 µs – 7.16 µs and the repetition rate of 51.51 kHz - 31.42 kHz for a moderate pumping level and non-optimized cavity losses. The Q switched output pulse trains were also obtained for different pumping levels at a natural lasing wavelength of 1567 nm in the cavity. The results show that Q-switching performance of wavelength tunable EDFRL design proposed can further be upgraded by optimizing the cavity length and losses. However, low damage threshold of GaAs based SA is serious limiting factor to be considered for high power applications. This kind of EDFRL Q switched pulse source can be widely used as a tunable laser source in DWDM optical communication systems operating in 1.55 µm region and for spectral response measurements in fiber optical sensor applications. In our future work, we will work on optimizing the cavity length and loss for a better Q-switching performance regarding wavelength tuning range, pulse width, repetition rate and output power.

ACKNOWLEDGEMENTS

This work was supported by Kütahya Dumlupınar University (Project No.DPU.2020-20).

REFERENCES

[1] El-Sherif, A.F. and King, T.A., (2003), High-energy, high-brightness Q-switched Tm^{3+}-doped fiber laser using an electro-optic modulator, Opt. Commun., 218(4),337-344.

[2] Li, W., Liu, H., Zhang, J., Long, H., Feng. S. and Mao, Q., (2016), Q-switched fiber laser based on an acousto-optic modulator with injection seeding technique, Appl. Opt., 55(17), 4584-4588.

[3] Wang, M., Chen, C., Huang, C., and Chen, H., (2014), Passively Q-switched Er-doped fiber laser using a semiconductor saturable absorber mirror, Optik (Stuttg)., 125(9), 2154–2156.

[4] J. J. Zayhowski, J.J., and Wilson, A.L., (2003), Pump-induced bleaching of the saturable absorber in short-pulse Nd:YAG/Cr/sup 4+/:YAG passively Q-switched microchip lasers, IEEE J. Quantum Electron., 39(12), 1588–1593.

[5] Zulkipli, N.F., Rosol, A.H.A., Sadik, S.A., Durak, F.E., Altuncu, A., Yasin, M. and Harun, S.W., (2021), Q-Switched Pulse Generation in a Bidirectionally Pumped EDFL Utilizing Lu_2O_3 as Saturable Absorber, Optoelectronics Letters, 17 (9), 529–533.

JSR A
Journal of Scientific Reports

Sadık, et all., Journal of Scientific Reports-A, Number 51, 73-80, December 2022.

[6] Kasim, N., Al-Masoodi, A.H.H., Ahmad, F., Munajat, Y., Ahmad, H., and Harun, S.W., (2014), Q-switched ytterbium doped fiber laser using multi-walled carbon nanotubes saturable absorber, Chinese Opt. Lett.,12(3), 31403.

[7] Yu, Z., Song, Y., Tian, J., Dou, Z., Guoyu, H., Li, K., Li, H., and Zhang, X., (2014), High-Repetition-Rate Q-Switched Fiber Laser with High Quality Topological Insulator Bi_2Se_3 Film, Optics Express, 22(10), 11508–11515.

[8] Luo, Z.,Zhou, Z., Weng, J., Huang, G., Xu, H., Ye, C., and Cai, Z., (2010), Graphene-Based Passively Q-Switched Dual-Wavelength Erbium-Doped Fiber Laser. Optics Letters,35(21), 3709–3711.

[9] Chen, B., Zhang, X., Wu, K., Wang, H., Wang, J., and Chen, J., (2015), Q-switched fiber laser based on transition metal dichalcogenides MoS_2, $MoSe_2$, WS_2, and WSe_2, Opt. Express, 23(20), 26723–26737.

[10] Zhang, Q., Chang, J., Wang, Q., Wang, Z., Wang, F., and Qin, Z., (2018), Acousto-optic Q-switched fiber laser-based intra-cavity photoacoustic spectroscopy for trace gas detection, Sensors, 18(1), 42.

[11] Shi, W., Petersen, E., Moor, N., Chavez-Pirson, A., and Peyghambarian, N., (2011), All fiber-based single-frequency Q-switched laser pulses at 2 um for lidar and remote sensing applications, in Proc.SPIE, 2011, vol. 8164.

[12] Celen, S. , Özden, H. and Uyar, E. (2014), İterbiyum-katkili fiber lazerle Q-anahtarlamalı modda implant yüzeyi mikro-imalatı ve karekterizasyonu . Gazi University Journal of Science Part C: Design and Technology , 2 (2) , 197-202 .

[13] Ismail, M.A., Ahmad, F., Harun, S.W., Arof, H., and Ahmad, H., (2013), A Q-switched erbium-doped fiber laser with a graphene saturable absorber, Laser Phys. Lett.,10(2), 25102.

[14] Chen, Y., Zhao, C., Chen, S., Du, J., Tang, P., Jiang, G., Zhang, H., Wen, S., and Tang, D., (2013), Large Energy, Wavelength Widely Tunable, Topological Insulator Q-Switched Erbium-Doped Fiber Laser, IEEE Journal of Selected Topics in Quantum Electronics,20(5),315–322.

[15] Sadik, S. A., Durak, F. E., & Altuncu, A. (2020), Widely tunable erbium doped fiber ring laser based on loop and double-pass EDFA design. Optics & Laser Technology, 124, 105979.

REFERENCES

Adachi, S., & Koyamada, Y. (2002). Analysis and design of Q-switched erbium-doped fiber lasers and their application to OTDR. *Journal of Lightwave Technology, 20*(8), 1506-1511.

Agrawal, Gonvind. P. (2013). *Semiconductor lasers.* (2nd ed.). Boston: Kluwer Academic Publishers.

Ahmad, H., Lee, C., Ismail, M., Ali, Z., Reduan, S., Ruslan, N., . . . & Harun, S. W. (2016). Zinc oxide (ZnO) nanoparticles as saturable absorber in passively Q-switched fiber laser. *Optics Communications, 381*, 72-76.

Ahmad, H., Reduan, S. A., Ali, Z. A., Ismail, M., Ruslan, N., Lee, C., . . .& Harun, S. W. J. I. P. J. (2016). C-band Q-switched fiber laser using titanium dioxide (TiO 2) as saturable absorber. *Institute of Electrical and Electronics Engineers Photonics Journal,* 8(1), 1-7.

Ahmad, H., Ruslan, N., Ismail, M., Reduan, S., Lee, C., Sathiyan, S., . . .& Harun, S. W. (2016). Passively Q-switched erbium-doped fiber laser at C-band region based on WS 2 saturable absorber. *Applied optics*, *55*(5), 1001-1005.

Ahmad, H., Ruslan, N., Ismail, M., Reduan, S., Lee, C., Sathiyan, S., . . . & Harun, S. W. (2016). Passively Q-switched erbium-doped fiber laser at C-band region based on WS 2 saturable absorber. *Applied optics, 55*(5), 1001-1005.

Ahmad, H., Samion, M. Z., Kamely, A., Ismail, M. F. J. (2019). Mode-locked thulium doped fiber laser with zinc oxide saturable absorber for 2 μm operation. *Infrared Physics & Technology*, *97*,142-148.

Ahmed, N.M. Ali, Z.S. Salleh, A.A. Rahman, S.W. Harun, M. & Manaf, H. Arof. (2014). All fiber mode-locked erbium-doped fiber laser using single-walled carbon nanotubes embedded into polyvinyl alcohol film as saturable absorber. *Optics & Laser Technology, 62*(10), 40-43.

Al-Hayali, Sarah K. M., Mohammed, D. Z., Khaleel, W. A., & Al-Janabi, A. H. (2017). Aluminum oxide nanoparticles as saturable absorber for C-band passively Qswitched fiber laser. *Applied optics, 56*(16), 4720-4726.

Al-Hiti, Ahmed Shakir, Rahman, M.F.A. Harun, S.W. Yupapin, Yasin, P. M. (2019). Holmium oxide thin film as a saturable absorber for generating Q-switched and mode-locked erbium-doped fiber lasers. *Optical Fiber Technology, 52*(11), 1-7.

Alyasiri T. A. R. , Aşkın A. , Kaya B. , Sadık Ş. A. , Durak F. E. , Altuncu A. (2022). Wavelength tunable passively Q-switched fiber ring laser using gallium arsenide based microchip saturable absorber. *Journal of Scientific Reports-A,* (051), 73-80.

Alyasiri, T. A., et al. (2022, August). Nanosecond mode-locked erbium doped fiber laser based on few layer bismuth telluride ultra thin film saturable absorber. S.B.A. Anas (Chair), *IEEE 9th International Conference on Photonics* (pp. 35-36). IEEEXplore. https://doi.org/10.1109/ICP53600.2022.9912495

Alyasiri, T. A., et al. (2022, May). Passively mode-locked fiber ring laser using Lu2O3 thin film based saturable absorber. In F. T. Yarman Vural (Chair), *30th Signal Processing and Communications Applications Conference* (pp. 1-4). IEEEXplore. https://doi.org/10.1109/SIU55565.2022

Anderberg, B. & Wolbarsht, M.L. (1992). *Laser Weapons: The Dawn of a New Military Age* (1st ed.). New York: Plenum Publishing.

Apandi, N. H. Ahmad, F. Zuikafly, S. N. F. Ibrahim, M. H. & Harun, S. W. (2016). Bismuth (III) telluride (Bi2Te3) embedded in PVA as a passive saturable absorber in a 2 micron region. *Photonics Letters of Poland, 8*(4), 101-103.

Bohua Chen, Xiaoyan Zhang, Kan Wu, Hao Wang, Jun Wang, and Jianping Chen. (2015). Q-switched fiber laser based on transition metal dichalcogenides MoS2, MoSe2, WS2, and WSe2. *Optics Express, 23*(10), 26723-26737.

Bourzeix, S., Plimmer, M. D., Nez, F., Julien, L., & Biraben, F. (1993). Efficient frequency doubling of a continuous wave titanium: sapphire laser in an external enhancement cavity. *Optics communications, 99* (1-2), 89-94.

Brabec, T. et al., (1992). Kerr lens mode locking. *Optics Letters, 17* (18), 1292-1294.

Bret, G., Gires F. (1964). Giant-pulse laser and light amplifier using variable transmission coefficient glasses as light switches. *Applied Physical Letters, 4* (10), 175-176.

Brom, J.E. et al., (2012). Structural and electrical properties of epitaxial Bi2Se3 thin films grown by hybrid physical-chemical vapor deposition. *Application Physics Letters. 100* (16), 1-4.

Brunel, M. et al., (1999). Experimental and theoretical study of monomode vectorial lasers passively Q switched by a Cr4+: yttrium aluminum garnet absorber. *Physical Review A, 60* (5), 4052-4058.

Carter, Ashley H., (2002). *Classical and Statistical Thermodynamics*. (1st ed.). New Jersey: Prentice-Hall.

Castellani, E. (2002). On the meaning of Symmetry Breaking. To appear in Brading, K. and Castellani, E. (eds) (2003), *Symmetries in Physics: Philosophical Reflections* (pp.1-17). Cambridge: Cambridge University Press.

Chen, Y., Jiang, G., Chen, S., Guo, Z., Yu, X., Zhao, C., . . . & Tang, D. (2015). Mechanically exfoliated black phosphorus as a new saturable absorber for both Q-switching and mode-locking laser operation. *Optics Express, 23*(10), 12823-12833.

Chen, Y.-F., Tsai, S., & Wang, S. J. O. l. (2000). High-power diode-pumped Q-switched and mode-locked Nd: YVO 4 laser with a Cr 4+: YAG saturable absorber. *Optics Letters, 25*(19), 1442-1444.

D. Chu, E.K. Kim. (2018). Recent advances in synthesis and assembly of van der Waals materials. *Journal of The Korean Physical Society*, *73*(6), 805-816.

Degnan, J.J. (1989). Theory of the optimally coupled Q-switched laser. *Institute of Electrical and Electronics Engineers Jurnal of Quantum Electron*, *25* (2), 214-220.

Digonnet, M.J.F. (2001). *Rare-Earth-Doped Fiber Lasers and Amplifiers Revised and Expanded* (2nd ed.). Florida: Chemical Rubber Company Press, Boca Raton.

Du, J., Wang, Q., Jiang, G., Xu, C., Zhao, C., Xiang, Y., . . . & Zhang, H. (2014). Ytterbium doped fiber laser passively mode locked by few-layer Molybdenum Disulfide (MoS2) saturable absorber functioned with evanescent field interaction. *Scientific reports, 4*, 1-7.

Eichhorn, M., & Jackson, S. D. J. O. L. (2007). High-pulse-energy actively Q-switched Tm 3+-doped silica 2 μm fiber laser pumped at 792 nm. *Optics Letters, 32* (19), 2780-2782.

Elisa Sani, & Aldo Dell'Oro. (2016). Spectral optical constants of ethanol and isopropanol from ultraviolet to far infrared. *Optical Materials, 60*, 137-141.

El-Sherif, A. F., & King, T. A. (2003). High-energy, high-brightness Q-switched Tm3+-doped fiber laser using an electro-optic modulator. *Optics communications, 218* (4-6), 337-344.

Femtosecond laser micromachining: a back-to-basics primer (July 2, 2012). Retrieved from: https://www.laserfocusworld.com/industrial-laser-solutions/article/ 142 161 83/ femtosecond-laser-micromachining-a-backtobasics-primer

Fleck J. A., (1970). Ultrashort-pulse generation by Q-switched lasers. *Physical Review B, 1* (1), 84-100.

Fran, D. A. (1999). Theory of Everything. *Journal of New Energy, 5*, 76-84.

Freudiger, C. W., Yang, W., Holtom, G. R., Peyghambarian, N., Xie, X. S., & Kieu, K. Q. J. N. p. (2014). Stimulated Raman scattering microscopy with a robust fibre laser source. *Nature Photonics, 8* (2), 153-159.

Fultz, B. (2014). *Phase Transitions in Materials. Cambridge* (1st ed.). Cambridge: Cambridge University Press.

Fuqiang, J. et al., (2015). Nanosecond-pulsed, dual-wavelength passively Q-switched c-cut Nd:YVO4 saturable absorber. *Institute of Electrical and Electronics Engineers Journal of Selected Topics in Quantum Electronics, 21*(1), 369-374.

Gangwar, R., Singh, S. P., & Singh, N. J. (2007). Soliton based optical communication. *Progress in Electromagnetics Research-pier*, *74*, 157-166.

Gattass, R. R., & Mazur, E. J. N. p. (2008). Femtosecond laser micromachining in transparent materials. *Optical Society of Technical Digest, 2* (4), 219-225.

Geim,A. Novoselov, K., (2007). The rise of graphene. *Nature Materials, 6* (3), 183-191.

Gerstner, E. (2010). Nobel Prize 2010: Andre Geim & Konstantin Novoselov. *Nature Physics, 6*, 1-2.

Ginley, T., Wang, Y. & Law, S., (2016). Topological insulator film growth by molecular beam epitaxy: a review. *Crystals, 6* (11), 1-26.

Gomez, L. A. , L. Orsila, T. Jouhti and Okhotnikov, O. G. (2004). Picosecond SESAM-Baed Ytterbium Mode- Locked Fiber Laser. *Institute of Electrical and Electronics Engineers Journal of Selected Topics in Quantum Electronics ,10* (1), 129-136.

Griffiths, David J. (2005). *Introduction to Quantum Mechanics* (2nd ed.). New Jersey: Prentice Hall.

Guo, B., Wang, S.-H., Wu, Z.-X., Wang, Z.-X., Wang, D.-H., Huang, H., . . . & Zhang, H. (2018). Sub-200 fs soliton mode-locked fiber laser based on bismuthene saturable absorber. *Optics express, 26* (18), 22750-22760.

Hao, R. and Sun, G. (2015). Design of Photonic Crystal Fiber with Large Negative Dispersion and High Nonlinearity. *Optik-International Journal for Light and Electron Optics, 126* (22), 3353-3356

Hasan, M.Z. & Kane, C.L., (2010). Colloquium: topological insulators. *Reviews of Modern Physics, 82* (4), 3045-3067.

Haus, H. A. (2000). Mode-locking of lasers. *Institute of Electrical and Electronics Engineers Journal of Selected Topics in Quantum Electronics, 6* (6), 1173-1185.

Heiba, Z.K., Mohamed, M.B. (2020). Effect of Gamma radiation on structural and optical parameters of Sm2O3: Mn/PVA nanocomposite film. *Optical* and *Quantum Electronics, 52*, 1-14.

Hernandez, Y., Nicolosi, V., & Lotya, M. et al. (2008). High-yield production of graphene by liquid-phase exfoliation of graphite. *Nature Nanotechnology, 3*, 563-568.

Hjelme, D. R., & Mickelson, A. (1992). Theory of timing jitter in actively mode-locked lasers. *Institute of Electrical and Electronics Engineers Journal of Quantum Electronics, 28* (6), 1594-1606.

Jackson, S. D., (2007). Passively Q-switched Tm 3+-doped silica fiber lasers. *Applied Optics, 46*(16), 3311-3317.

Jiang, Y., Narushima, T., & Okamoto, H. (2010). Nonlinear optical effects in trapping nanoparticles with femtosecond pulses. *Nature Physics*, *6*, 1005-1009.

Jinying Wang, Shibin Deng, Zhongfan Liu, & Zhirong Liu, (2015). The rare two-dimensional materials with Dirac cones. *National Science Review*, *2*(1), 22-39.

Kasim, N. Al-Masoodi, A. H. H. Ahmad, F. Munajat, Y. Ahmad, H. & Harun, S. W. (2014). Q-switched ytterbium doped fiber laser using multi-walled carbon nanotubes saturable absorber. *Chinese Optics Letters*, *12*(3), 1-4.

Keller, U. (2003). Recent developments in compact ultrafast lasers. *Nature*, *424* (6950), 831-838.

Klitzing, K. (1986). The quantized Hall effect. *Reviews of Modern Physics*, *58* (3), 519-531.

Krumrain, J. et al.,. (2011). MBE growth optimization of topological insulator Bi2Te3 films. *Journal of Crystal Growth*, *324* (1), 115-118.

Kurkov, A. S. (2011). Q-switched all-fiber lasers with saturable absorbers. *Laser Physics Letters*, *8*(5), 335-342.

Lee, J., Koo, J., Joonhoni, Y. M., & Lee, J. H. (2015). Femtosecond harmonic modelocking of a fiber laser based on a bulk-structured Bi 2 Te 3 topological insulator. *Optics Express*, *23*(5), 6359-6369.

Li, J., Luo, H., Zhai, B., Lu, R., Guo, Z., Zhang, H., & Liu, Y. (2016). Black phosphorus: a two-dimension saturable absorption material for mid-infrared Q-switched and mode-locked fiber lasers. *Scientific Reports*, *6*, 1-11.

Lin, Z. et al., (2016). 2D materials advances: from large scale synthesis and controlled heterostructures to improved characterization techniques, defects and applications. *2D Materials*, *3* (4), 1-38.

Lu, S. B. et al., (2015). Broadband nonlinear optical response in multi-layer black phosphorus: An emerging infrared and mid-infrared optical material. *Optics Express*, *23*(9), 11183-11194.

Luo, Z., Zhou, M., Weng, J., Huang, G., Xu, H., Ye, C., & Cai, Z. (2010). Graphene based passively Q-switched dual-wavelength erbium-doped fiber laser. *Optics Letters*, *35*(21), 3709-3711.

Luo, Z.-C., Luo, A.-P., & Xu, W.-C. (2010). Tunable and switchable multiwavelength passively mode-locked fiber laser based on SESAM and inline birefringence comb filter. *Institute of Electrical and Electronics Engineers Photonics Journal, 3*(1), 64-70.

M. Hajlaoui, et al., (2012). Ultrafast surface carrier dynamics in the topological insulator Bi2Te3. *Nano Letters, 12* (7), 3532-3536.

Miller, Arthur I.(2010). *137: Jung, Pauli and the Pursuit of a Scientific Obsession* (1st ed.). New York: W. W. Norton & Company.

Miransky, Vladimir A. (1993). *Dynamical Symmetry Breaking in Quantum Field Theories* (1st ed.). Singapore: World Scientific.

Moss, R. (2009). *The Secret History of Dreaming* (1st ed.). California: World Library.

Nagy Z, Takacs A, Filkorn T, Sarayba M. (2009). Initial clinical evaluation of an intraocular femtosecond laser in cataract surgery. *Journal of Refractive Surgery, 25*(12), 1053-1060.

Nizamani, B., Salam, S., Jafry, A. A. A., Zahir, N. M., Jurami, N., Khudus, M., . . . & Harun, S. W. (2020). Indium Tin Oxide Coated D-Shape Fiber as a Saturable Absorber for Generating a Dark Pulse Mode-Locked Laser. *Chinese Physics Letters, 37*(5), 1-6.

Noh H.-J., et al. (2008). Spin-orbit interaction effect in the electronic structure of Bi2Te3 observed by angle-resolve photoemission spectroscopy. *Euro physics Letters, 81* (5), 1-7.

Okhotnikov, O., Grudinin, A., & Pessa, M. (2004). Ultra-fast fibre laser systems based on SESAM technology: new horizons and applications. *New journal of physics,6*(1), 1-22.

Paschotta, R., Häring, R., Gini, E., Melchior, H., Keller, U., Offerhaus, H., & Richardson, D. (1999). Passively Q-switched 0.1-mJ fiber laser system at 1.53 micro meter. *Optics Letters, 24*(6), 388-390.

Paschotta, R., Nilsson, J., Tropper, A. C., & Hanna, D. C. (1997). Ytterbiumdoped fiber amplifiers. *Institute of Electrical and Electronics Engineers Journal of Selected Topics in Quantum Electronics, 33*(7), 1049-1056.

Peter, W., Milonni, J., & Eberly, H. (2010). *Laser physics* (2nd ed.). New Jersey: John Wiley & Sons, Hoboken.

Rosdin, R.Z.R.R. and Afiq Arif Aminuddin Jafry and Sulaiman Wadi Harun and Nur F. Zulkipli and Jusoh, Z. and Moh. Yasin (2019). Nanosecond pulsed laser generation with bismuth (III) tellurite saturable absorber. *Chalcogenide Letters, 16* (5), 209-214.

Rosol, A. H. A., Latiff, A. A., Khudus, M., & Harun, S. W. (2020). Nanosecond pulses generation with rose gold nanoparticles saturable absorber. *Indian Journal of Physics, 94*(7), 1079-1083.

Rüdiger Paschotta Effect of Self-phase Modulation on the Pulse Bandwidth. (2015, 05 Jun). Retrieved from: https://www.rp-photonics.com/self_phase_ modulation.html

Rüdiger Paschotta, (October 2008). Article on four-wave mixing (1st ed.). *Encyclopedia of Laser Physics and Technology*. Retrieved from: https://www.rp-photonics.com/four_wave_mixing.html.

Rusdi, M., Rosol, A., Rahman, M., Mahyuddin, M., Latiff, A., Ahmad, H., . . . & Yasin, M. (2019). Q-switched and mode-locked thulium doped fiber lasers with nickel oxide film saturable absorber. *Optics Communications, 447*, 6-12.

Russo V., Bailini A., Zamboni M., Passoni M., Conti C., Casari C. S., Li Bassi A. and Bottani C. E. (2008). *Journal of Raman Spectroscopy, 14,* 205-210

Salehi, J. A., Weiner, A. M., & Heritage, J. P. (1990). Coherent ultrashort light pulse code-division multiple access communication systems. *Journal of Lightwave Technology 8*(3), 478-491.

Samsamnun, F. S. M., N. F. Zulkipli, M. I. M. A. Khudus, A. S. A. Bakar, W. H. A. Majid, & S. W. Harun,. (2019). Nanosecond pulse generation with a gallium nitride saturable absorber. *Optical Society of America Continuum, 2,* 134-141.

Sennaroglu, Alphan (Ed.). (2007). *Solid-state lasers and applications*. Florida Chemical rubber company press, Boca Raton.

Set, S. Y., Yaguchi, H., Tanaka, Y., & Jablonski, M. (2004a). Laser mode locking using a saturable absorber incorporating carbon nanotubes. *Journal of Lightwave Technology*, *22*(1), 51-56.

Shirk, M.D. & Molian, P.A. (1998). A review of ultrashort pulsed laser ablation of materials. *Journal of Laser Applications, 10* (1),18-28.

Sinha, D. & Amaratunga, G. A. J. (2016). *Explicit Symmetry Breaking in Electrodynamic Systems and Electromagnetic Radiation.* (1st edition). California: Morgan Claypool.

Soffer, B. H. (1964). Giant pulse laser operation by a passive, reversibly bleachable absorber. *Journal of Applied Physics, 35*(8), 2551-2551.

Sotor, J. Sobon, G. Kowalczyk, M. Macherzynski, W. Paletko, P. & Abramski, K. M. (2015). Ultrafast thulium-doped fiber laser mode locked with black phosphorus. *Optics letters, 40,* 3885-3888.

Spühler, G., Paschotta, R., Fluck, R., Braun, B., Moser, M., Zhang, G., . . . & Keller, U. J. J. B. (2001). Experimentally confirmed design guidelines for passively Qswitched microchip lasers using semiconductor saturable absorbers. *Journal of the Optical Society of America B,16*(3), 376-388.

Steen, W. Mazumder, M. J.(2003). *Laser Material Processing* (4th ed.). Berlin: Springer Science & Business Media.

Stolen, R. H. & Bjorkholm, J. E. (1982). Parametric amplification and frequency conversion in optical fibers. *Institute of Electrical and Electronics Engineers Journal of Quantum Electronics, 18* (7), 1062-1072.

Sun, Y.-J. et al.,(2015). Passively Q-switched tri-wavelength Yb^31:GdAl3(BO3)4 solid-state laser with topological insulator Bi2Te3 as saturable absorber. *Photonics Research, 3* (3), 97-101.

Sun, Z. et al., (2016). Selenium-assisted controlled growth of grapheme-Bi2Se3 nanoplates hybrid Dirac materials by chemical vapor deposition. *Applied Surface Science, 365*, 357-363.

Sun, Z., Hasan, T., Torrisi, F., Popa, D., Privitera, G., Wang, F., . . . & Ferrari, A. (2010). Graphene mode-locked ultrafast laser. *American Chemical Society Nano, 4* (2), 803-810

The Longevity and Use of Index-Matching Gel in the UniCam® Connector and CamSplice® Mechanical Splice AEN046. (March 28, 2017). Retrieved from:

https://www.corning.com/catalog/coc/documents/application-engineering notes/AEN046.pdf

Tsai, T.-Y., & Birnbaum, M. J. J. o. a. p. (2000). Co 2+: ZnS and Co 2+: ZnSe saturable absorber Q switches. *Journal of Applied Physics, 87*(1), 25-29.

Vogel, A. Venugopalan, V. (2003). Mechanisms of pulsed laser ablation of biological tissues. *Chemmical Review, 103* (2), 577-644.

Walsh, T., Ilkov, F., & Chin, S. (1997). The dynamical behaviour of H2 and D2 in a strong, femtosecond, titanium: sapphire laser field. *Journal of Physics B: Atomic, Molecular and Optical Physics, 30*(9), 2167-2175.

Wang, J., Yang, P., Wei, X., & Zhou, Z. (2015). Preparation of NiO two-dimensional grainy films and their high-performance gas sensors for ammonia detection. *Nanoscale research letters, 10*(1), 1-6.

Wang, J., Yang, P., Wei, X., & Zhou, Z. (2015). Preparation of NiO two-dimensional grainy films and their high-performance gas sensors for ammonia detection. *Nanoscale Research Letter,* ***10*** (1), 1-6.

Wang, W., Yue, W., Liu, Z., Shi, T., Du, J., Leng, Y., . . . & Liu, X. J. (2018). Ultrafast Nonlinear Optical Response in Plasmonic 2D Molybdenum Oxide Nanosheets for Mode-Locked Pulse Generation. *Advanced Optical Materials, 6*(17), 1-8.

Wang, Y.R. et al., (2017). Optical nonlinearity engineering of a bismuth telluride saturable absorber and application of a pulsed solid state laser therein. *Nanoscale, 9* (48), 19100-19107.

Wang, Y.-R. et al.,(2018). Ultralow saturation intensity topological insulator saturable absorber for gigahertz mode-locked solid-state lasers. *Institute of Electrical and Electronics Engineers Photonics Journal, 10* (5), 1-10.

Wang, Z., Molina-Sanchez, A., Altmann, P., Sangalli, D., De Fazio, D., Soavi, G., . . & Finazzi, M. J. (2018). Intravalley spin-flip relaxation dynamics in singlelayer WS2. *Nano Letters, 18*(11), 6882-6891.

Wilson, J. & Hawkes, J. (1987). *Lasers, Principles and Applications* (1st ed.). London: Prentice Hall.

Xu, C., & Wise, F. J. N. p. (2013). Recent advances in fibre lasers for nonlinear microscopy. *Nature Photonics, 7*(11), 875-882.

Xu, J.L. et al. (2015). Ultrasensitive nonlinear absorption response of large-size topological insulator and application in low-threshold bulk pulsed lasers. *Scientific Reports, 5,* 1-12.

Y.-H. Lin, et al. (2015). Using n-and p-type Bi2Te3 topological insulator nanoparticles to enable controlled femtosecond mode-locking of fiber lasers. *American Chemical Society of Photonics, 2* (4), 481-490.

Young Min Jhon & Ju Han Lee. (Eds.). (2020). *2D Materials for Nanophotonics in Nanophotonics*. Amsterdam: Elsevier Science Publishing Company.

Yu, Y., Li, X., Hong, X., Deng, Y., Song, K., Geng, Y. and Tong, W. (2010) Some Features of the Photonic Crystal Fiber Temperature Sensor with Liquid Ethanol Filling. *Optics Express, 18*, 15383-15388.

Zayhowski, J. J. & Dill, C. (1995). Coupled-cavity electro-optically Q-switched Nd:YVO 4 microchip lasers. *Optics Letters, 20*(7), 716-718.

Zayhowski, J.J., Dill, C. (1994). Diode-pumped passively Q-switched picosecond microchip lasers. *Opticall Letters, 19* (18), 1427-1429.

Zhang Y, Xiong W, Chen W, Zheng Y. (2021). Recent progress on vanadium dioxide nanostructures and devices: fabrication, properties, applications and perspectives. *Nanomaterials, 11*(2), 1-48.

Zhang, H. et al. (2009). Topological insulators in Bi2Se3, Bi2Te3 and Sb2Te3 with a single Dirac cone on the surface. *Nature Physics, 5* (6), 438-442.

Zhang, H., Tang, D. Y., Zhao, L. M., Bao, Q. L., & Loh, K. P. (2009). Large energy mode locking of an erbium-doped fiber laser with atomic layer graphene. *Optics Express, 17*(20), 17630-17635.

Zhou, G., Wang, D. (2015). Few-quintuple Bi2Te3 nanofilms as potential thermoelectric materials. *Scientific Reports, 5,* 1-6.

Zulkipli N. F. et al., (2021). Q-switched pulse generation in a bidirectionally pumped EDFL utilizing Lu2O3 as saturable absorber. *Optoelectronics Letters, 17*(9), 529-533.

INDEX